1969

Electrical conduction in high resistivity particulate solids

K J. McLean
University of Wollongong

ELECTRICAL CONDUCTION IN HIGH RESISTIVITY PARTICULATE SOLIDS

Thesis for the Degree of

DOCTOR OF PHILOSOPHY

Submitted by

K.J.McLean, M.E.(N.Z.), B.D.(Melb.), M.I.E.Aust.

Department of Electrical Engineering,

Wollongong University College,

University of New South Wales.

December, 1969.

PREFACE

The problem of current conduction through high resistivity particles first arose while I was participating in a research programme on the electrostatic precipitation of high resistivity fly-ash. It became quite clear early in the investigation that it was going to be necessary to have a thorough understanding of the mechanism of current conduction through compressed layers of particles. Although the approach to the subject is made as general as possible, there are certain aspects which have been investigated more fully than others, these being those areas which are of particular interest to Engineers concerned with electrostatic precipitator performance.

In order to assist the reader, a concise statement of the approach adopted in this thesis is given in Section 1.1.1 together with a brief outline of the theoretical and experimental work covered. In Section 1.1.2 an outline is given of the original contribution this thesis makes to the body of knowledge on this subject. To assist in following the development of the theme throughout the thesis, a summary of each chapter is given in the Introduction to each chapter, together with a statement as to where the results and conclusions will be used in other parts of the thesis.

This project could not have been completed without the assistance of many people. I am thankful to Professor

C.A.M. Gray, Warden of Wollongong University College, for permission to carry out this research and for making the facilities of the College available, and to the Electricity Commission of New South Wales and the National Coal Research Advisory Committee of Australia who have financed the overall research programme. I am also indebted to my colleagues, Messrs. O.J. Tassicker and Z. Herceg of the Electrical Engineering Department who, through being involved in the research programme on electrostatic precipitators have assisted in creating an environment which has made the working on this thesis much easier.

The working on this thesis has been made most satisfying by the encouragement and helpful guidance given by my supervisor, Associate Professor R.M. Huey, and by the personal interest he has taken in this project. For all this I express my special thanks.

Finally, I wish to thank my wife Jean and children, David, Bruce and Helen who have had to show much patience and understanding during the final stages of this project.

K.J. McLean,
Wollongong University College.
November, 1969.

ABSTRACT

The mechanism of current conduction through particulates compressed between two parallel metal electrodes is investigated. The analysis assumes the absence of any surface conduction over the particles. It is shown that the overall electrical characteristics are determined by the characteristics of the individual contacts of the particles themselves, their bulk resistivity and the mode of compaction.

Silica glass and borosilicate glass are chosen to represent typical characteristics of electronic and ionic conducting, high resistivity materials. After investigating their bulk characteristics in high electric fields, the characteristics of the different types of contacts are examined experimentally by the use of scaled up models of the contacts.

The glass-glass contacts and glass-metal contacts all show non linear voltage-current characteristics. This is attributed to the existence of high electric fields which reduce the bulk resistivity of the glass and induce charge transfer across the small airgaps near the points of contact.

With metal-borosilicate contacts, the current is time dependent. The current increase for negative electrode polarity is attributed to excess electrons entering the glass, and the decrease in current with the opposite polarity is attributed to the depletion of mobile ionic carrier density.

Some analytical results of the effective resistivity of regular and random compactions of spherical particles are obtained, and the effect of mixtures of particle size are investigated qualitatively. A general equation for the effective resistivity of a particulate solid is derived.

The two glasses are ground into a powder, compressed between two parallel metal plates, and their overall electrical characteristics measured. These are explained in terms of the characteristics of the scaled up models of the contacts, the resistivity and the mode of compaction. To illustrate the work, a set of fly-ash characteristics are interpreted in terms of the theory developed in this thesis.

CONTENTS

CHAPTER 1.0

I N T R O D U C T I O N

1.1 Introduction.

1.1.1 Detailed Outline of Thesis.

The topic of this thesis arose out of a research programme on the electrostatic precipitation of high resistivity fly-ash. Although the approach has been made as general as possible, some of the aspects which are of particular interest in electrostatic precipitator operation have been more fully developed than others.

In chapter 1. the general philosophy of approach is developed. The thesis is concerned with finding and explaining the electrical characteristics of high resistivity particles compressed between two parallel metal plates. If the surface conduction over the particle surface is assumed negligible then it is argued that the three main factors responsible for the characteristics of the current conduction are the electrical characteristics of the particle contacts between themselves and with the metal electrodes, the bulk resistivity and the mode of compaction. In order to make the investigation more useful, both ionic and electronic conducting materials are used. A survey is made of the existing work on current conduction through particulate solids, and of the measuring techniques used.

The area of contact, contact resistance and the magnitudes of the electric fields are investigated theoretically in Chapter 2. It is shown that very high electric fields can

be generated in the particles themselves and between adjacent surfaces in the region around the points of contact. The existence of these high electric fields is used to explain the characteristics of the contacts observed in the following chapters. A "field magnitude" factor is introduced to indicate the magnitude of the electric fields around the contact points.

Optically clear silica and borosilicate glass respectively are chosen as typical examples of electronic and ionic conducting materials. The bulk characteristics of these materials under high electric fields and temperatures are investigated in Chapter 3, together with their absorption current characteristics. The presence of spurious pulses was observed in silica and this is further examined in the Appendix.

The electrical characteristics of the contacts are investigated experimentally by the use of scaled up models. By using a system of small diameter rods as one electrode, the bulk characteristics of the contacts are determined. A similar set of characteristics is then obtained by replacing the rod electrode with a metal ball. By comparing the two sets of characteristics, it is shown that electron transfer takes place between two adjacent surfaces around the point of contact of any two particles. By varying the polarity of the metal electrodes and observing the results, the behaviour of the contacts between the particles and the anode and cathode

metal electrodes is determined. The metal to glass contact characteristics using electronic conducting glass are given in Chapter 4 and those using ionic conducting glass in Chapter 5. The characteristics of glass-glass contacts are also investigated and the results recorded in Chapter 6. In each of these cases, the results are related to the bulk characteristics of the glass and additional models are proposed to account for the phenomena observed.

In Chapter 7, the effect of different modes of compaction are investigated. In the first instance, the effective resistivity of regular arrays of uniform sperical particles is determined analytically. This is then extended to randomly packed uniform spheres and then to particles with a wide size distribution. A general equation for the effective resistivity of a particulate solid is given:

$$\rho = \left[H' A \epsilon^{\phi/kT} \right] \epsilon^{-N'E_{av}}$$

Samples of the two types of material used in the previous tests are then ground to a powder and their electrical characteristics recorded in Chapter 8. These are then explained in terms of the bulk characteristics of the material, the characteristics of the point contacts and the compaction. In order to illustrate the results, the characteristics of a sample of fly-ash are interpreted in terms of the theory developed in the thesis.

1.1.2 Original Contribution of Thesis.

In this section, an attempt is made to give a concise statement of the original contribution made by this Thesis to the understanding of the mechanism of current conduction in particulate solids. The main areas where this contribution has been made are listed below.

(i) The first of these is in the general philosophy of the approach adopted for this investigation. In the past, very little attempt has been made to relate the overall characteristics of the current conduction through particulate solids to the characteristics of the particles themselves and their effect on one another. This is the first time that this has been attempted for a compacted layer of particles in which the surface conduction over the particles is eliminated. The relationship is established in two ways:

(a) By using scaled up models of the particle contacts to obtain their electrical characteristics. These are then related to the characteristics of the contacts in the particulate solid and to the overall characteristics.

(b) By analysing in detail the effect of different modes of compaction of the particles on the current conduction through the particulate solid.

(ii) This is the first time that the Holm equation

has been used in a theoretical investigation of the electrical field strength around the contact points of the particles. It is demonstrated that high electric fields may exist in the particles themselves and between surfaces in the region of their points of contact. The 'FM' factor is introduced as a means of indicating the order of magnitude of these electric fields.

(iii) Some of the characteristics of the point contacts between two glass samples and between glass and metallic electrodes in high electric fields have been observed for the first time. The two important ones are;

(a) the non-linear voltage-current relationship, and

(b) the time dependence of the current in the case of metal to ionic conducting glass contacts.

New experimental techniques have been developed to investigate these characteristics and new models proposed to account for the observed results.

(iv) This is the first occasion on which an effective resistivity of a particulate solid is related to the mode of compaction of the particles. A complete theoretical analysis is made of an ideal situation where

spherical particles of uniform size are compacted in regular arrays. A method is also suggested for determining the effective resistivity of the random packing of uniform particles. The effect of a random distribution of particle size on the effective resistivity is discussed.

(v) A semi-empirical equation is derived for the effective resistivity of a particulate solid. This takes into account the bulk characteristic of the particle material, the mode of compaction and the electrical characteristics of the contact points of the individual particles. As far as the overall characteristics are concerned, the model proposed accounts for the non-linear voltage-current characteristics, the temperature dependence and effect of compaction. The origin of the current transient components observed in resistivity measurements has been determined.

(vi) This is the first occasion on which a rod electrode system has been used to investigate the origin of the spurious pulses observed in silica and fly-ash. A new model is proposed to account for these pulses.

1.2 Philosophy of Approach.

1.2.1 Relationship to Electrostatic Precipitators.

The problem of current conduction through high resistivity particles first arose in connection with a research programme now being undertaken by the Electrical Engineering Department at Wollongong University College. The aim of this programme is to investigate the basic physical processes taking place in electrostatic precipitators, especially when precipitating high resistivity particles, and to relate these processes to the precipitator performance. The ultimate aim is to use this knowledge to improve their overall efficiency and performance. In general terms the overall programme is concerned with the following projects:

(a) Investigation of the corona current characteristics with clean and contaminated electrodes.

(b) The electric field distribution.

(c) Mechanism of particle charging.

(d) Factors affecting particle adhesion.

(e) Mechanism of current conduction through compressed layers of particles.

(f) Resistivity measuring techniques.

(g) The prediction of full scale precipitator performance from data obtained from bench type precipitators.

This thesis represents part of the investigation associated with Projects (e) and (f).

To understand the relationship of the topic of this thesis to that of electrostatic precipitators, it is necessary to give a brief outline of the general principles of their operation. Good, comprehensive and detailed accounts are given in the books by White (1), and Rose and Wood (2). An electrostatic precipitator comprises a series of earthed parallel plates or tubes called collecting electrodes, which enclose wire discharge electrodes. When a high negative voltage is applied to the discharge electrode, a corona current flows between it and the collecting electrode. As the gas containing the suspended particles flows through the precipitator, the suspended particles are charged negatively, and under the influence of the electrostatic field, are deposited on the collecting plate causing a thick layer to be formed. The accumulated deposit on the collecting electrode is removed by occasionally rapping the electrode thus causing the deposited particles to fall into hoppers.

The main corona current is carried across the air gap between the electrodes by charge attachment to the gas molecules and suspended particles, which, on reaching the surface of the deposited layer are discharged through the layer to the metal electrode. Under some circumstances there are also free electrons in the air gap. If the particle

resistivity is high, the current flow through the particles establishes high electric fields in the layer, which affects the operation of the precipitator and reduces its efficiency.

The relationship between the reduction in efficiency and particle resistivity is usually attributed to 'back corona'. This phenomenon appears as blue point discharges on the surface of the deposited layer of particles and has the effect of reducing the spark over voltage, increasing the corona current, generating local disturbances of the electric field, reversing the charge of the oncoming suspended particles and causing erosion of the particle layer. In addition to this, the author(3) has shown that even if the effects of back corona are ignored, the voltage drop across the deposited layer reaches such a magnitude that the effective voltage in the air gap between the electrodes is reduced. This reduces the charging and accelerating electric fields for the suspended particles and reduces the precipitator efficiency.

An understanding of the mechanism of current conduction through a layer of compacted particles and of the manner in which the over all resistance is governed by the particulate form of the layer is basic in any programme aimed at understanding the processes taking place in electrostatic precipitators.

1.2.2 Manner of Current Injection.

It is necessary at this stage to decide on the manner in which the current is to be injected into the compacted layer of particulate solids. In electrostatic precipitator work, the current conduction problem arises in two quite different circumstances. The first is on the collecting plate of the precipitator. In this case the particle layer is bombarded by a stream of negatively charged ions and particles which discharge through the layer to the metal electrode. The other occasion is where resistivity measurements are being made of the particles compressed between two metal electrodes. The method of charge injection is different in these two cases and this results in different overall characteristics of the layer. In the former case for instance, for high resistivity particles, a back discharge in the form of luminous spots appears on the layer surface and this complicates the mechanism of conduction through the layer. It is apparent that the latter case is the more basic one and it is proposed to restrict this investigation to the study of current conduction in particulate layers compressed between two parallel metal electrodes. The other aspect is to be the subject of another project.

1.2.3 General Considerations.

The aim of this investigation into the mechanism of current conduction through particulate solids can be better understood by posing the problem in an alternative form. The basic objective of the thesis is to determine how the characteristics of an insulating material, broken into small particles and compressed between metal electrodes, will differ from its characteristics when in the solid form. There are a number of factors responsible for the differences that occur but the ones which dominate the conduction mechanism are:

(a) The large specific area of the layer when in the particulate form. Hence it follows that the surface characteristics will play a much more important part in the conduction process when in the particulate than when in the solid form.

(b) Points of contact. In the particulate form, the layer is made up of a large number of small particles compressed together and making contact with the adjacent particles at a number of points. The area of these points of contact will depend on the particle shape, type of compaction, and forces involved, but in any case it will be small compared with the diameter of the particles. As the current flows through the layer it must pass through these points of contact. Since their areas are small, the current density, and hence the electric fields in this region must be higher than the average

electric field. The effect of this will vary with circumstances but under some conditions will cause heating, reduction in the bulk resistivity, carrier depletion, space charge build up and charge transfer across the airgap between the particles.

(c) Particle compaction. The conduction of the current will be governed by such factors as the particle shape, the size distribution, type of compaction, and the compaction forces as well as the elastic characteristics of the particles themselves.

In order to have a clear picture of the conduction mechanism it is convenient to consider two extreme cases. One where the current flows only over the surface of the particles and the other where the current flows entirely through the volume of the particles and only comes to the surface at the points of contact. Of the two cases the latter is the more basic and it is therefore proposed to investigate this in the thesis.

The problem is therefore reduced to one involving an investigation of the electrical characteristics of point contacts and the influence of the mode of compaction with volume conduction taking place through the particles.

1.2.4 Material

In choosing a suitable material the following requirements have to be met:

(a) The material must have a high resistivity and a negative temperature co-efficient.

(b) It must be obtainable in solid form in order that its bulk and surface properties can be investigated before it is ground to a powder.

(c) Its chemical composition must be similar to that of fly-ash.

(d) In order to keep the investigation as general as possible it is necessary to select two different materials; one of which must be essentially ionic conducting and the other electronic conducting.

As shown in Appendix I, the main chemical constituent of fly-ash is silica. On the basis of the chemical composition, X-Ray diffraction analysis and the presence of trace elements in the fly-ash, it is reasonable to assume that both electronic and ionic conduction may take place. Fly-ash itself however is not a suitable material for these tests as it is not possible to obtain it in a solid form so that its bulk characteristics can be investigated.

The two materials chosen were borosilicate glass and optically clear silica. Both of these meet the chemical requirement of containing a large percentage of silica. A number of ionic conduction materials were investigated but it was decided to use borosilicate glass as it is readily available, has good temperature properties and some experi-

mental work had already been carried out on its electrical properties. A purely electronic conducting material was not immediately available. However, optically clear silica appeared to be suitable. Very little is known about its conducting mechanism but, as will be shown in Chapter 4, the author's work indicates that it is essentially an electronic conducting material.

1.3 Survey.

1.3.1 Conduction Mechanism

In general, there has not been very much interest in the problem of current conduction in particulate solids. Outside of the work associated with electrostatic precipitators most of the published work (4)(5)(6) is concerned with the overall electrical characteristics of low resistivity powders in which very little attempt has been made to develop a theoretical analysis of the conduction mechanism. Some of the main applications of the conductivity characteristics of powdered materials have been to determine the moisture content of substances as sand(7) and wheat grain (8), and to determine the dew point of gases(9).

The most extensive investigations into this topic have been carried out in research programmes associated with electrostatic precipitators. It has been a common practice of investigators working in this field to speak of two modes

of current conduction;

(i) volume conduction,

and (ii) surface conduction.

There are special circumstances where either one or the other of these conduction mechanisms will dominate but often they occur together.

For volume conduction alone to exist, the particle surfaces must be cleaned to remove any high conducting outer layer. Under these conditions, the main current flows through the volume of the particle, coming to the surface only at the points of contact. It has been observed that for a fixed set of compaction conditions, the variation of conductivity with temperature obeys the Rash Henrickensen Law.

$$\sigma = A \epsilon^{-\phi/kT} \quad \ldots\ldots\ldots\ldots\ldots\ldots\ldots \quad 1.1$$

Where ϕ is called the activation energy, k is Boltzmanns' constant, T the absolute temperature and A a constant. Little attempt has been made to investigate these constants. White(10) has compared the activation energies of leached fly-ash with that of common materials.

Surface conduction occurs when particles adsorb gas molecules, chemicals or water onto their outer surface causing a high conductivity layer to be formed. Although conduction through the volume must always occur, in the case where the surface conductivity of the layer is high compared with that of the volume, it is reasonable to neglect the

volume conduction. Much of the interest has been in comparing the overall conductivity of the compacted layers of particles with variations of environmental conditions. Sproull and Nakada(11) have made one of the most thorough investigations of the effect of varying the temperature and relative humidity on the apparent resistivity of a number of industrial dusts. Daniel(12) has measured the apparent resistivity as a function of the amount of water adsorbed at various temperatures. Surface conduction is also influenced by adsorbed gases. One well established practice for reducing the resistivity of the particles is to condition the gas carrying the suspended particles by adding small quantities of ammonia, sulphur-trioxide, chlorides or hydrocarbon vapours as conditioning agents. These are adsorbed on to the particle surfaces thus reducing the surface resistivity. Although the reduction in resistivity has been measured, no systematic attempt has been made to relate experimentally the temperature, conditioning agent concentration, humidity and particle material to the apparent resistivity.

The influence of such factors as particle compaction and that of the applied electric field have only been observed and superficially investigated(13).

The first person to attempt to establish a theoretical model relating some of the basic parameters of the dust to its overall electrical characteristics was Nasuda(14)(15). He began his analysis by considering spherical

particles arranged in a simple cubic array. By calculating the area of contact between two adjacent particles from the Hertz Equation and determining the effective resistance of the points of contact he developed a theoretical expression for the conductivity. In addition to volume and surface conductivity terms he introduced another term taking into account the effect of capillary condensation.

His experimental results tend to be more informative than those of the earlier workers. He has results showing the variation of conductivity with particle size, for different temperatures and humidities. He also compared the conductivities of soda glass and marble in both the solid and particulate state for different temperatures and relative humidities.

1.3.2 Measuring Techniques.

There are two basic techniques used to measure the resistivity of particulate solids. The first method is to compact the particles between two parallel plates and measure the voltage current characteristic. The second method makes use of a metal plate electrode and a point discharge electrode mounted directly above it. The particles may be either placed or precipitated on the metal electrode. The potential drop across the layer is measured by means of a grid or probe placed on the surface of the layer. For both methods it is usual to use guard rings to eliminate the effects of surface and stray currents.

It is also possible to classify the resistivity measurements according to the condition under which it is desired to make the measurements. There are three classifications:

(i) Bulk resistivity measurements. These are conducted in the laboratory with the conditions adjusted so as to eliminate any surface conduction over the particles.

(ii) Environmental measurements. These are also conducted in the laboratory with the environment varied so that at least some conduction takes place over the particle surface (11).

(iii) In-situ measurements. These measurements are made with the particles in contact with the actual flue gas which will pass through the precipitator. In general, a sample of the particle laden gas is extracted from the main flue and passed through the resistivity measuring apparatus. The White and Anderson apparatus(16), which has been adopted by the Air Pollution Control Association of America as a standard (17), comprises a needle electrode suspended above a metal plate. The particles are precipitated onto the plate and then a second metal plate is lowered onto the surface to make the resistivity measurement. Isahaya and Echizenya(18) have developed a refinement in which a probe is lowered onto the surface of the precipitated layer. Cohen and Dickinson(19) collected the particles with a mechanical cyclone and then dropped the particles into a

measuring chamber. One of the limitations of these methods is that they do not always collect a representative sample of the suspended particles. Since the chemical composition of the particles tends to vary with particle size, this may introduce errors into the resistivity measurement.

The author, with Tassicker & Herceg(20)(21), has overcome this problem by using a small precipitator of high efficiency to do the collecting. This apparatus also has the advantage of making voltage-corona current, sparkover voltage, and efficiency measurements. These can be related to full scale precipitator performance.

Eishold(22) has devised an original apparatus which is placed in the main gas flow and the particles are precipitated into the space between the measuring plates.

CHAPTER 2.0

THEORY OF CONTACTS

2.1 Introduction.

The mechanism of current conduction through a particulate solid is determined to a large extent by the electrical characteristics of the points of contact between individual particles. As the current flows from one point to another, it is constricted by geometrical considerations to flow through the relatively small area of the contact point. Because of this constriction, the current density in the region of the contact is high and this results in the establishment of high electric fields in the particle itself and in the air gap between adjacent particles.

In order to obtain analytical expressions for the resistance of the contacts and for the magnitude of the electric fields, it is necessary, in the first instance, to consider an idealized contact. In this chapter the idealized contact is analysed. After considering a number of approximate solutions for the contact resistance and electric field, the approach used by Holm for calculating contact resistance is selected as the one most suitable for the purpose of this thesis. It is shown that for this idealized contact, very high electric fields may exist in the region of the point of contact.

Because of the magnitude of these electric fields, some of the basic assumptions made for this idealized model do not apply to real contacts. The effect of the electric field on the resistivity of the particulate material and on the temperature rise due to losses is discussed in Chapter 3. Its effect on the electrical characteristics of the particle contacts is detailed in Chapters 4, 5 and 6.

2.2 Constriction Resistance.

2.2.1 Basic Assumptions.

The calculation of the constriction resistance of contacts between two surfaces has been widely investigated and well summarised in books by Jones(23), Windred(24) and Holm(25). For the purpose of this thesis however, it is necessary to extend their work. The main reasons for doing this are:

(a) These investigators have been mainly concerned with the characteristics of contacts between two metallic components, whereas in this thesis, the main interest is in the contacts in which at least one component is an insulator. When this occurs, high electric fields may be generated in the region around the contacts thus causing changes in their electrical characteristics.

(b) No solution has been obtained for the constriction resistance of two spherical particles in contact or of a spherical particle in contact with a plane.

Although no simple analytical solution has been found for the exact constriction resistance of two spheres in contact, it has been possible to obtain solutions based on three different approximations.

The basic assumptions which are common to all three approximate solutions are listed below;

(i) The conductivity of the material is independent of the electric field.

(ii) The material is homogenous.

(iii) No conduction takes place over the surface of the particle.

(iv) The contact is ohmic.

(v) There is no build up of space charge, depletion of mobile carriers or any charge transfer across the air gap.

(vi) The particles are spherical with perfectly smooth surfaces.

(vii) There is no heating at the contacts points.

2.2.2 Holm's Equation.

One approximation which may be made, is to assume that the radius of the contact circle is very small compared with the radius of the particle. In this case, it is a reasonable approximation to assume that the surface of contact and that of the adjacent surface of the particle are all in the one plane. Under these conditions, the problem reduces to the consideration of the pattern of current flow through a contact point of a semi infinite body. The mathematical solution of Laplace's Equation for this geometry is given in standard text books.

Holm (25), in his work on metallic contacts developes an expression for the effective resistance of point contacts between parallel plates. So as to generalise the expression he assumed an elliptic point of contact with

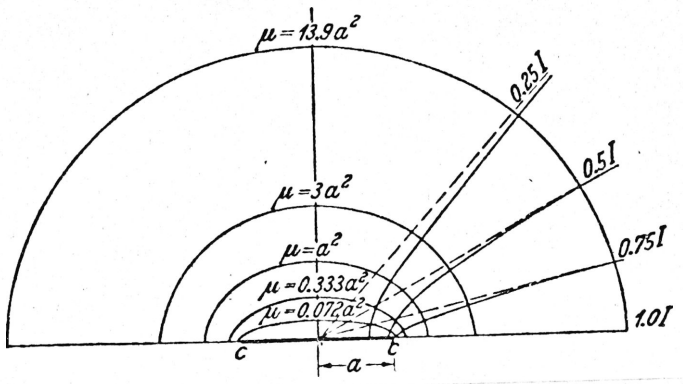

FIGURE 2.1 LINES OF CURRENT FLOW AND EQUIPOTENTIAL SURFACES

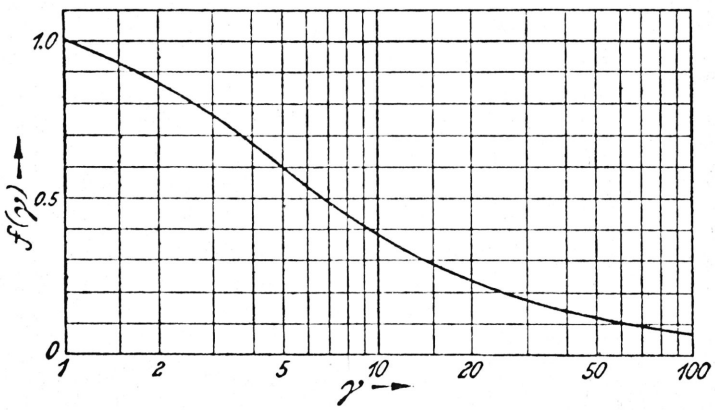

FIGURE 2.2 VARIATION OF SHAPE FACTOR

(The above two figures are reproduced from Reference 25)

the semi-axes α and β. It may be shown that the equi-potential surfaces in the solid are semi-ellipsoids with the equation;

$$\frac{x^2}{\alpha^2 + \mu} + \frac{y^2}{\beta^2 + \mu} + \frac{z^2}{\mu} = 1.0$$

Where μ is a parameter and the ellipse axes coincide with the direction of x and y. The height of a semi-ellipsoid normal to the x-y plane is $\sqrt{\mu}$ and its axis in the x direction is $\sqrt{\alpha^2+\mu}$

The constriction resistance from the plane of contact to the equi-potential surface μ is,

$$R_\mu = \frac{\rho}{4\pi} \int_0^\mu \frac{d\mu}{\sqrt{(\alpha^2 + \mu)(\beta^2 + \mu)\mu}}$$

where ρ is the resistivity of the material.

If the area of contact is circular instead of ellipic, $\alpha = \beta = a$, the radius of the contact, then the resistance to the equi-potential surface μ is,

$$R_\mu = \frac{\rho}{2\pi a} \tan^{-1} \frac{\sqrt{\mu}}{a} \quad \ldots\ldots\ldots\ldots\ldots\ldots \quad 2.1$$

By letting the value of $\mu = \infty$, the total constriction resistance of the contact can be determined. Hence the resistance is:

$$R = \rho / 4a \quad \ldots\ldots\ldots\ldots\ldots\ldots \quad 2.2$$

Figure 2.1 shows the current flow and equipotential surfaces.

This equation gives the effective resistance of the contact between a particle and a flat metal surface. It assumes that the constriction resistance of the metal electrode is negligible compared with that of the particle.

The total effective resistance of a particle is twice that given by Equation 2.2 and is,

$$R = \rho / 2a \quad \ldots\ldots\ldots\ldots\ldots\ldots\ldots \quad 2.3$$

This also gives the total contact resistance between two particles.

For the elliptic contact, it may be shown that the current density is given by;

$$J(x,y) = \frac{1}{2\pi\alpha\beta\sqrt{1 - (x/\alpha)^2 - (y/\beta)^2}}$$

For a circular conducting surface this reduces to the form,

$$J(r) = \frac{1}{2\pi a\sqrt{a^2 - r^2}} \quad \ldots\ldots\ldots\ldots \quad 2.4$$

The influence of the elliptic shape of the contact area on the constriction resistance can be determined by letting $\alpha = \gamma a$ and $\beta = a/\gamma$, where γ is a measure of the ovalness of the elliptic contact. The area of the elliptic contact with ordinates α and β is the same as the circular area with radius 'a'. The resistance of an elliptic contact may be written in the form,

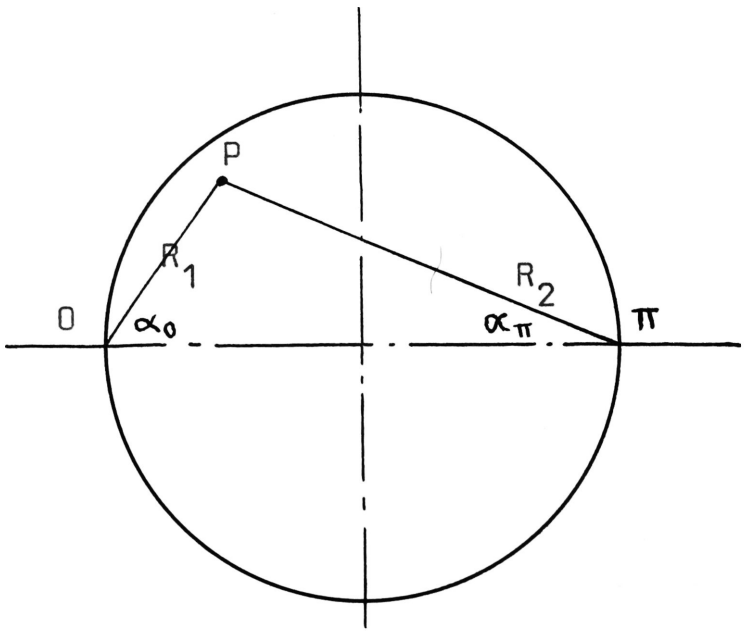

FIGURE 2.3 DIAGRAM FOR SMYTHS EQUATION

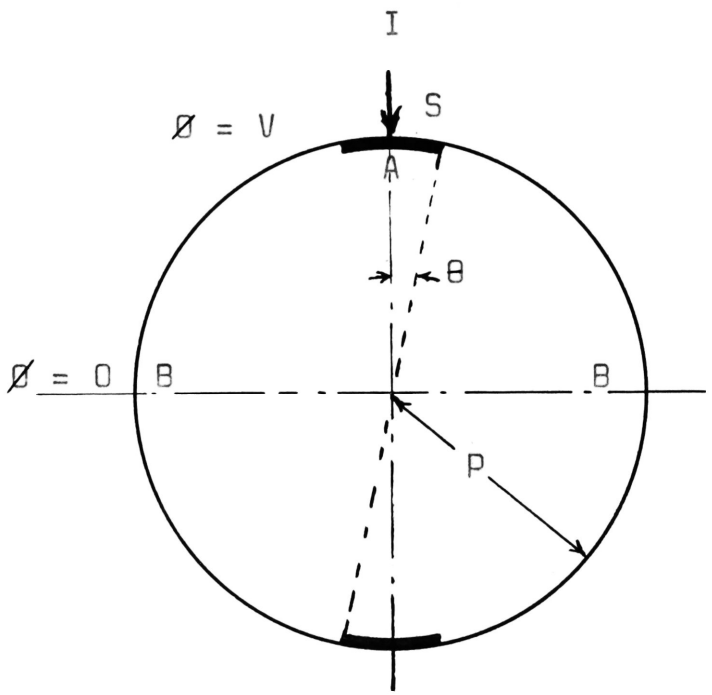

FIGURE 2.4 DIAGRAM FOR EQUIPOTENTIAL CAP EQUATION

$$R = (\rho/4a) f(\gamma) \quad \ldots\ldots\ldots\ldots\ldots\ldots \quad 2.5$$

The variation of the shape factor $f(\gamma)$ with the ovalness of the ellipse is given in Figure 2.2.

2.2.3 Smyth's Equation.

Smyth(26) has developed an equation for the voltage distribution in a sphere when the current enters at one pole and leaves at the other. See Figure 2.3. The voltage is given by,

$$V = \frac{\rho I}{2\pi}\left[\frac{1}{R_1} - \frac{1}{p}\ln\left(R_1(1+\cos\alpha_0)\right)^{0.5} - \frac{1}{R_2} + \frac{1}{p}\ln\left(R_2(1+\cos\alpha_n)\right)^{0.5}\right]$$

Since this equation assumes the Legendre Function $P_n(\cos\theta) = P_n(1)$, it gives infinite values for the potential at the electrodes. Hence the equation cannot be used in this form to evaluate the resistance between the electrodes.

As the point P approaches the electrodes, the equipotential surface becomes a hemispherical surface with a magnitude of $\rho I/2\pi R_1$ volts. If it is assumed that the contact forms a solid conducting hemisphere of radius R_1, the resistance of one half of the particle is given by the relationship,

$$R = \rho / 2\pi R_1 \quad \ldots\ldots\ldots\ldots\ldots\ldots\ldots \quad 2.6$$

The effective resistance of a particle is twice the value given by Equation 2.6.

2.2.4 Equipotential Cap.

Assume that the area of contact between adjacent particles follows the surface of the sphere and that these contact areas are at opposite poles, as shown in Figure 2.4.

If the spherical co-ordinate system is used, the general solution of Laplaces Equation is of the form;

$$\phi = \sum_{n=0}^{\infty} An\, x^n\, Pn(\cos\theta) \quad \ldots\ldots\ldots\ldots \quad 2.7$$

Because of the symmetry, the equatorial plane may be taken as zero potential and only odd harmonics can appear in the expansion.

The boundary conditions are;

At $x = p$

$$\frac{\partial \phi}{\partial x} = 0 \quad \text{except over area S}$$

$$\phi = V \quad \text{over area S}$$

$$\frac{\partial \phi}{\partial x} = \rho J(\mu) \quad \text{over area S}$$

Where $\mu = \cos\theta$

The current distribution over the area S must be

regarded as being unknown at this stage. If the first two boundary conditions are given, then by the Uniqueness Theorem, the current distribution over the area of the contact can only have one form. Weber's (27) assumption of a constant current density cannot be correct.

Differentiating the potential ϕ,

$$\frac{\partial \phi}{\partial x} = \sum_{n=1}^{\infty} An\, n x^{n-1} Pn(\cos\theta)$$

where n is odd.

Multiply both sides by $Pn(\cos\theta)$, put $x = p$ and integrate between limits of -1 and 1.

Since the equatorial plane is taken as zero potential, integrate between 0 and 1.

Since $\frac{\partial \phi}{\partial x} = 0$ for $\mu = 0$ to $\mu = \mu_1$

$$\int_{\mu_1}^{1} \rho\, J(\mu)\, Pn(\mu) = An\, p^{n-1}\, (n/(2n+1))$$

$$\text{Hence} \quad An = \frac{2n+1}{n\, p^{n-1}} \int_{\mu_1}^{1} \rho\, J(\mu)\, Pn(\mu)\, d\mu \quad \ldots\ldots\ldots \quad 2.8$$

The potential at any point is found by substituting Equation 2.8 in Equation 2.7.

$$\phi = \rho\, p\, (x/p)^n \left[\sum_{n=1}^{n=\infty} (2n+1)/n \int_{\mu_1}^{1} J(\mu)\, Pn(\mu)\, d\mu \right] Pn(\mu)$$

At $\theta = 0$, $Pn(\mu) = 1$. The voltage difference between A and B is given by,

$$V = \rho p \sum_{n=1}^{\infty} (2n+1)/n \int_{\mu_1}^{1} J(\mu)\, Pn(\mu)\, d\mu \qquad \ldots\ldots\ldots\ldots \quad 2.9$$

The effective resistance of one half of the sphere is given by,

$$R = V / I = V / \int_S J(\mu)\, ds \qquad \ldots\ldots\ldots\ldots \quad 2.10$$

No simple explicit expression can be found for equation 2.10. A numerical solution was found for a contact angle of two degrees. The technique used was to assume some distribution for the current over the contact surface and then use equation 2.9 to calculate the voltage distribution around the surface. If the calculated potential is constant over the surface of the cap, then the assumed current distribution is the correct one. In order for the Legendre Functions to converge, it is necessary to generate harmonics up to the order of 200. This makes computing on the IBM 1620 rather slow.

Other than producing one sample calculation, this method was not persued as it had limited usefulness.

2.2.5 Conclusions

Of the three approximate methods considered for calculating the constriction resistance of two spheres in

contact, the latter two were rejected.

One of the main requirements of the method adopted is that explicit expressions must be available so that the electric field strength may be calculated. On this basis the equipotential cap approximation is unsatisfactory. Of the other two approximations, the assumptions leading to the Holm equation give a field pattern much closer to the actual one than is given by the Smyth equation. In the latter case, the final equation 2.6 implies that the contact forms a solid conducting hemisphere of radius R_1. Hence the Holm equation is used for further calculations.

2.3 Area of Contact.

2.3.1 Hertz Equation.

The deformation which determines the load bearing area, is usually elastic up to pressure limits in the order of the hardness of the material, but for greater pressures plastic flow commences.

If two like spheres, each of radius p, are compressed by a force Fc directed along their line of centres, then with in the limits of elastic deformation, the theory due to Hertz (28) predicts a plane circular contact of radius 'a'.

$$a = \sqrt[3]{\frac{3(1-\nu^2)\,Fc\,p}{4Y}} \qquad \ldots\ldots\ldots\ldots \quad 2.11$$

Where ν = Poissons ratio.

Y = Youngs modulus.

The normal pressure on the contact area is given by;

$$\sigma = \frac{3\,Fc}{2\pi a^2}\sqrt{(a^2 - x^2)}$$

x = radial distance from centre of the contact circle.

The relative approach of the spheres is given by;

$$\propto = 2\left[\frac{3(1 - \nu^2)\,Fc}{4\,Y\sqrt{p}}\right]^{2/3}$$

The basic assumptions implied by the Hertz equation are;

(i) Dimensions of the contact area are small compared with the radii of the spheres.

(ii) Warping of the surface of contact is negligible.

(iii) Tangential components of the traction across the contacts are negligible.

2.3.2 Effective Electrical Contact Area.

The actual electrical contact area is not necessarily the same as the area calculated from the Hertz equation. In the case of contacts between metal surfaces, the actual physical contact occurs as a number of clusters of microcontacts. Their position is determined by the flatness

of the surfaces and their sizes by the microscopic surface roughness. If this is true for nominally smooth surfaces, it will also be true for the contact surfaces between two particles.

If the microcontacts are assumed to be circular and at a sufficient distance from one another so that their potential fields do not interfere, the effective resistance of the contact is given by;

$$Ra = \frac{\rho}{4 \sum_{i} a_i} \quad \ldots\ldots\ldots\ldots\ldots\ldots \quad 2.12$$

Where a_i is the radius of any single contact.

If the microcontacts are close enough to influence one another, then the above equation is not valid. Holm (25) has shown that for a uniform distribution of the microcontacts, which are of circular shape, the effective resistance is;

$$Ra = \frac{\rho}{2\pi n b} \tan^{-1} \frac{l}{b} - \frac{\rho l}{Aa} + \frac{\rho}{4a} \quad \ldots\ldots\ldots \quad 2.13$$

Where n = the number of microcontacts,

b = the radius of microcontacts,

l = average distance between centres,

Aa = apparent contact area.

Greenwood(29) quotes an alternative formula used by Holm in his more inaccessible publications. In the simplest case where there are a large number of small equal contacts distributed uniformly over a circular area the effective resistance is;

$R_a = \rho (1/2nb - 1/2a)$

Where b = radius of the microcontact

a = radius of the cluster.

Greenwood has shown that the effective resistance may be regarded as the sum of the parallel resistances of the microcontacts and an interaction term often related to the extent of the cluster but independent of the number and size of the individual contacts.

2.4 Electric Field Strength.

2.4.1 Introduction.

It has already been pointed out that because of the high density of current in the region of the contact points and the magnitude of the resistivity, very high electric fields are generated in the particle itself and across the airgap between adjacent surfaces. It is necessary to find expressions for these electric fields and to calculate their magnitudes in order that their effect on the conduction mechanism in this region may be determined.

If it is assumed that the particles are all of one size and are packed to form a simple cubic array as shown in Figure 7.1, and subjected to a constant voltage gradient of E_{av} v/m, the voltage across each particle is given by,

$$V_p = E_{av} 2p \quad \ldots\ldots\ldots\ldots\ldots \quad 2.14$$

This is the total voltage across the particle, the voltage

drop across one side of the contact is therefore $E_{av}p$ volts.

If it is assumed that the material is homogeneous and of constant conductivity, the current flow pattern, as determined by Holm's equation, is the same shape irrespective of the applied voltage and the diameter of the contact circle. It is shown in Appendix III that the strength of the electric field at any given point in the pattern is proportional to the voltage across the contact and inversely proportional to the radius of the contact circle. Hence,

$$E_p = K\,V/a \qquad \ldots\ldots\ldots\ldots\ldots \quad 2.15$$

By substituting Equation 2.14 in 2.15, this may be related to the average applied field across a compacted layer of particles.

$$E_p = K\,E_{av}(p/a)$$

$$= K\,FM$$

$$\text{Where} \qquad FM = V/a = E_{av}(p/a) = V_p/2a \ldots \quad 2.16$$

Hence the electric field strength in the particle itself is proportional to the Field Magnitude (FM) factor.

Table 2.1 shows the voltage across different sizes of particles when subjected to average voltage gradients from 10^4 to 10^6 v/m. Since the average breakdown voltage across a compacted layer of particles is approximately that of air, an E_{av} of 10^6 v/m is taken as the maximum value.

TABLE 2.1

VOLTAGE ACROSS PARTICLES FOR SIMPLE CUBIC ARRAY

E_{av} v/m	Voltage across particle Volts		
	p = 10μ	p = 1 mm	p = 1 cm
10^4	0.2	20	200
10^5	2.0	200	2,000
10^6	20.0	2,000	20,000

Table 2.2 sets out the 'FM' factors for different values of average applied electric field and p/a ratios for a simple cubic array. For other regular arrays, this must be multiplied by the relative magnitude factor (RFM) constant as given in Table 7.2.

TABLE 2.2

FIELD MAGNITUDE FACTORS FOR

SIMPLE CUBIC ARRAY

p/a	'FM' Mv/m		
	$E_{av} = 10^4$ v/m	$E_{av} = 10^5$ v/m	$E_{av} = 10^6$ v/m
50	.5	5	50
100	1	10	100
500	5	50	500
1,000	10	100	1,000

In the following Sections, the actual field strengths at fixed points in the field pattern are calculated for different values of 'FM'. This value is given by Table 2.2 but may be modified if necessary, by the RFM constant so as to take into account other modes of compaction.

2.4.2. Internal Electric Fields.

In order to determine the possible effects of the electric fields around the contact points, it is desirable to obtain some numerical values.

(a) Field Strength Along Axis.

The potential along the axis perpendicular to the plane of the contact circle and passing through its centre, is given by equation 2.1. The distance along the z axis is $\sqrt{\mu}$. The electric field is obtained by differentiating the expression for the potential with respect to $\sqrt{\mu}$.

$$E = \frac{I\rho}{2\pi a} \frac{a}{(a^2 + \mu)} \qquad \ldots\ldots\ldots\ldots \quad 2.17$$

If the distance along this axis is expressed as a fraction of the radius of the contact circle a, a more general expression for the electric field may be found.

Let $\sqrt{\mu} = ma$

hence $\mu = m^2a^2$ $\qquad \ldots\ldots\ldots\ldots \quad 2.18$

Since $I\rho/2a$ is the voltage drop across a particle, this must also equal $E_{av}2p$. Substituting this and 2.18 in equation 2.17, the electric field at any point ma along the

perpendicular axis is;

$$E = \frac{2}{\pi}\left[\frac{E_{av}\, p}{a}\right]\frac{1}{(1+m^2)} \quad \ldots\ldots\ldots$$

$$= \frac{2}{\pi}(FM)\frac{1}{(1+m^2)} \quad \ldots\ldots\ldots\ldots\ldots \quad 2.19$$

Table 2.3 gives some typical values of electric field strength for different values of FM.

(b) Field Strengths Along Contact Surface.

From equation 2.4 the current density along the contact surface is given by;

$$J = \frac{I}{2\pi a\sqrt{a^2 - r^2}}$$

Let $r = ma$, where $m < 1$.

The electric field at any point along this surface is,

$$E = \rho J = \frac{\rho I}{2\pi a^2\sqrt{1 - m^2}}$$

$$= \frac{2}{\pi}\left[\frac{E_{av}\, p}{a}\right]\frac{1}{\sqrt{1 - m^2}}$$

$$= 2/\pi\,(FM)\frac{1}{\sqrt{1 - m^2}} \quad \ldots\ldots\ldots\ldots \quad 2.20$$

The direction of this electric field will be perpendicular to the contact surface. Table 2.4 gives some typical values of the magnitude of the field strength for different values of FM.

TABLE 2.3

ELECTRIC FIELD STRENGTH ALONG AXIS PERPENDICULAR TO PLANE OF CONTACT

FM Mv/m	Local Field Mv/m				
	m = 0.0	0.5	1.0	2.0	5.0
1.0	.638	.510	.319	.127	.025
10.0	6.38	5.10	3.19	1.27	.25
100.0	63.8	51.0	31.9	12.7	2.5
1,000.0	638.	510.	319.	127.	25.

TABLE 2.4

ELECTRIC FIELD STRENGTH ALONG SURFACE OF CONTACT

FM Mv/m	Local Fields Mv/m				
	m = 0.00	0.90	0.96	0.98	1.00
1.0	.638	1.47	2.26	3.19	∞
10.0	6.38	14.7	22.6	31.9	∞
100.0	63.8	147.	226.	319.	∞
1,000.0	638.	1470.	2260.	3190.	∞

(c) Field Strength Along External Surface

The general expression for the potential of the field in the solid is given by equation 2.4. The distance x along this surface is,

$$x = \sqrt{a^2 + \mu}$$

$$\text{hence} \quad \sqrt{\mu} = \sqrt{x^2 - a^2}$$

Substituting this in equation 2.4, the potential along this surface may be written,

$$\phi = \frac{I\rho}{2\pi a} \tan^{-1} \frac{\sqrt{x^2 - a^2}}{a} \quad \ldots\ldots\ldots \quad 2.22$$

The electric field is found by differentiating this with respect to x. By letting x = ma, the following expressions may be found,

$$E = \frac{I\rho}{a^2 2\pi m \sqrt{m^2 - 1}}$$

$$= (2/\pi)(E_{av}\, p/a) \frac{1}{m\sqrt{m^2 - 1}}$$

$$= (2/\pi)(FM) \frac{1}{m\sqrt{m^2 - 1}} \quad \ldots\ldots\ldots \quad 2.23$$

If the surface is a true flow line, the direction of this field will be acting along the surface. Some typical values of the electric field for different values of FM are given in Table 2.5

TABLE 2.5

ELECTRIC FIELD STRENGTH ALONG THE EXTERNAL PARTICLE SURFACE

FM Mv/m	Local fields Mv/m				
	m = 1.0	1.1	1.5	2.0	5.0
1.0	∞	1.24	0.38	.185	0.026
10.0	∞	12.4	3.8	1.85	0.26
100.0	∞	124.0	38.0	18.5	2.6
1,000.0	∞	1240.0	380.0	185.0	26.0

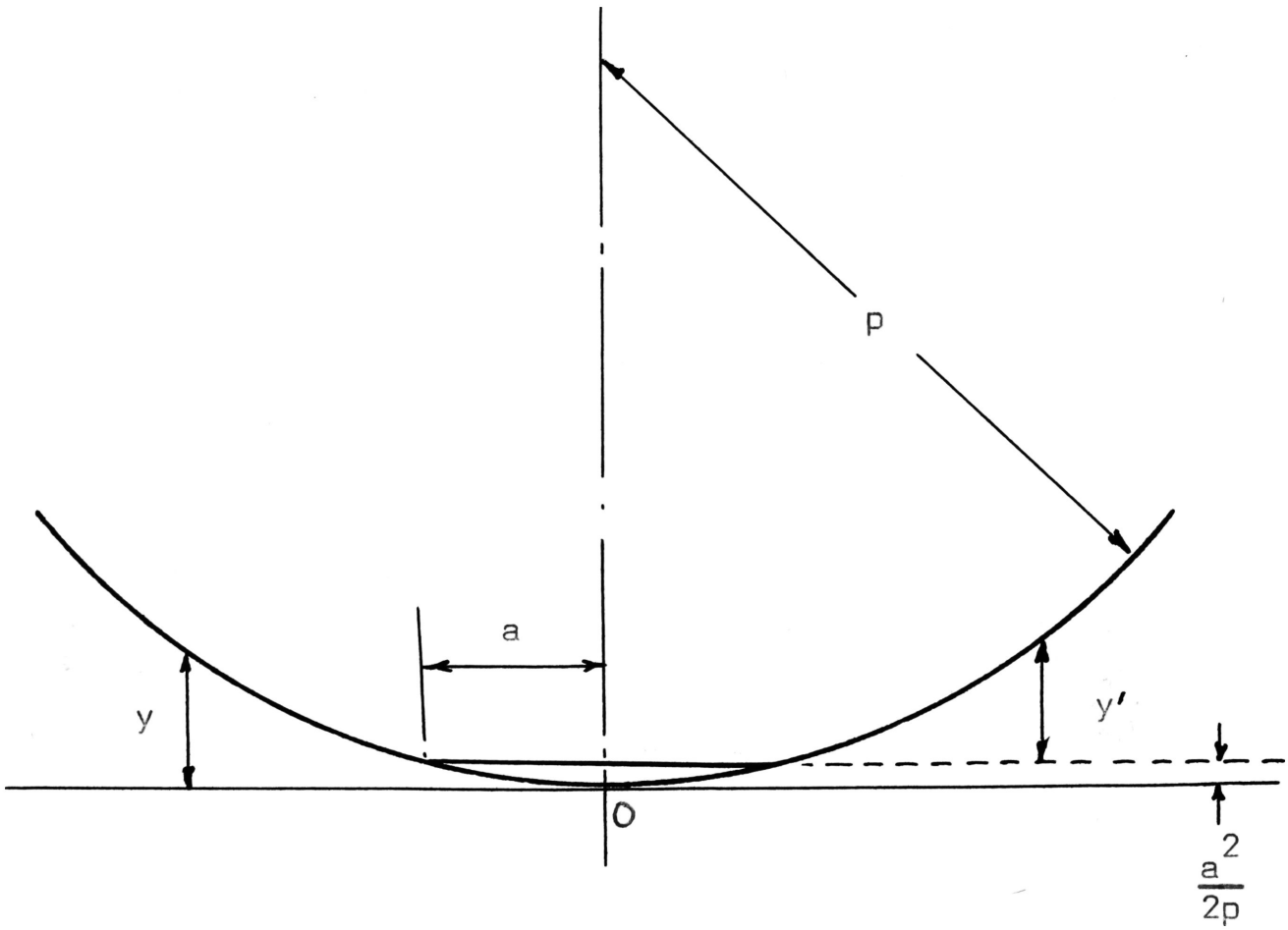

FIGURE 2.5 DIMENSIONS AT THE CONTACT POINT OF A SPHERE AND A PLANE

2.4.3 Electric Fields Between Particles.

The electric field between the surfaces of two particles will depend on the voltage difference between corresponding points on the two surfaces and the distance between them.

Consider the case of a sphere in Figure 2.5 touching the plane at point O.

The equation of the great circle is;

$$x^2 = 2p\,y - y^2$$

Solving for y;

$$y = p \pm p\,(1 - (x/p)^2)^{0.5}$$

Expanding the term in the bracket by means of the Binomial Theorem,

$$y = x^2/2p + x^4/8p^3 + 3x^6/48x^5 + \ldots,$$

If only small distances from the origin O are considered, the higher powers of x may be neglected.

$$y = x^2/2p \qquad \ldots\ldots\ldots\ldots\ldots\ldots\ldots \quad 2.24$$

When the two particles are compressed together, elastic deformation takes place at the point of contact. If the radius of the contact circle is 'a', the distance the initial point of contact is depressed is $a^2/2p$. If the distance along the x axis is expressed as a multiple of the

radius of the contact, then y is given by;

$$y = (ma)^2 / 2p$$

and the actual height of the surface of the sphere from the plane containing the area of contact is;

$$y' = y - a^2/2p$$

$$= (a^2/2p)(m^2 - 1) \quad \ldots\ldots\ldots\ldots\ldots \quad 2.25$$

Table 2.6 gives some typical values for y'.

The potential at a distance x along the outside surface of the particle with respect to that at the contact surface is given by equation 2.22. If the distance is expressed as a multiple of the contact radius, the potential is given by;

$$\phi = \frac{I\rho}{2\pi a} \tan^{-1}\sqrt{m^2 - 1}$$

This voltage may be expressed as a perunit value of the total voltage drop in one half of the particle.

$$V_{pu} = \frac{\phi}{I\rho / 4a}$$

$$= (2/\pi) \tan^{-1}\sqrt{m^2 - 1} \quad \ldots\ldots\ldots\ldots\ldots \quad 2.26$$

TABLE 2.6

SOME TYPICAL AIR GAP DISTANCES

Þ/a	m	Gap Distance Microns	
		Þ = 10 Microns	Þ = 1.0 cm
100	1.25	.00056	0.56
100	1.50	.00063	0.63
100	2.00	.00150	1.50
100	3.00	.00400	4.00
100	4.00	.00750	7.50
100	5.00	.01200	12.00
100	10.00	.04500	45.00

The electric field in the airgap at some point along this axis is given approximately by the voltage difference between the two surfaces at that point divided by the vertical distance between them. This assumes that the flow lines are straight and are perpendicular to the plane of the contact area. In practice, they follow slightly curved paths but this approximation is reasonable considering the approximation involved in using Holm's equation and the accuracy of the experimental techniques. Hence the electric field in the air gap is,

$$E_g = \frac{2p\ E_{av}\ V_{pu}}{2y'}$$

$$= \frac{E_{av}(\ 2p/\ \pi\ )\ \tan^{-1}\sqrt{m^2 - 1}}{(a^2/2p)\ (\ m^2 - 1\ )}$$

$$= \left[\frac{E_{av}p}{a}\right]\left[\frac{p}{a}\right]\frac{4}{\pi}\ \frac{\tan^{-1}\sqrt{m^2 - 1}}{(\ m^2 - 1\ )} \quad \ldots\ldots\ldots \quad 2.27$$

In this case the field strength depends not only on the 'FM' factor but also on the ratio of 'p' to 'a'. Table 2.7 gives some typical numerical values for the air gap field strength for different values of FM and p/a.

TABLE 2.7

ELECTRIC FIELD STRENGTH IN AIR GAPS BETWEEN PARTICLES

FM Mv/m	m	Local field 10^8 v/m	
		p/a = 100	p/a = 1000
1	1.25	1.460	14.60
	1.5	.860	8.60
	2.0	.440	4.40
	3.0	.195	1.95
	4.0	.112	1.12
	5.0	.073	.73
	10.0	.019	.19
10	1.25	14.60	146.0
	1.5	8.60	86.0
	2.0	4.40	44.0
	3.0	1.95	19.5
	4.0	1.12	11.2
	5.0	.73	7.3
	10.0	.19	1.9
100	1.25	146.0	1460.0
	1.5	86.0	860.0
	2.0	44.0	440.0
	3.0	19.5	195.0
	4.0	11.2	112.0
	5.0	7.3	73.0
	10.0	1.9	19.0

CHAPTER 3.0

BULK CHARACTERISTICS.

3.1 Introduction.

One of the important preliminary steps in this study is to determine the current conduction mechanism and some of the experimental constants of the materials to be used in the particulate form.

Because of the many complex processes taking place in dielectrics and the nature of their interactions with one another, the conduction of current through this type of material is a complicated and little understood phenomenon. Many diverse theories have been proposed to explain the variety of effects observed with this material, but no general theory has been developed. In the case of glass, a theory for ionic conduction has been developed which will account for the general shape of the experimental results. Electronic conduction in glass has been observed although no clear theory has been developed.

In this chapter the theory of ionic and electronic conduction in insulators, and particularly glass, is reviewed and theoretical relationships are established for conduction in both low and high electric fields. The existence of absorption current in glass is reviewed and the relationship between the electric field, resistivity and temperature rise due to internal heating is determined.

Experiments are carried out to determine the activation energy of the silica and borosilicate glass samples and the deviation of their resistivities with electric field.

From the borosilicate glass results, some numerical values of the ion jump distances and density of mobile ions are determined.

The results of this chapter will be used in subsequent ones to explain the characteristics of contacts and finally the conduction characteristics of particulate solids.

3.2 Ionic Conduction.

3.2.1. Structure of glass.

The structure of glass has been subject to very thorough investigation and a number of good accounts are available (30)(31)(33). For the purpose of this thesis it will be necessary to give a brief summary of the modern structural theory so that some explanation may be given to account for the electrical phenomenon observed in the experimental work.

Glass has been defined by the American Society of Testing Materials as 'an inorganic product of fusion which has been cooled to a rigid condition without crystallizing', or according to Carman (32), 'a liquid which is supercooled till its viscosity is high enough to make it behave as an amorphous solid'. There is a group of substances which are capable of doing this of which the most outstanding are SiO_4, B_2O_3, and P_2O_5. They are generally referred to as

the network formers. These substances can take a limited amount of basic oxides as Na_2O, K_2O, CaO, PbO into solution and also some fluorides without losing their vitreous form although some of their properties may be modified. These additives are referred to as network modifiers.

The most generally accepted theory for the structure of glass was first put forward by Zachariasen(33) and later confirmed by Warren's(24) X-ray studies. Their random network theory assumes that the manner in which the atoms and ions are ordered in the vitreous state is the same as the crystalline state in the short range order, but in the long range order the lattice does not exhibit any general symmetry as it would in the crystalline state.

Vitreous silica for example, comprises SiO_4 tetrahedra linked through the O^{2-} ion to an adjacent SiO_4 tetrahedra to form a three dimensional network without regularity of a crystalline structure or lattice. Warren's work showed that the Oxygen atoms are at a distance of 1.62 Å and each silicon is separated from four others by an average distance of 3.2 Å. None of the commercially available forms of vitreous silica has the exact structure postulated by the Zachariasen-Warren model. Infra-red adsorption and fluorescence under ultraviolet radiation studies indicate the presence of OH^- ions and electron pairs in place of some of the O^{2-} ions. In areas where this takes place, the tetrahedra must be described by;

SiO_2- x(OH)2x or SiO_2- x($\bar{e}$)x

Weyl and Marbor(30) have pointed out that 'it is well established that all large optically clear crystals do contain a fine amount of Al^{3+}, Li^+, and Na^+ ions in addition to protons'. These impurities probably exist in commercial silica.

Commercial silica glasses are made from SiO_4 to which is added one or more fluxes which modify the properties of the glass. These fluxes may comprise the easily fusible glass forming oxides themselves as for example B_2O_3, the fluorides as NaF etc. or the basic oxides Na_2O, CaO, etc. Many of the commercial glasses have a number of these extra components. Borosilicate glass (Pyrex) uses B_2O_3 as an additional network former to that of SiO_4 and Na_2O and K_2O as network modifiers. A typical composition for borosilicate glass is given in Table 3.1.

The addition of the network former B_2O_3 changes the network structure, the oxygen ion links the B_2O_3 triangles to the SiO_4 tetrahedra, (B-O-Si) as well as linking similar polyhedras (Si-O-Si and B-O-B). The addition of the basic oxides Na_2O acts as a network modifier flux. The oxygen ion of Na_2O attaches itself to the silicon or boron ion and the sodium ion is then free. These cations fit into the voids in the network structure and can be easily moved. The basic action can be described by the equation;

$$Si\text{-}O\text{-}Si + Na_2O \longrightarrow Si\text{-}O^- + 2Na^+ + {}^-O\text{-}Si\text{-}$$

TABLE 3.1

A TYPICAL COMPOSITION OF

BOROSILICATE GLASS

COMPONENT	PERCENT
SiO_4	80.5
B_2O_3	12.9
Al_2O_3	2.2
Na_2O	3.8
K_2O	0.6

3.2.2 Conduction.

The volume conduction in glass is due to the network modifying ions moving from one interstice to another. Generally, only the monovalent ions K^+ and Na^+ make a marked contribution to the conduction. These ions are relatively small and have a small charge so are able to jump easily through the network. In the presence of an electric field the cations move towards the cathode and the nonbridging oxygen defects move towards the anode.

The model, which is generally accepted to explain the ionic conduction in glass, comprises these loosely bound ions undergoing thermal vibration in a potential well. These have a finite probability of surmounting the potential barrier and moving into an adjacent well. The probability of an ion making this jump is given by Boltzmann's Equation.

$$p = b\,\epsilon^{-\phi/kT} \qquad \ldots\ldots\ldots\ldots\ldots\ldots \quad 3.1$$

b = vibration of ion in the well

k = Boltzmann's constant

ϕ = the potential barrier.

On the application of an electric field, the energy barrier levels are distorted and lowered in one direction and increased in the other. This increases the probability of a net ion movement in the direction of the electric field and causes a current to flow.

Although the model had been used before to explain conduction in ionic crystals, it was Stevels(31) who most successfully applied it to glass. He considers an arbitary direction θ with the direction of the electric field E and shows that the barrier is altered by

$$\frac{\lambda e E}{2} \cos\theta \qquad \ldots\ldots\ldots\ldots\ldots\ldots \quad 3.2$$

and calculates the probability of a mobile ion jumping in that direction. By finding an expression for the incremental current and then integrating, he arrives at an expression for the resistivity.

Owen(35) arrives at effectively the same result by assuming the ions move in one dimension parallel to the x axis.

The following analysis accepts Owen's approximation but arrives at his result following a slightly different argument.

Let N = number of possible mobile ions per m^3.

The number of ions per second with sufficient thermal energy to jump the adjacent energy barrier and move to a neighbouring potential well λ meters away, is given by Boltzmann's Equation;

$$n = N b \epsilon^{-\phi/kT}$$

If an electric field E is applied then the energy levels between adjacent wells is altered by,

$$\frac{e E \lambda}{2}$$

The number of ions in the positive direction is

$$n_+ = \frac{1}{2} N b \epsilon^{-(\phi - \frac{1}{2} e E \lambda)/kT}$$

and in the opposite direction

$$n_- = \frac{1}{2} N b \epsilon^{-(\phi + \frac{1}{2} e E \lambda)/kT}$$

Hence the net flow of ions is given by;

$$n_c = (n_+ - n_-)$$

$$= \frac{1}{2} N b \epsilon^{-\phi/kT} \left[\epsilon^{e E \lambda / 2kT} - \epsilon^{-e E \lambda/2kT} \right]$$

$$= N b \epsilon^{-\phi/kT} \sinh(e E \lambda / 2k T) \quad \ldots\ldots\ldots\ldots \quad 3.3$$

The current density is given by;

$$J = e \lambda n_c$$

$$= e \lambda N b \epsilon^{-\phi/kT} \sinh \frac{e \lambda E}{2 k T}$$

$$\sigma = \frac{e \lambda N b}{E} \epsilon^{-\phi/kT} \sinh \frac{e \lambda E}{2kT}$$

$$\rho = \frac{E \epsilon^{\phi/kT}}{e \lambda N b \sinh \frac{e \lambda E}{2kT}} \quad \ldots\ldots\ldots\ldots \quad 3.4$$

For the purpose of making certain approximations, it is desirable to expand the hypobolic function.

$$\rho = \frac{2\,k\,T\,\epsilon^{\phi/kT}}{e^2\,\lambda^2\,N\,b\left[1 + \frac{1}{6}\left(\frac{e\lambda E}{2kT}\right)^2 + \frac{1}{120}\left(\frac{e\lambda E}{2kT}\right)^4\right]} \quad \ldots\ldots\ldots \quad 3.5$$

It is convenient at this stage to simplify this expression by considering three special cases.

(i) Low Electric Fields.

If the applied electric field is small, then all but the first term of the series expansion of the hypobolic function may be neglected. The resistivity then becomes;

$$\rho = \frac{2\,k\,T}{e^2\lambda^2\,N\,b}\,\epsilon^{\phi/kT} \quad \ldots\ldots\ldots\ldots\ldots\ldots \quad 3.6$$

This is the same result as obtained by Stevels if 'λ' is assumed to be numerically equal to 3 as he has done.

(ii) Medium Electric Fields.

For values of E where the resistivity is just starting to be a function of the electric field, the second term of the series cannot be ignored.

$$\rho = \frac{2\,k\,T}{e^2\lambda^2 N b}\left[1 - \frac{1}{6}\left(\frac{e\lambda E}{2kT}\right)^2\right]\epsilon^{\phi/kT} \quad \ldots\ldots \quad 3.7$$

(iii) High Electric Fields.

For high values of electric fields, the hyperbolic function approximates to

$$\rho = \frac{E}{e \lambda N b} \epsilon^{\phi/kT} \epsilon^{-e\lambda E/2kT}$$

For a given temperature this reduces to

$$\rho = A E \epsilon^{-B E} \quad \ldots\ldots\ldots\ldots\ldots\ldots \quad 3.8$$

There is a group of investigators who have used slightly different models to represent the energy barrier. Maurer(36) uses two energy barrier terms; W, the work done to move an ion from a normal position to an interstice position and U, the potential barrier in the interstitial space due to the repulsive forces between the free ions and the fixed ions. By taking into account the effect of the applied field on the potential barrier U, it can be easily shown that the resistivity is given by the expression,

$$\rho = \frac{\gamma k T}{e^2 \lambda^2 N b} \epsilon^{(0.5W + U)/kT} \quad \ldots\ldots\ldots\ldots \quad 3.9$$

Charles (37) also found it necessary to modify Stevels model in order to account for orientation polarization and d.c. conductivity in glass. The alkali ion in the silica network is considered to spend most of its time ionically associated with a nonbridging oxygen ion. The model postulates the existence of a number of equivalent positions of stability around each nonbridging oxygen atom. Each of these

equivalent positions are separated by energy barriers. Hence if W_o and U_o are the absolute zero energies of formation and migration of the defects, then

$$\rho = \rho_o \epsilon^{(0.5Wo + Uo)/kT} \quad \ldots\ldots\ldots\ldots\ldots \quad 3.10$$

Muray(38), using the results of Charles, introduces $e\phi$ as the dissociation energy, and $e\psi$ as the energy barrier of the main lattice work. He arrives at an expression for the resistivity,

$$\rho = \frac{6kT}{e^2\lambda^2 N b} \epsilon^{(\phi + \psi)e / kT} \quad \ldots\ldots\ldots \quad 3.11$$

All these theoretical formulae agree in general with the Rash and Henrichsens empirical law.

$$\rho = A \epsilon^{B/T} \quad \ldots\ldots\ldots\ldots\ldots\ldots\ldots \quad 3.12$$

3.3 Electronic Conduction.

3.3.1 Introduction.

The general problem of electron conduction in insulators has not been as thoroughly investigated as electron conduction in semi-conductors or metals. The main interest in this has been in the electrical breakdown of dielectric materials and more recently in the conduction mechanism through thin insulating films. Only a limited

amount of work has been carried out on the problem of electron conduction in glass.

Before considering the mechanism of electron conduction in glass, it is desirable to give a brief statement of the theories of conduction in insulators.

3.3.2 Conduction in Insulators.

Electronic conduction in insulators is usually explained by making use of the Band Theory. The model assumes that the forbidden zone between the filled band and the empty band is in the order of 1 to 5 eV so that the transition of electrons from the filled zone to the empty zone requires impossibly high temperatures. In practice, conduction is observed in insulators and is often related to the temperature by the expression,

$$\rho = A \epsilon^{B/T} \quad \ldots\ldots\ldots\ldots\ldots\ldots\ldots \quad 3.13$$

To account for this, it is necessary to explain the existence of free mobile electrons and to describe how they move through the material.

The presence of free electrons in an insulating material may be accounted for by assuming the existence of imperfection levels in the forbidden region. These may be due to the existence of dissimilar atoms in the lattice work or to dislocations and other defects. These imperfections may be of the donor or acceptor type as in semi-

conductors. Conduction becomes possible because of one of the following reasons:

(i) The thermal excitation of electrons from the impurity levels into the empty zone or due to the electrons being excited out of the filled zone into the conduction zone by using the imperfection levels as stepping levels (39).

(ii) The thermal excitation of electrons out of the impurity levels may also be assisted by the applied electric field. The effect of the electric field is to lower the height of the potential barrier between the trapped electrons and the conduction band and is generally referred to as the Pool-Frenkel effect (40).

(iii) Field ionization. In the case where the applied electric field is sufficiently high, electrons may tunnel through to the conduction band from these localized impurity levels into the conduction band. If this takes place from the valence band, it is known as Zener breakdown (41).

(iv) Impurity conduction. This speculates the movement of electrons from one impurity level to another without being activated into the conduction zone. A necessary condition is the existence of both donor and acceptor levels. There are two possible mechanisms of electron transfer. The electrons may tunnel through the barrier or they may jump over the potential barrier (42).

Once the electrons have been excited into the conduction band they are not free to move through the material as easily as they do in metals and semi-conductors. The mobile electrons will lose energy due to an interaction between them and the lattice work. For fast moving electrons it is convenient to use the same terminology as is used in semi-conductor theory. There are two types of collisions.

(a) Lattice Scattering. This is due to the thermal vibration of the atoms in the lattice work which, in the case of insulators would be more complicated than for semi-conductors, due to the dissimilarity of the atoms and the greater variations of potential through the lattice work. It is not unreasonable to assume that the mobility of the electrons will increase with a decrease in temperature in an analogous manner to the way it occurs in semi-conductors.

(b) Impurity scattering. This is due to the electrostatic forces acting on the carriers because of the impurity charges. Since the model assumes a high level of impurities, this is expected to be a significant factor in the case of insulators. If this model is a reasonable one, then from semi-conductor theory it may be expected that the mobility of the electrons will increase with temperature due to the increase in their average velocity.

3.3.3 Electron Conduction in Glass.

The whole subject of electron conduction in glass has not received very much attention, and only a few attempts have been made to examine it experimentally.

One aspect of this work which has been investigated, is the manufacture of a glass which is essentially electronic conducting. This has been achieved through the use of transition element oxides, usually in combination with modifier oxides of alkali and alkaline earth metals (44)(45). The main interest in this area has been to determine the effects of different combinations of the elements.

Electron conduction in glass has also been investigated by the excitation of electrons into the conduction state by photoelectric effect (46), bombarding the surface of the glass with a stream of electrons from an electron gun (46)(47) and observing the decay of charge placed on the surface by making a metal to glass contact (48). Although these techniques are used mainly to obtain an understanding of the basic properties of materials, they also demonstrate that electron conduction can take place in a glass which would normally be ionic conducting.

In the case of fused silica, the mechanism of conduction is not very well understood. Doremus(49) has suggested that this is due to alkali and hydroxyl ion movement although he does admit to the possibility of some electronic conduction'. The work of the author on the time dependence of the current with a rod to plane electrode

geometry, indicates that with the sample used in this thesis, the conduction mechanism is essentially electronic. In Section 3.2.1 it has been shown that electron pairs and various impurities are known to exist in the lattice work which must introduce impurity levels into the band structure of the silica. Conduction may take place by any of the methods described in the preceeding section.

3.3.4 Conduction in High Electric Fields.

For high applied electric fields, the current increases at a greater rate than the electric field. There have been a number of explanations offered for this phenomenon (40)(41) but the one which is most widely accepted and which fits the experimental results obtained later in this chapter is that offered by Frohlich(43).

By assuming that the net gain in electron energy is proportional to the square of the electric field strength, and by considering the interaction with trapped electrons, Frohlich showed that the resistivity varies as:

$$\rho = \rho_o \epsilon^{-\frac{V E^2}{\Delta V Em^2}} \qquad \text{.....} \qquad 3.14$$

Where V = Potential barrier of the trapped electrons.

ΔV = Energy barrier of the average excited trapped electron.

Em = The intrinsic electric strength.

3.4 Temperature Rise in High Electric Fields.

3.4.1 Theory.

One factor which limits the maximum value of the applied electric field during resistivity measurements is the temperature rise in the bulk of the material due to the $J^2\rho$ loss. If it is assumed that there is no heat lost from the volume in which it is generated, then an indication of the allowable electric field may be found for a given rate of temperature rise.

Consider a unit volume of the material in a uniform and constant electric field E. If there is no heat lost from this volume, the temperature rise in time dt is,

$$dT = \frac{E^2\, dt}{\rho\, MS}$$

$$\frac{dT}{dt} = \frac{E^2}{\rho\, MS} \qquad \text{.....} \qquad 3.15$$

Where T = temperature,

M = mass of unit volume of the material,

S = specific heat constant.

In the case of silica, the dependence of the resistivity on temperature and the magnitude of the electric field is given by the empirical equations 3.13 and 3.24 respectively. Substituting these in equation 3.15, the rate of temperature rise is,

$$\frac{dT}{dt} = \frac{E^2}{MS\, A\epsilon^{B/T_\epsilon - CE}} \qquad \text{.....} \qquad 3.16$$

For borosilicate glass, preliminary checks showed that the electric field at which a temperature rise of 0.10 °C per sec. occured is below the value at which the electric field affects the resistivity of the glass at the given temperature. Hence equation 3.6 is applicable and if this is substituted in 3.15,

$$\frac{dT}{dt} = \frac{E^2}{MS\ A'T\epsilon^{B/T}} \qquad \ldots\ldots\ldots\ldots \qquad 3.17$$

Neither of the equations 3.16 and 3.17 can be solved analytically to obtain an expression for the temperature as a function of time and electric field strength.

3.4.2 Calculations.

Although it is not possible to obtain general solutions for T as a function of E and t from equations 3.16 and 3.17, never the less, if a given rate of temperature rise is assumed, then a set of particular relationships between resistivity, temperature and applied electric field may be determined for each sample.

If a temperature rate of rise of 0.10 °C per sec. is taken as the maximum that can be tolerated, then over a period of 10 seconds this would represent a temperature rise of 1.0 °C. At an operating temperature of 225 °C, this would correspond to a reduction of 6 percent in the resistivity.

Let $M = 2.5 \times 10^3$ Kg/m^3

$S = 1.34 \times 10^3$ J/Kg.

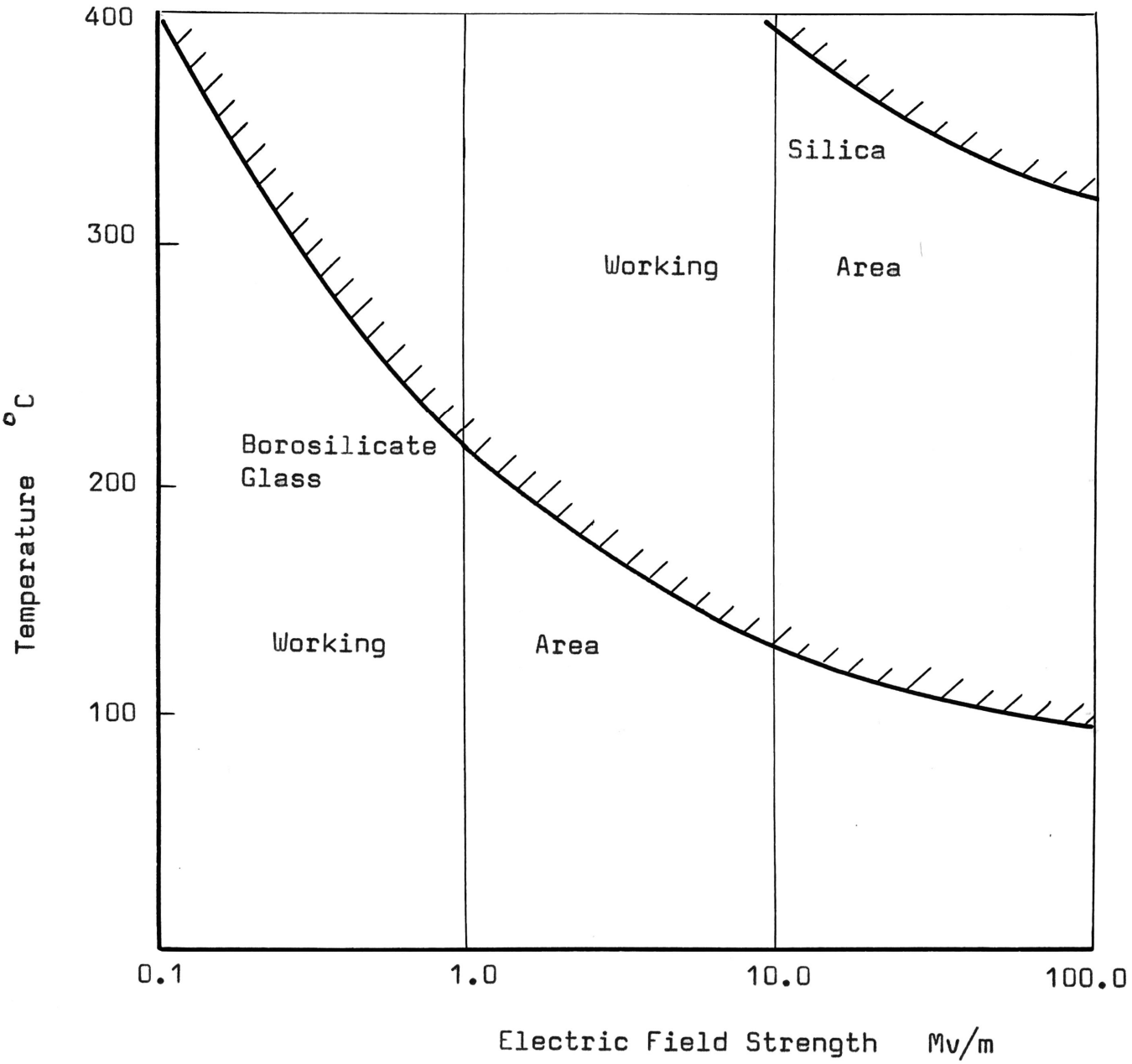

FIGURE 3.1 RELATIONSHIP BETWEEN ELECTRIC FIELD AND TEMPERATURE FOR 0.1°C/SEC RATE OF TEMPERATURE RISE

From equation 3.15

$$E = 578.0\sqrt{\rho} \quad \ldots\ldots\ldots\ldots\ldots\ldots \quad 3.19$$

By inserting values for the resistivity, the electric field which will give this rate of temperature rise can be calculated. By making use of the experimental results in section 3.6 and the equations for the variation of the resistivity at high electric fields, curves may be plotted for silica and borosilicate glass giving the temperature - electric field relationship for the given rate of temperature rise. This is shown in Figure 3.1.

3.5 Absorption Current.

3.5.1 Introduction.

If a step voltage is applied to a dielectric material between two metal electrodes, the initial current will decay with time to the true conduction current. Part of this current transient can be identified with the time constant of the circuit but there is usually a component which is dependent only on the characteristics of the dielectric material itself. This component is called the dielectric absorption current.

One approach to this phenomenon is to explain it in terms of dielectric relaxation. According to Lamb (42) this "dielectric relaxation may occur due to a time-dependent

dipole formation (i.e. separation of positive and negative charges), or it may be due to a time dependent re-orientation of permanent dipoles already present in the material". The work of Sutter and Norwich(50) on NaCl crystals supports this interpretation. Joffe(51) on the other hand has explained this by means of the space charge polarization theory. Muray(38) attributed part of the transient to 'carrier number' limited flow. A quite different approach has been to describe the transient in terms of the absorption of electrons into traps in the material(52).

The experimental work on the characteristics of glass shows that the absorption component of the current decreases with increasing electric field strength and increasing temperature. The results of Vermeer(53) show that for temperatures above 100°C, the absorption current vanishes within a few seconds.

3.5.2 Experimental Results.

In the experimental work in Section 3.6 it is shown that, for the temperatures at which the tests were carried out, the absorption current for both silica and borosilicate glass is of such short time duration that it does not affect the results and may be neglected.

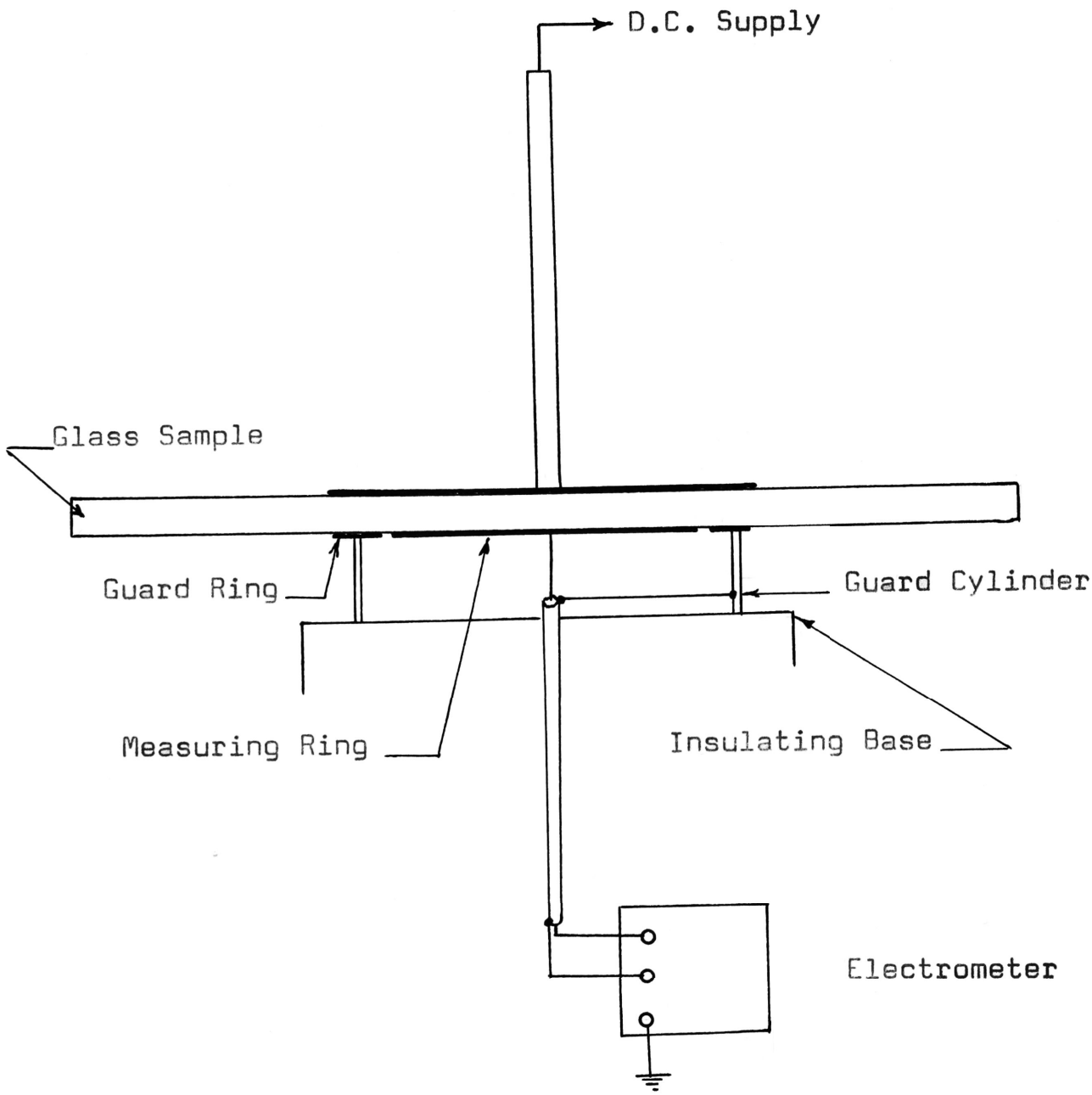

FIGURE 3.2 SCHEMATIC DIAGRAM OF CONNECTIONS

3.6 Experimental.

3.6.1 Introduction.

The objective of this section is to determine the bulk characteristics of the silica and borosilicate glass samples to be used in future experiments. Measurements at low electric fields enable the activation energies to be determined and those at high electric fields show how the resistivity of these samples vary with the electric field. This latter characteristic plays an important part in the characteristics of particulate solids.

3.6.2 Measuring Techniques.

The sample is prepared by metallizing both surfaces with Dag Dispersion 915 (Silver in M.I.B.K.) and providing a guard ring on one side. The specimen is placed in an oven and the measuring circuit connected as shown in Figure 3.2. A fully smoothed d.c. voltage is applied to the top electrode and the current from the measuring electrode is carried by a screened cable and measured by a Keithley Electrometer 610B. The guard ring is connected to the screen and earthed via the guard terminal on the electrometer. To provide additional protection from stray corona currents at high voltage, the measuring ring is surrounded by a guard cylinder.

The specimen was heated to the required temperature

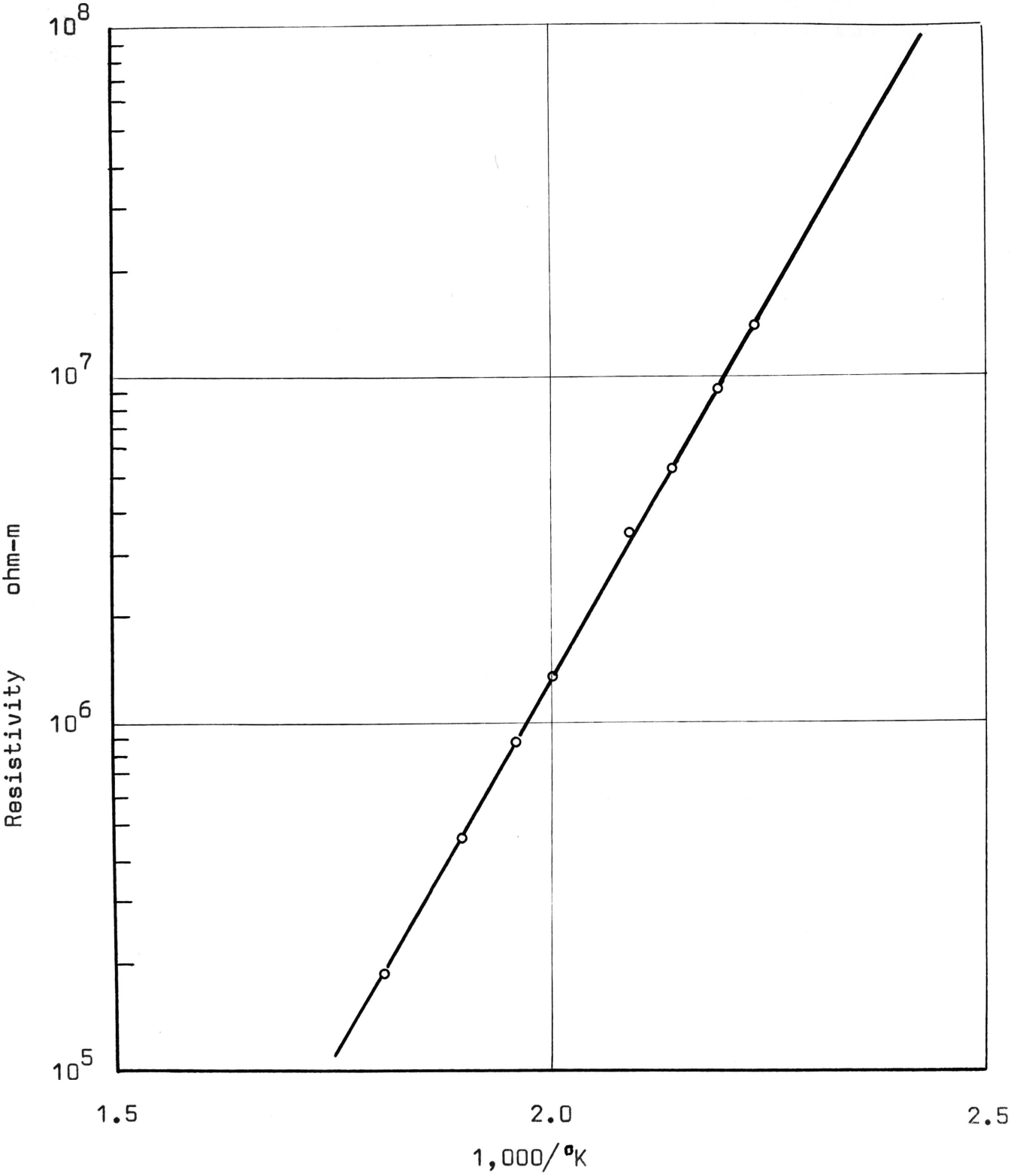

FIGURE 3.3 BOROSILICATE GLASS RESISTIVITY-TEMPERATURE CHARACTERISTIC

and the low electric field voltage-current characteristic obtained. This was then plotted and the mean resistance and hence the resistivity calculated. This was then repeated for other temperatures.

A set of voltage-current characteristics into the high electric field range was also obtained. With borosilicate glass the voltage was applied for the minimum time necessary to allow measurements to be made. This reduced to a minimum the build-up of any space charge at the electrodes. The maximum upper voltage that could be applied was limited by the internal heating of the glass and this was in close agreement with the curve shown in Figure 3.1. In the case of silica, there were no problems with internal heating but the maximum applied electric field was limited by the facilities available. The presence of spurious pulses with silica made current measurements difficult at the higher electric fields but since they subsided with time their effect could be overcome. The characteristics and origin of these pulses are discussed in Appendix II.

3.6.3 Results and Discussions, Borosilicate Glass.

From the low electric field tests, the variation of the resistivity with temperature was determined. The resistivity was plotted against 1,000/T on semi-log paper and is shown in Figure 3.3. If this is now compared with Equation 3.6 then its constants can be evaluated. Hence the equation becomes;

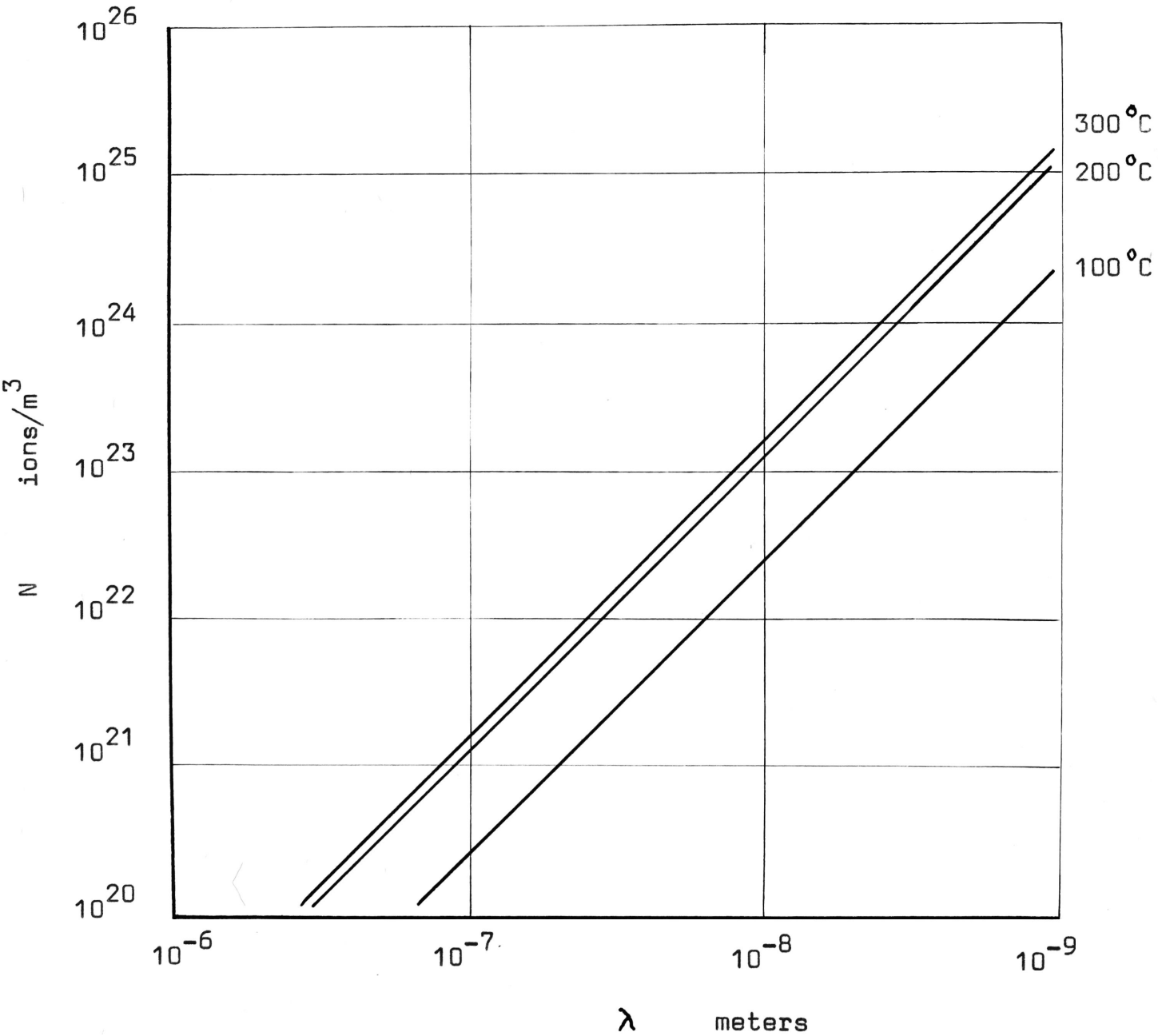

FIGURE 3.4 RELATIONSHIP BETWEEN N AND λ FOR TEMPERATURES OF 100, 200 AND 300°C. BOROSILICATE GLASS.

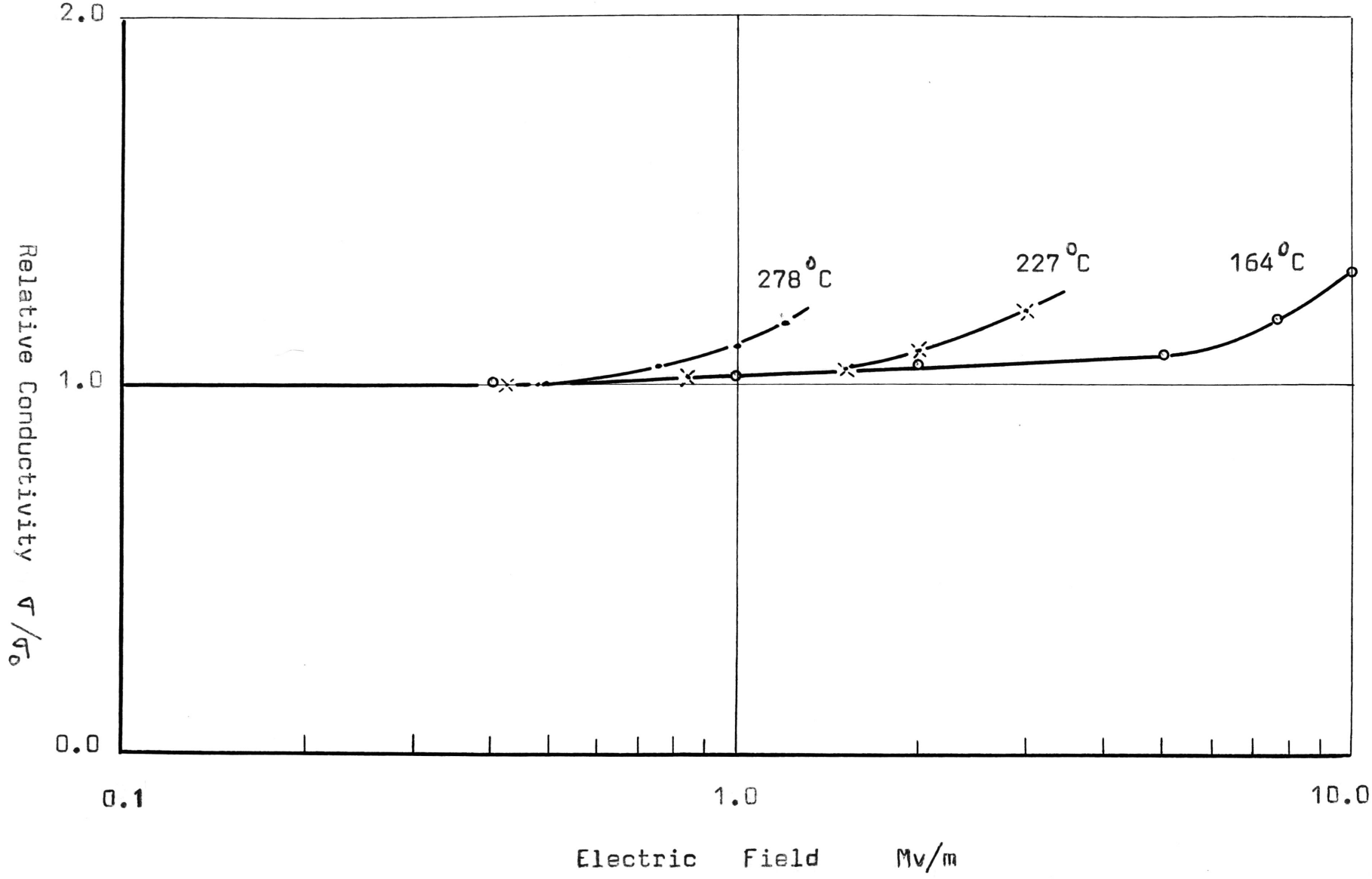

FIGURE 3.5 VARIATION OF MEASURED CONDUCTIVITY WITH APPLIED ELECTRIC FIELD FOR BOROSILICATE GLASS

$$\rho = 0.0038\, \epsilon^{9,810/T} \quad \ldots\ldots\ldots\ldots\ldots\ldots \quad 3.20$$

A relationship between the ion concentration, λ, and the temperature can be obtained from these low field results. If the vibrational frequency of the ion in the well is assumed to be 10^{13} cps and the value of λ is taken to be 10^{-7}, 10^{-8} and 10^{-9} m. From equation 3.6,

$$N = \frac{2kT}{e^2 \lambda^2 b \rho}\, \epsilon^{\emptyset/kT} \text{ ions m}^{-3} \quad \ldots\ldots\ldots\ldots \quad 3.21$$

By using Figure 3.3 to determine ρ, the values of N may be calculated for the three temperatures of 100, 200 and 300°C and the three values of λ. The results are shown plotted in Figure 3.4.

The results of the high electric field tests are shown in Figure 3.5, where the conductivity is expressed as a fraction of the low field conductivity. Because of the temperature rise, it is not possible to obtain the characteristics for electric fields higher than those recorded, hence it is necessary to use Equation 3.7 to determine the jump distance. For a 20 percent deviation in the resistivity, it follows from Equation 3.7,

$$\frac{1}{6}\left(\frac{e\lambda E}{2kT}\right)^2 = 0.2$$

Hence

$$\lambda = \sqrt{1.2}\,\frac{2kT}{eE} \quad \ldots\ldots\ldots \quad 3.22$$

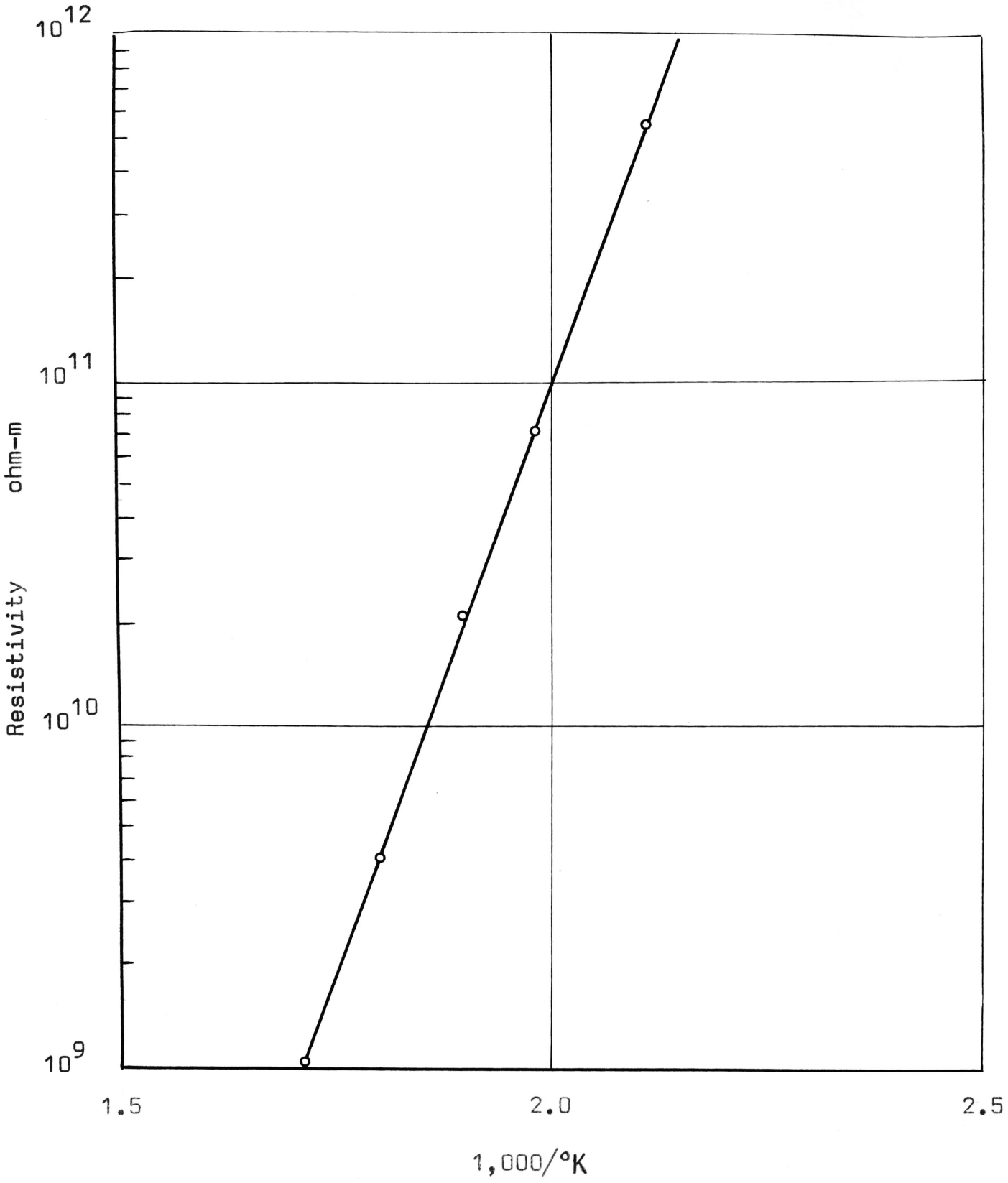

FIGURE 3.6 SILICA GLASS RESISTIVITY-TEMPERATURE CHARACTERISTIC

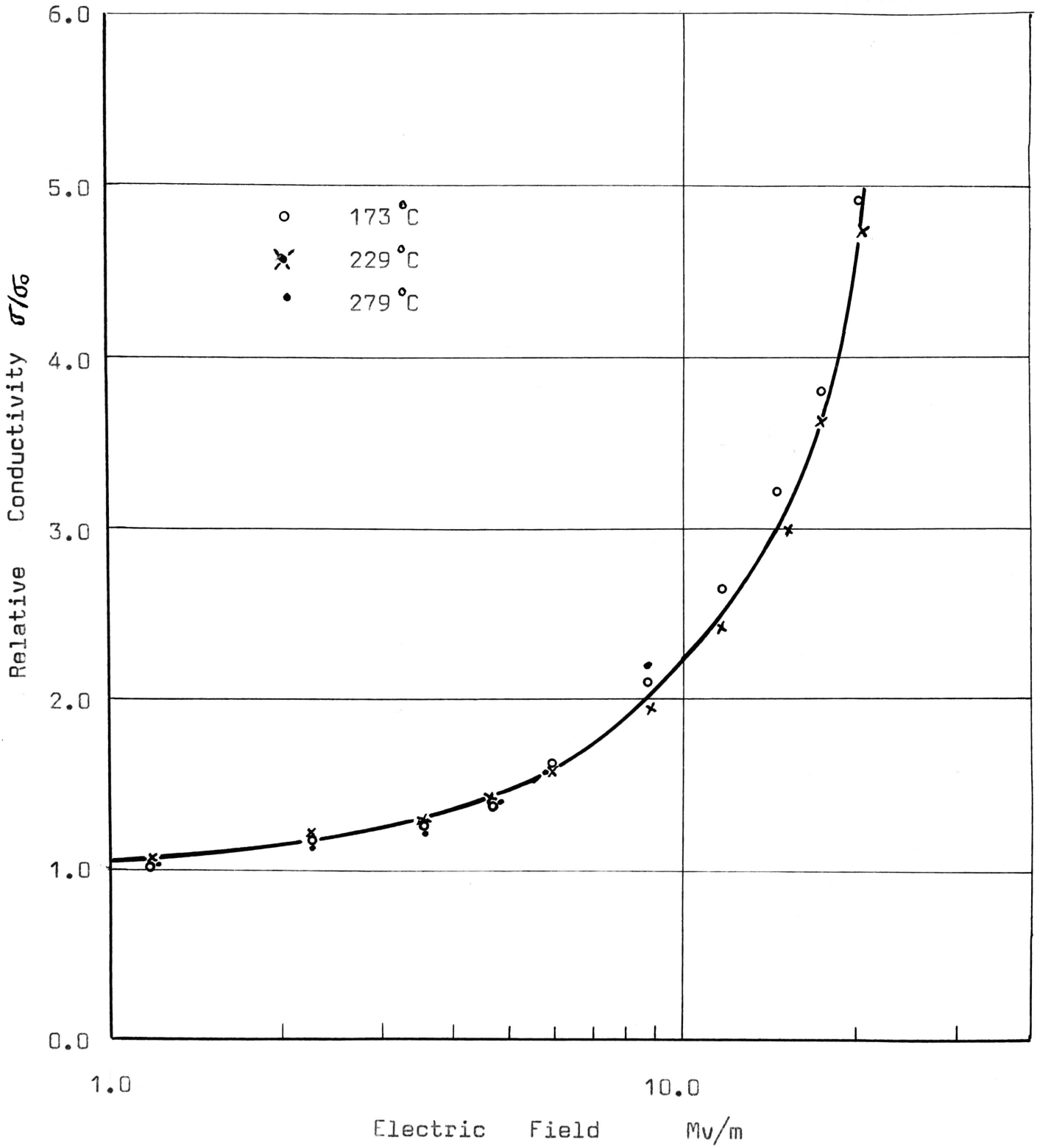

FIGURE 3.7 VARIATION OF MEASURED CONDUCTIVITY WITH APPLIED ELECTRIC FIELD FOR SILICA GLASS

The value of the ionic jump distance for the different temperatures as calculated by this equation is given in Table 3.2.

TABLE 3.2

ION JUMP DISTANCES FOR

BOROSILICATE GLASS

Temp. °C	λ 10^{-8}m
164	1.03
228	3.15
278	8.00

This increase in ion jump distance was observed by Maurer(36) and Vermeer(53). Maurer's results show that at temperatures above 65 °C, the jump distance increased rapidly to a value greater than 50 Å at 100 °C. This has been attributed to structual changes in the lattice network at the higher temperatures. Bean, Fisher and Vermilyea(54) have proposed a model to explain a similar phenomenon observed with metal oxide films and have suggested that it may also apply to glass.

Owen(35, p. 130) is of the opinion that " the simple model of an ion hopping over a potential barrier between equilibrium positions

is in reasonable agreement with experiment". The experimental work of this chapter confirms the model with respect to the variation of temperature and electric field. However, the high calculated value of the jump distance at 278 °C suggests that the model may need slight modification if it is to be used to calculate jump distances at the higher temperatures.

The range of jump distances shown in Fig. 3.5 are only hypothetical values and do not necessarily represent values found in practice.

3.6.4 Results and Discussion - Silica.

From the low electric field tests, the variation of the resistivity with temperature can be determined. In Figure 3.6 the resistivity is plotted against 1,000/T on semi-log scales. From this the activation energy may be calculated and numerical values determined for Equation 3.13.

$$\rho = 0.004\, \epsilon^{15,320/T} \quad \ldots\ldots\ldots\ldots \quad 3.23$$

The high electric field tests were carried out at temperatures of 173, 229 and 279 °C, the results of which are shown plotted in Figure 3.7. The conductivity, expressed as fraction of the low field conductivity, is plotted against the electric field. It is of interest to note that the deviation from 1.0 begins at about 1.0 Mv/m and is the same for all three temperatures.

The mean curve through these points is shown plotted again in Figure 3.6 using semi-log axes. The relative conductivity is

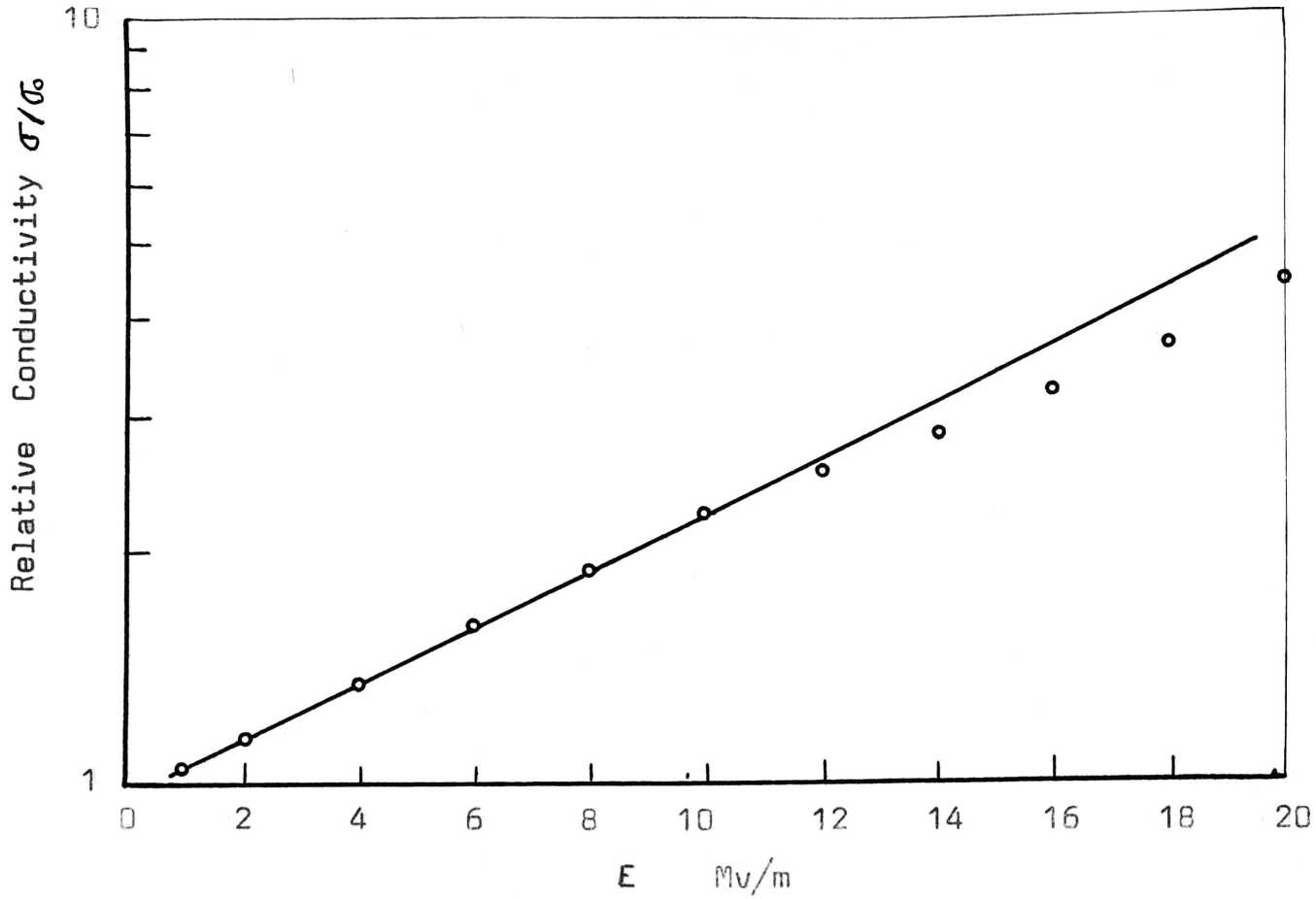

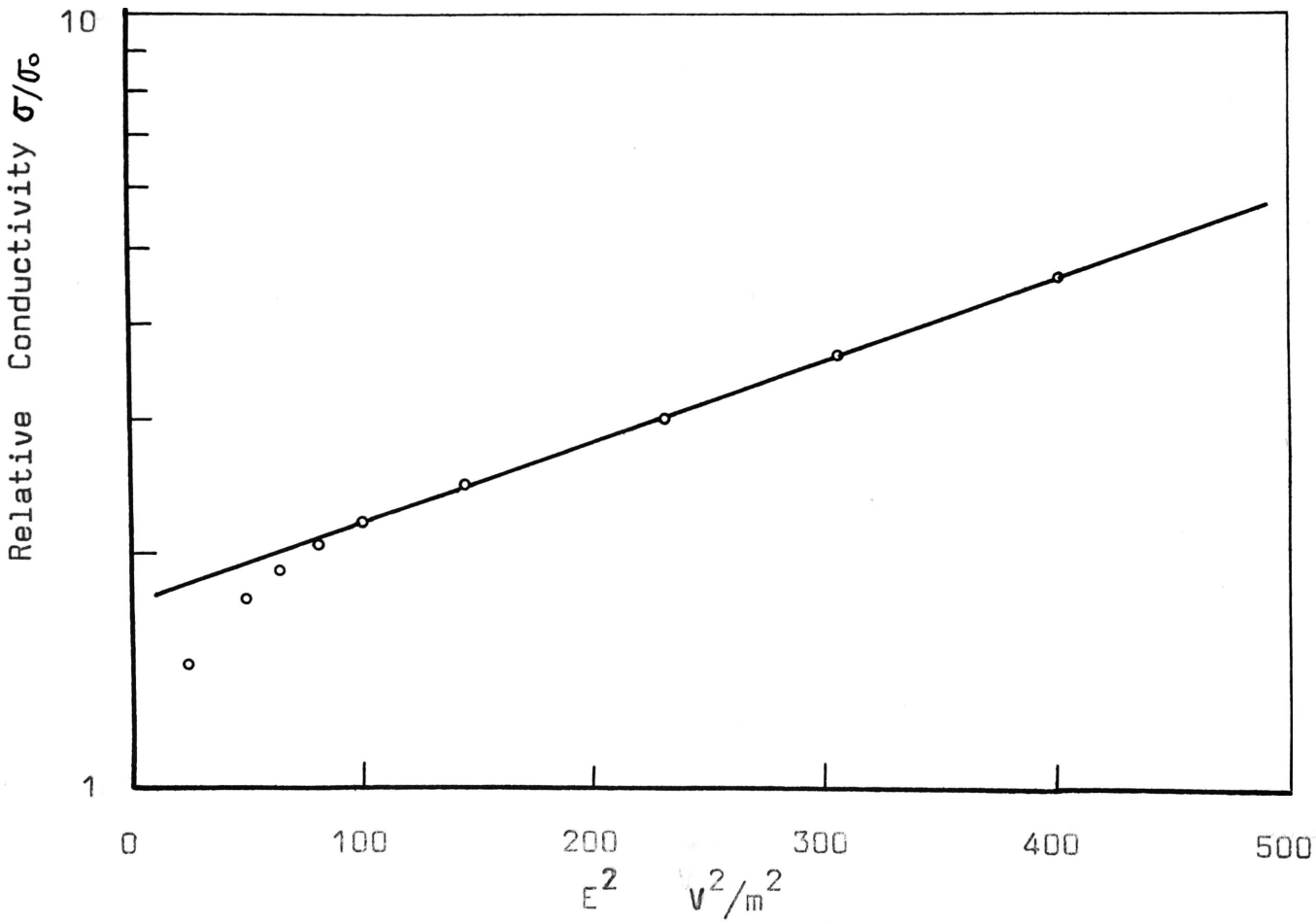

FIGURE 3.8 PLOTS TO DETERMINE HIGH ELECTRIC FIELD RELATIONSHIPS

plotted on the log scale and the electric field and square of the electric field along the linear scale.

For electric fields below 10.0 Mv/m, the experimental points fit the linear relationship with E. The empirical relationship is of the form,

$$\rho = \rho_o \epsilon^{-B E} \quad \ldots\ldots\ldots\ldots\ldots\ldots \quad 3.24$$

Inserting numerical values,

$$\rho = \left[0.004 \epsilon^{15,320/T}\right] \epsilon^{-8.1 \times 10^{-6} E} \quad \ldots\ldots \quad 3.25$$

For values of electric field greater than 10.0 Mv/m, the experimental curve fits the square law relationship in E. It is interesting to note that this is not inconsistant with Equation 3.14, the relationship derived by Frohlich. Inserting numerical values for the constants, the resistivity at these higher values of electric field is given by,

$$\rho = \left[0.0058 \epsilon^{15,320/T}\right] \epsilon^{-0.25 \times 10^{-14} E^2} \quad \ldots\ldots \quad 3.26$$

CHAPTER 4.0

METAL TO SILICA CONTACTS.

4.1 Introduction.

In Chapter 1, it is shown that an important factor in controlling the conduction mechanism in particulate solids is the electrical characteristic of the contacts between the particles themselves and between the particles and the metal electrodes. To fully describe their effects, it is necessary to consider three cases.

(i) Metal to glass contacts with the metal electrode at negative potential.

(ii) Metal to glass contacts with the metal electrode at positive potential.

(iii) Glass to glass contacts.

Since the glass may be either ionic or electronic conducting, additional tests are necessary so as to take this factor into account.

One method of investigating the characteristics of these contacts is to use scaled up models of the particles themselves. The ideal arrangement is to use a hemispherical insulating particle of about 1 cm diameter with its flat surface metallized. If this is placed on a flat metal surface it would model the contacts between the metal electrode and the first layer of particles. There are however a number of practical difficulties in doing this, the most important being the difficulty in obtaining suitable spherical particles of the right material. As an alternative,

a satisfactory representation of the configuration can be obtained by placing a spherical metal ball on a flat sample of the insulating material to be investigated. The essential geometrical difference is that in the approximate representation, the metal surface curves away from the plane of the contact circle, whereas in the real situation they are both in the one plane. It has already been shown in Chapter 2 that most of the voltage drop occurs within ten times the radius of the contact area and also, that the separation between the surfaces is small compared with the overall dimensions if the ratio of the radius of the ball to that of the contact is in the order of 100 or more. Under these conditions, there is very little difference in the field patterns between the two cases. This approximation is consistent with that made by adopting the Holm Equation to calculate the contact resistance. Considering the order of the magnitude of the currents being measured, the accuracy of the instrumentation and the random errors involved, the approximation is a reasonable one.

In Section 2.4.3 it is shown that very high electric fields may exist between the surfaces of adjacent particles in the region around the point of contact. Under these conditions, it is reasonable to speculate on the possibility of there being some kind of charge transfer across the air gap. In order to detect this experimentally, the rod to plane test has been devised. Contact with the insulator surface is made with the squared off end of a long cylindrical

rod. Since the sides of the rod electrode are perpendicular to the insulator surface, any possibility of charge transfer across an air gap is reduced to a minimum. The results of this test are called the "bulk characteristics" of the electrode system, since they are due only to changes taking place in the glass itself. By comparing the rod to plane tests with the ball to plane tests, it can be shown that charge transfer takes place.

In order to compare the results of different tests, the field magnitude factor 'FM' is introduced. It is shown in Appendix III, that for a fixed value of the ratio of the applied voltage to the contact radius, the electric field pattern in the insulating material and its magnitude are the same irrespective of the actual radius of the contact. Hence by using this factor it is possible to compare the results of different tests. In addition, it is also shown that if v/a is plotted against $\rho I/4a^2$, it is possible to compare the results obtained at different temperatures.

In this chapter, the characteristics of metal to silica contacts are investigated. Experimental results are obtained for the ball to plane and rod to plane tests and these are compared on a common graph.

The ball to silica characteristic is explained in terms of the reduction of the bulk resistivity of the silica and the charge transfer across the air gap in the region adjacent to the contact by the high electric fields.

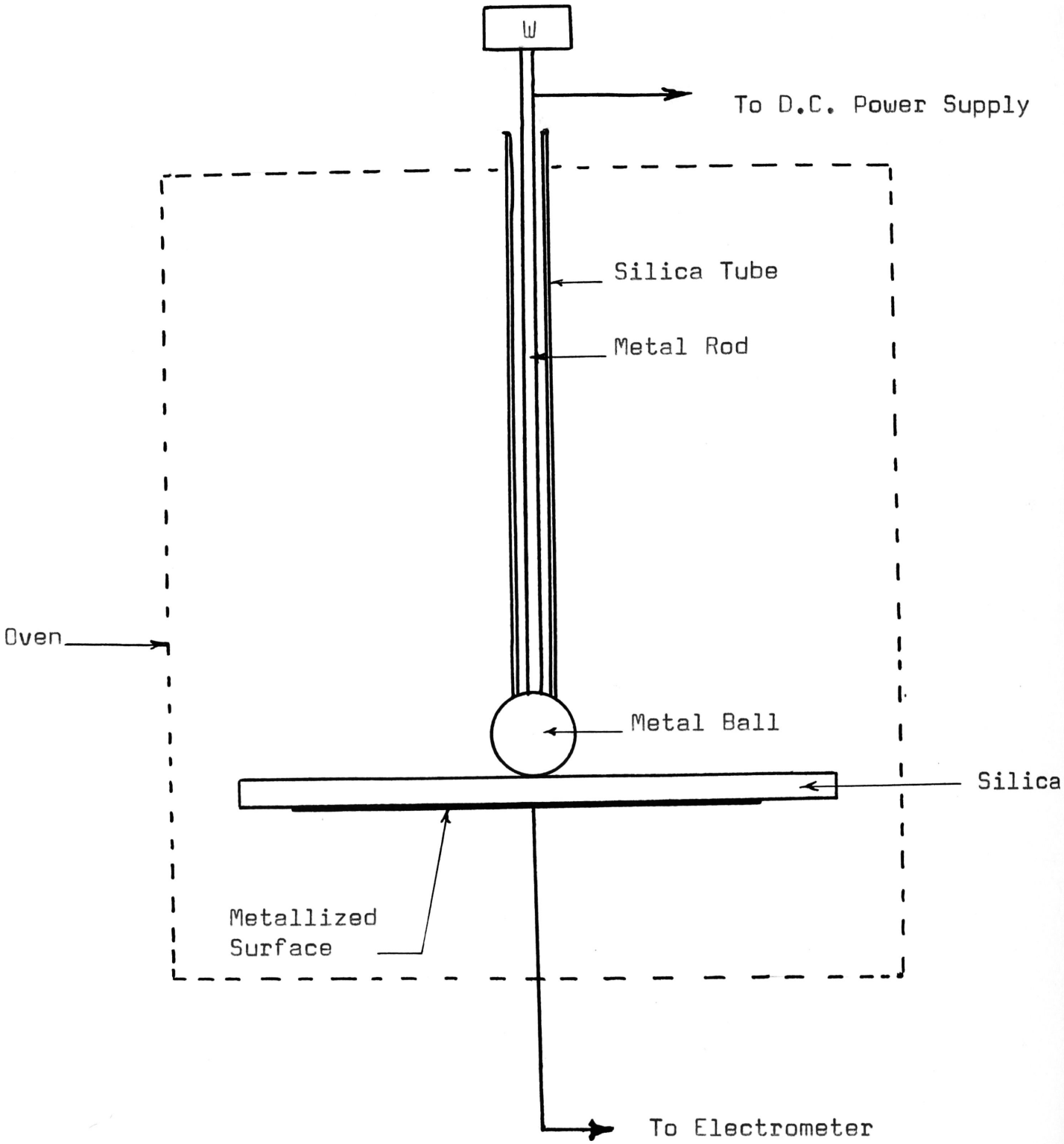

FIGURE 4.1 ARRANGEMENT FOR THE METAL BALL TO SILICA TEST

The results of this chapter will be used in Chapter 8 to account for the overall characteristics of particulate solids.

4.2 Metal Ball to Silica Contacts.

4.2.1 Experimental Method.

It is shown in Section 4.1 that the most convenient way of representing a particle in contact with a metal electrode is to place a metal ball on the flat surface of the silica sample.

The apparatus used is shown in Figure 4.1. The metal ball electrode is held in position on the silica surface by a silica tube which projects through the top of the oven. This enables the position of the ball on the silica to be easily changed and external loads to be applied. Electrical connection to the ball is made by means of a rod which fits inside the tubing and rests on the metal ball electrode. The other end is connected to a variable voltage d.c. power supply. The radius of contact between the ball and silica is adjusted by varying the applied external load and is calculated from the Hertz Equation 2.11. The total current flow is measured by a Keithley Electrometer connected between the metallized under-surface of the silica specimen and ground.

Before carrying out the tests, the surface of the

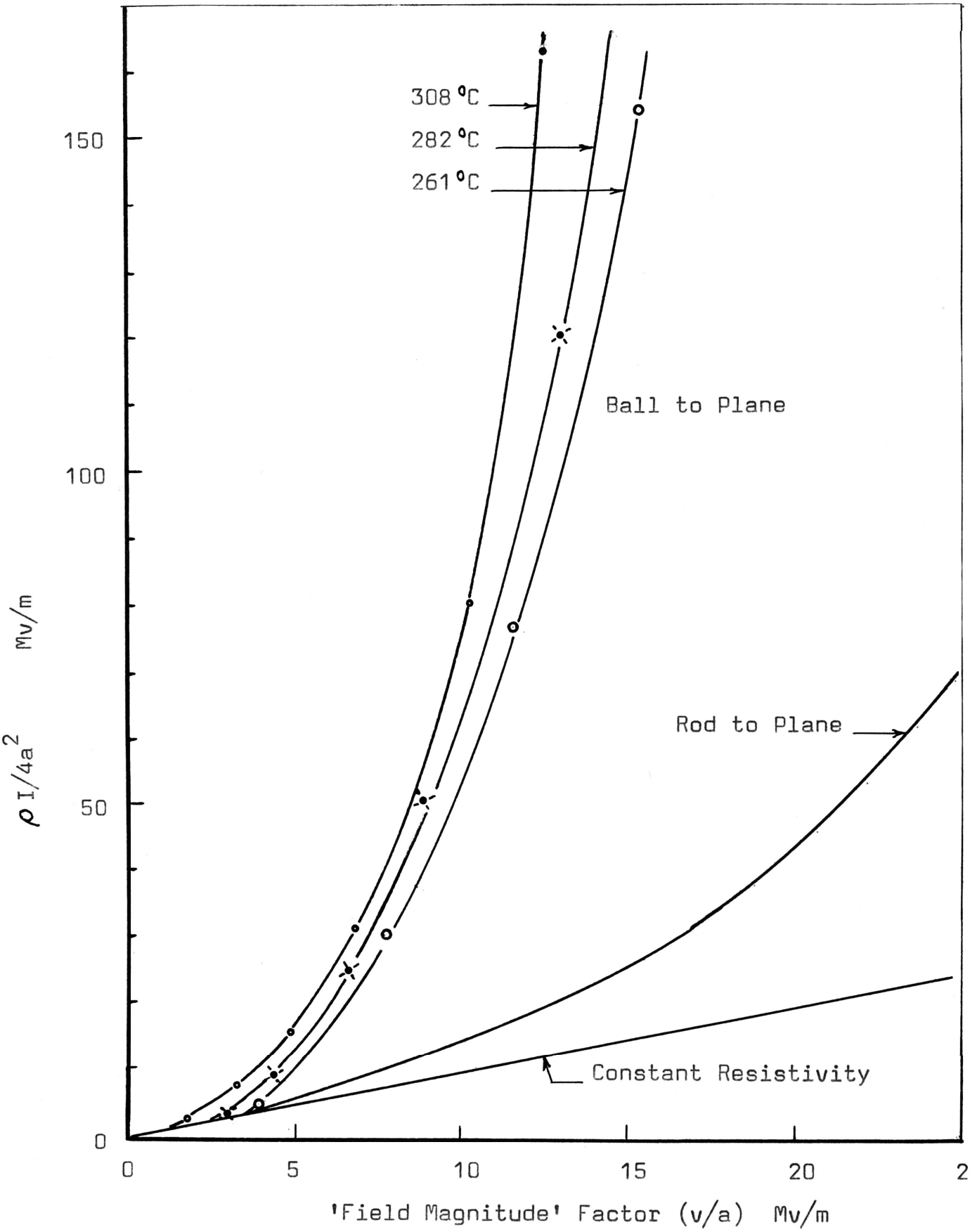

FIGURE 4.2 DEVIATION FROM LINEARITY OF THE METAL BALL TO SILICA CHARACTERISTICS

silica was cleaned with chromic acid and washed in distilled water. The metal ball surface was carefully polished.

A series of voltage-current measurements were made at three different temperatures with the metal ball held at a positive potential and then at a negative potential. For each set of readings the ball was moved to a new position on the silica surface.

Table 4.1 gives the important parameters for this test.

4.2.2 Results.

The results are shown plotted in Figure 4.2, where v/a or the Field Magnitude factor is plotted against $\rho I/4a^2$. By using the 'FM' factor, it is possible to compare the results of a number of tests where the actual contact radius differs from one test to another. By plotting $\rho I/4a^2$ on the other axis, the results for different temperatures are easily compared.

In order to determine the radius of contact, the initial slope of the voltage-current curve was carefully determined from the plot. This gave the effective resistance of the contacts at low electric fields. From the temperature measurements, the resistivity was determined from Figure 3.6, and the effective contact radius calculated from Holm's Equation 2.2

Hence radius of contact $a = \rho/4R_o$

where R_o is the resistance of the contact at low

TABLE 4.1

MAIN PARAMETERS OF METAL BALL TO SILICA TESTS

Material		Silica
Applied force		0.54 kgms
Ball diameter		2 cms
Youngs Modulus	Ball	1.81×10^6 kgm/cm^2
	Silica	0.72×10^6 kgm/cm^2
Poissons Ratio	Ball	0.33
	Silica	0.10
Hertz Equivalent Radius		100 microns
P/a		100

Adjustments have been made to some of these parameters to take into account the temperature of operation.

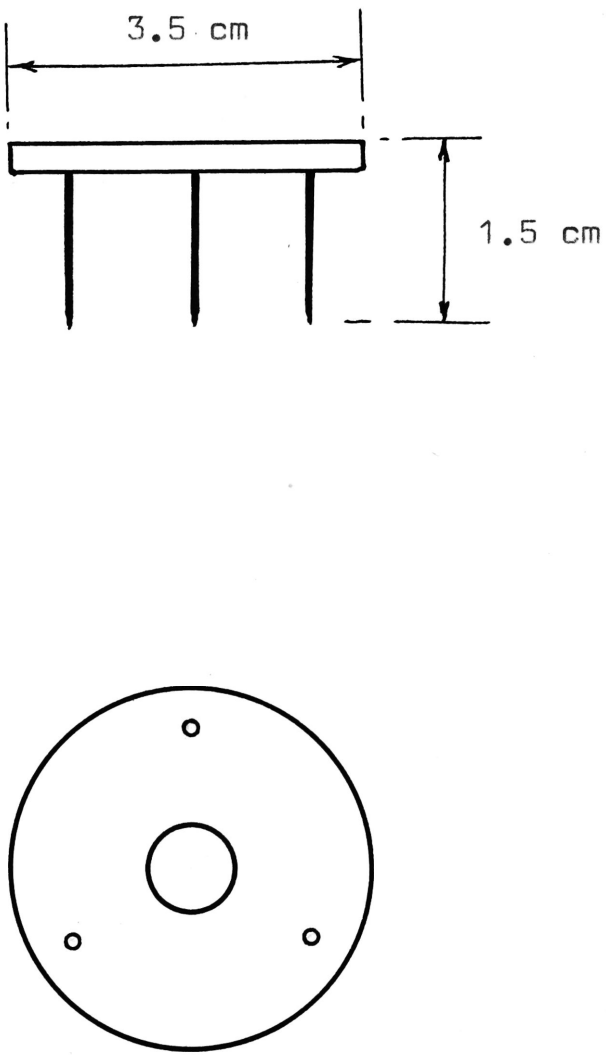

FIGURE 4.3 ARRANGEMENT OF THE ROD ELECTRODE

fields.

Table 4.2 gives the radii of contact as determined by the Holm and Hertz Equations for different temperatures.

There was no significant difference between the voltage-current readings obtained with the metal ball at negative polarity and those obtained with the ball at positive polarity.

It was also observed that there were no spurious pulses even for the higher voltages.

4.3 Metal Rod to Silica Contacts.

4.3.1 Experimental Method.

The purpose of the rod to silica test is to find the voltage-current characteristic of a metal to silica contact with electron emission across the air gaps reduced to a minimum.

The arrangement of the rod electrode is shown in Figure 4.3. It is comprised of three needles projecting down from a metal ring equispaced from one another by 2 cms. The flat surface on the needle points were obtained by first mounting them in the ring and then carefully rubbing them over a smooth flat abrasive surface until a flat end of 200 micron diameter was obtained. The points were finished off on a very flat and smooth silica glass surface lubricated with a metal polish. Each point was carefully examined and its diameter measured under a microscope. The surfaces of

TABLE 4.2

RADII OF CONTACT FOR METAL BALL TO SILICA DISC TESTS.

Temperature °C	Radius microns	
	Hertz Equivalent	Holm Equivalent
308	100	147
282	100	115
261	100	130

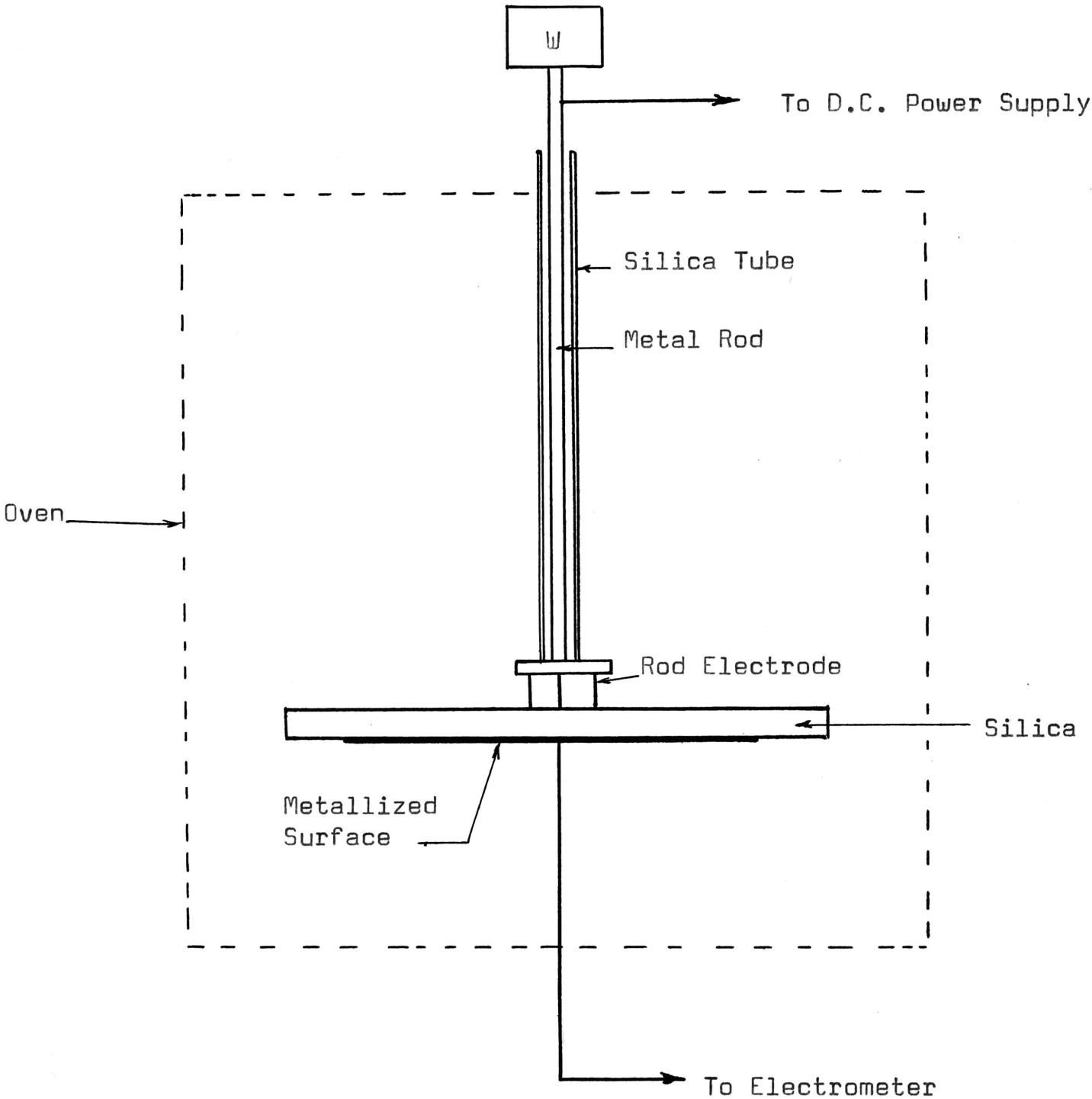

FIGURE 4.4 ARRANGEMENT FOR THE ROD TO SILICA TEST

the points were as smooth as could be made with this method and were all in the one plane. To ensure that the rod points sat squarely and firmly on the glass surface, a weight of 0.5 kgm was placed on the upper ring.

The silica specimen itself was first prepared by metallizing one side of the silica disc and then cleaning the other side with chromic acid and washing in distilled water. The point electrode was placed on the cleaned surface and the whole apparatus placed in an oven.

Figure 4.4 shows the general arrangement together with the electrical connections. The d.c. potential is supplied from a low ripple power supply and the current measured with a Keithley electrometer.

Voltage-current measurements were made for voltages up to 1750V for each temperature range selected. The maximum voltage was limited by the presence of spurious pulses which made current measurement difficult. These pulses were also encountered in the bulk measurements and are discussed in more detail in Appendix II. The temperature range for these tests was from 260°C to 310°C. The upper temperature was limited by the capacity of the oven and the lower, by the magnitude of the resistance of the contacts. At temperatures below 260°C, the current was too low to be measured satisfactorily with the instrumentation available.

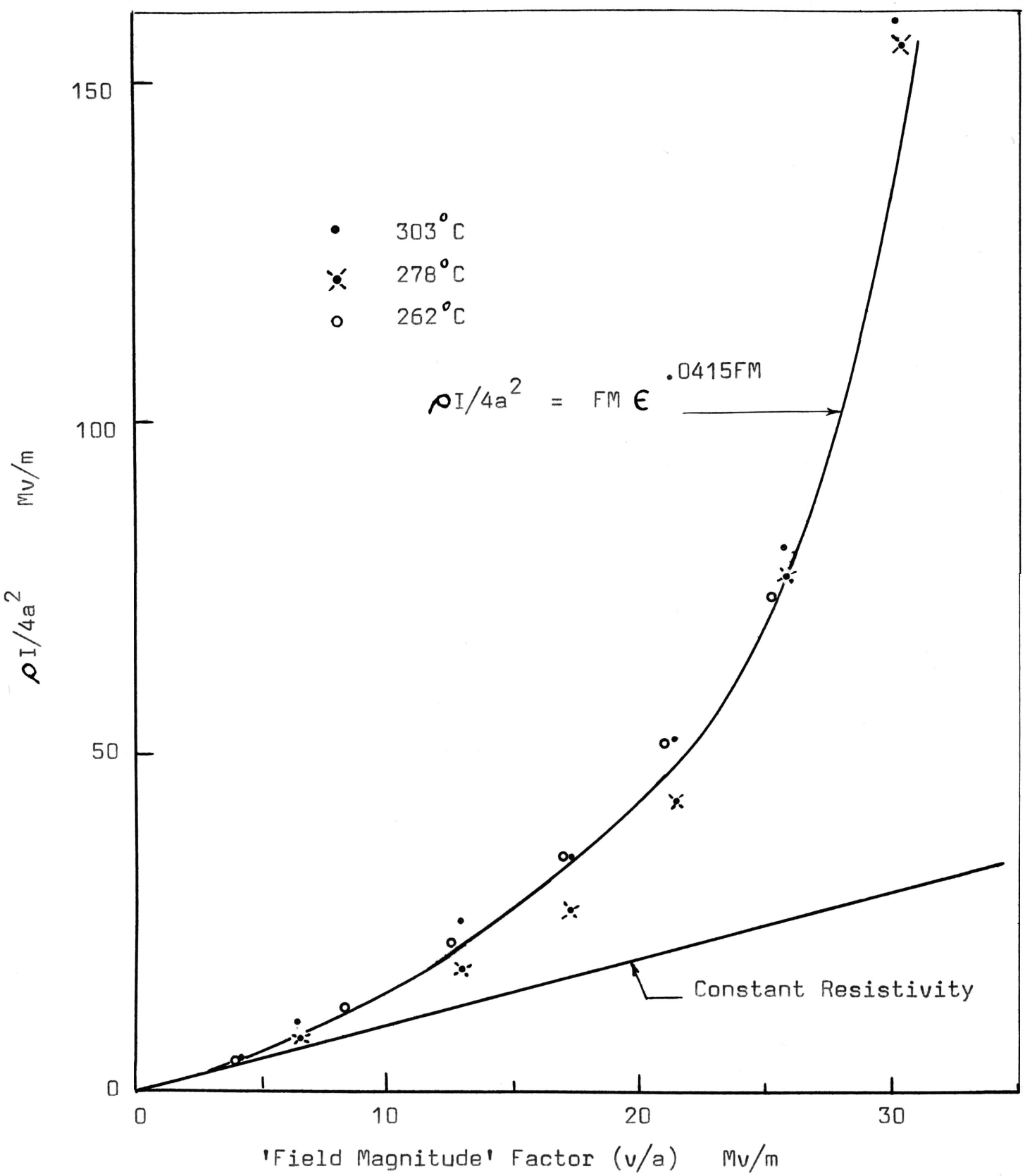

FIGURE 4.5 DEVIATION FROM LINEARITY OF THE METAL ROD TO SILICA CHARACTERISTIC

4.3.2 Results.

The results are shown plotted in Figure 4.5. By using the same co-ordinates as in Section 4.2.2, it is possible to compare the results of the two sections.

The low field contact resistance was determined from a plot of the voltage-current characteristic as in Section 4.2.2, and by obtaining the resistivity from Figure 3.6, the Holm Equivalent contact radius was calculated. Table 4.3 gives the radii of contact as determined by the Holm Equation and that measured with the microscope for three different temperatures.

As with the ball to silica tests there was no significant difference in the voltage-current characteristics with change of polarity of the metal ball.

However in this case the presence of spurious pulses was very obvious. This was particularly so when the points were held at negative potential. This is discussed in Appendix II.

4.4 Discussion.

4.4.1 Contact Radii.

The effective radius of contact calculated from the Holm Equation for the rod to plane geometry is less than the actual physical radius of the rods. This is not unexpected. Although every care was taken in finishing off

TABLE 4.3

CONTACT RADIUS METAL POINTS ON SILICA DISCS

Temperature °C	Radius (microns)	
	Optically Measured	Holm Equivalent
303	100	58
278	100	58
262	100	59

the surfaces of the points, it is most unlikely that the entire surface of the rod end is in the one plane. In addition, even for the area where contact does take place, it is most unlikely that it is circular, in which case Equation 2.2 does not strictly apply. If the contact shape is elliptic, then Figure 2.2 indicates that the effective resistance is less than that for a circular contact of the same area. Alternatively, for a given measured resistance, the actual area of contact will be greater than that calculated from Holm's Equation. If the ovalness factor is 3, the effective area is 77 percent greater than that calculated from the Holm equivalent radius.

With the ball to plane geometrical configuration, the Holm Equivalent radius is either equal to or greater than the Hertz Equivalent radius. This result is not unexpected. It is demonstrated in Section 2.4 that the distance between the curved surface of the ball and the flat surface of the silica disc is very small. At a distance of 1.5 times the contact radius, the two surfaces are separated by 0.63 microns. It would only require slight deviations in the flatness of the silica or smoothness of the metal ball to cause contact to be made.

4.4.2 Rod to Silica Characteristic.

This characteristic is linear for low values of applied voltage but becomes non-linear for higher

values of voltage where the 'FM' factor is greater than 2.0 Mv/m. This non-linearity can be explained in terms of the decrease in the bulk resistivity of the silica in the region around the point of contact.

It has already been shown in Section 2.4 that very high electric fields can be established in the silica specimen adjacent to the metal points, and in Section 3.6, that the resistivity of silica begins to decrease at electric fields of 1.0 Mv/m and is significant at fields of 10.0 Mv/m. For applied voltages low enough to give 'FM' factors below 2.0 Mv/m, the electric field throughout the silica sample is not of sufficient magnitude to affect its resistivity. See Tables 2.3, 2.4 and 2.5. Hence, for voltages up to this value the voltage-current characteristic is linear. When however the voltage is increased above this, the electric field strength in some areas become high enough to reduce the bulk resistivity of the silica. For example, when the 'FM' factor is 10.0 Mv/m, the electric field at the centre of the contact radius is 6.4 Mv/m and increases along the radius to the circumference but decreases along the perpendicular axis. Since the electric fields are now in the order where substantial changes can be expected in the bulk value of the resistivity, corresponding changes can be expected in the resistance of the contact. This is confirmed by Figure 4.5 which indicates that for an 'FM' factor of 10.0 Mv/m the original resistance of the contact is reduced by

50 percent.

It is also shown in Figure 4.5 that the experimental points fit reasonably well around the following equation, and are independent of the temperature over the range considered.

$$I = \frac{V}{R_o} \epsilon^{.0415\ FM} \quad \ldots\ldots\ldots\ldots \quad 4.1$$

Where R_o = low electric field resistance.

FM = field magnitude factor (Mv/m).

Hence the resistance of the contact varies as the 'FM' factor, and therefore as the magnitude of the electric field, in the exponent of the exponential. It is shown in Section 3.6, that the initial variation of the resistivity of silica with the electric field is also given by a similar relationship.

The temperature independence of these characteristics gives additional support to the model proposed. It is shown in Section 3.6 that the variation of the resistivity with the electric field is independent of temperature, and this independence must be expected in these tests if the process taking place occurs in the material itself.

The possibility of some form of charge transfer across airgaps must be considered. Since the sides of the rods rise almost vertically from the silica surface any contribution from them must be very small. However, since

the Holm equivalent radius is about 58 microns instead of 100 microns, it follows that only part of the area of the ends of the rods are in contact with the silica. In those areas where contact does not take place, it is possible that strong electric fields may exist and electron transfer take place. This mechanism cannot dominate because of the following reasons:

(i) The characteristics are independent of temperature. It is shown in the next section that if electron emission takes place, the characteristics are temperature dependent.

(ii) The maximum radius over which emission can take place is 100 microns. Careful examination of the rod end under a microscope shows that the actual surface tends to curve up even before this radius, so the actual area over which emission can take place is very limited.

It may be concluded that the results of this test approximately represent the bulk characteristics of this electrode arrangement. The true bulk curve will sit somewhere under the experimental one given in Figure 4.5.

One factor which could influence the voltage-current characteristic of this test is the potential barrier between the metal points and the silica. For low electric fields, only those electrons with sufficient thermal energy can enter the silica from the metal electrode. With high electric

fields, electron transfer is enhanced either by electrons tunnelling through from the metal to the conduction band of the insulator, or as is more likely, the effective height of the barrier is reduced by the Schottky Effect. Mead (55), when considering electron transport mechanism in insulating films, concluded that the current in the cases he considered was limited by the bulk processes in the material and not by the characteristics of the electrode. If this is the case in his studies, it is quite likely that the same applies here. Hence it may be assumed that the electrode - insulator potential barrier is not a significant factor in determining the overall voltage-current characteristic.

Since these characteristics are independent of time, it may be concluded that the sample of silica used in these tests is essentially electronic conducting. In addition to this it is also necessary to conclude from this characteristic that the internal heating effects are also negligible. It has already been shown in Section 3.4 that for heating to be significant, electric fields in the order of 100 Mv/m are necessary. Examination of Tables 2.3, 2.4 and 2.5 shows that, except at the circumference of the contact circle, the electric fields are below this value.

4.4.3 Ball to Silica Characteristic.

In Figure 4.2, the ball to plane characteristics are shown plotted with the rod to plane characteristics. This shows the ball to plane characteristics deviating from linearity to a greater extent than the rod to plane characteristic and that this is temperature dependent.

This confirms the original hypothesis that, due to the influence of the strong electric fields, some kind of charge transfer takes place across the air gap between the two surfaces. The non-linearity of the ball to plane characteristics is due to two main factors:

(i) The reduction of the resistivity of the silica around the region adjacent to the point of contact. This is represented approximately by the region between the constant resistivity and rod to plane curves and is described in some detail in Section 4.4.2.

(ii) Charge transfer across the air gap. A comparison of the rod to plane and the ball to plane curves in Figure 4.2 shows quite clearly that both sets of curves begin with the same initial slope but that the ball to plane characteristics deviate from the constant resistivity line at a much greater rate than the rod to plane characteristic. This characteristic can best be explained in terms of electron transfer across the air gap in the region of the point of contact. This has the effect of increasing the radius of the contact circle, reducing the effective contact resistance and hence increasing the current above what it

would be in the absence of electron emission.

There are two possible mechanisms by which this charge transfer may take place.

The first is electron tunnelling. The initial investigation into this type of emission was carried out by Fowler and Nordheim(56) although since then a great deal of additional work has been done (42). There are however two factors which would indicate that this is not the dominant mechanism in this case. For tunnelling to take place it is important that the distance between the two surfaces be within certain limits. In the case of tunnel diodes the distance between the two surfaces is in the order of 100 Å. With the scaled up model used in these tests, the actual air gap separates fairly quickly and soon exceeds this value. The other factor is the strong temperature dependence of the characteristics which is not consistant with tunnelling. Hence on the basis of these two considerations, it must be concluded that tunnelling cannot account for the order of the deviation obtained in the tests. Any tunnelling that does take place probably occurs very close to the point of contact.

The other possible mechanism is Schottky emission. This is analogous to thermionic emission except that the applied electric field lowers the potential barrier height and facilitates the escape of electrons. One of the main characteristics of this type of emission is its temperature

dependence. Since the characteristics of the ball to plane geometry are also temperature dependent it is reasonable to assume that the Schottky Effect dominates in this case. The mechanism by which this occurs can be described as follows. For given temperature and electric field conditions, electrons will be emitted from the surfaces and flow across the airgap. This reduces the effective area of the contact and causes the current to increase. At higher temperatures, the electron emission is made easier and consequently it can take place at greater distances from the physical contact area. This means that for a given voltage, and hence 'FM' factor, the effective area over which emission takes place is larger than at the lower temperatures, and this causes the resultant current to increase. When plotted on the axes shown in Figure 4.2, the curves for the higher temperatures fit above those for the lower temperatures.

When the metal surface is at negative polarity, an abundant supply of electrons are available. However, when they reach the silica surface they form a space charge which sets up a reverse field and limits the current flow. Muray(57) has observed this when bombarding a glass surface with a stream of electrons. When the metal surface is at a positive potential, the electrons must come from the free electrons in the silica. In this case the emission current is limited by the number of free electrons available near the silica surface.

In order to check the feasibility of this type of emission from the metal electrode, the theoretical current density was determined for an electric field of 10^6 v/m at a room temperature of 275°C. Using an activation energy of 4.48 ev, a current density of 4.5×10^{-6} amp/m^2 is obtained. After making an estimate of the approximate area that could be involved, it can be shown that the magnitude of the total current increase can be easily supplied by this emission current.

The actual mechanism of charge transfer across the air gap will vary with the length of the gap. Since the mean free path of air molecules is in the order of 10^{-7} meters, and the distance between surfaces at a point of twice the radius of the constant circle is approximately 1.5 microns, the probability of a collision is very small. At distances further out collisions may occur and charge may be transferred by electron attachment or even some limited ionization may take place. Ahmed(58) has discussed some aspects of current conduction at these greater distances. It is probable that most of the charge is transferred by the direct flow of electrons.

One additional factor which is in agreement with the model proposed is the absence of spurious pulses. As has been shown in Appendix II, these are easily generated with the rod electrode geometry, and are due to the high electric fields in the region of a metal electrode. In this

case with the ball to plane geometry, the effective area of contact is increased and the internal electric fields must be correspondingly reduced. The electric fields are high enough to cause electrons emission but not high enough to generate any spurious pulses.

CHAPTER 5.0

METAL TO BOROSILICATE GLASS CONTACTS.

5.1 Introduction.

The mechanism of current conduction by ions is sufficiently different from that by electrons, that a separate investigation into their characteristics is justified. This applies in particular when considering the effects of electrodes. If the electrodes are made of a suitable electrolyte, there is a free exchange of ions at both electrodes and no special contact effects take place. If the electrodes are metallic, the ions at one electrode cannot move out of the glass into the metal electrode nor can the deficiency of ions in the glass at the other electrode be replaced. This causes special effects to take place at each electrode.

In this chapter, the electrical characteristics of the following two contacts are investigated.

(i) Metal to glass contacts with the metal electrode at negative potential.

(ii) Metal to glass contacts with the metal electrode at positive potential.

The characteristics of these contacts are investigated by means of scaled up models. As was the case in Chapter 4, the contact between a spherical particle and the metal electrode is represented approximately by a metal ball placed on a flat sample of borosilicate glass. In order to determine the existence of charge transfer between adjacent surfaces of the electrode and the particle,

a series of tests were carried out using the rod to plane geometry. By comparing the results of these two tests on common axes, it is shown that the non-linear voltage-current characteristic of the ball to plane test is due in part to the reduction of the bulk value of the resistivity of the borosilicate glass around the point of contact and to electron transfer across the air gap.

With the metal electrode at a positive potential, the total current decays with time, and with it negative, the current increases with time. Models are developed to account for these phenomena.

The results of this chapter will be used in Chapter 8 to account for the overall characteristics of particulate ionic conducting solids.

5.2 Metal Ball to Borosilicate Glass Contacts.

5.2.1 Experimental method.

The preparation of the borosilicate glass specimen, the arrangement of the metal ball and the electrical connections is the same as for the corresponding tests on silica described in Section 4.2.

The radius of the contact circle between the metal ball and the borosilicate glass surface was controlled by applying an external force to the ball and its magnitude calculated from the Hertz Equation 2.11. Table 5.1 lists

TABLE 5.1

MAIN PARAMETERS OF METAL BALL TO BOROSILICATE GLASS TESTS

Material		Borosilicate glass
Applied force		1.33 kgms.
Ball diameter		2.0 cms.
Youngs Modulus	Ball	0.81×10^6 kgm/cm
	Glass	0.64×10^6 kgm/cm
Poissons Ratio	Ball	0.33
	Glass	0.224
Hertz Equivalent Radius		125 microns.
p/a		80

The magnitude of these values has been adjusted for temperature.

the main constants of the materials concerned and gives the Hertz equivalent radius.

Initially, considerable difficulty was experienced in obtaining consistent and repeatable results with this ionic conducting material until it was realised that the current was a function of the electrode polarity as well as the period of application of the electric field. Good consistent results were only obtained by conducting three different sets of tests.

(i) The bulk characteristic of the material could only be found by preventing any substantial variation of the ion concentration in the region of the points. This was done by varying the polarity of the electrodes. The actual procedure was to first adjust the voltage of the power supply to the required value and then apply it to the ball electrode for a period of five seconds while current readings were taken. The two electrodes were then shorted for a ten second period. The opposite polarity was then applied to the electrodes for a further period of five seconds. This was repeated for increasing steps of voltage to a maximum of 500 volts and then for decreasing values of voltage. Good reproducible results were obtained. The magnitude of the current readings for positive and negative polarities were the same for 'FM' factors up to 2.0 Mv/m, but for greater values there were slight differences. The positive reading was slightly lower than the negative reading. The

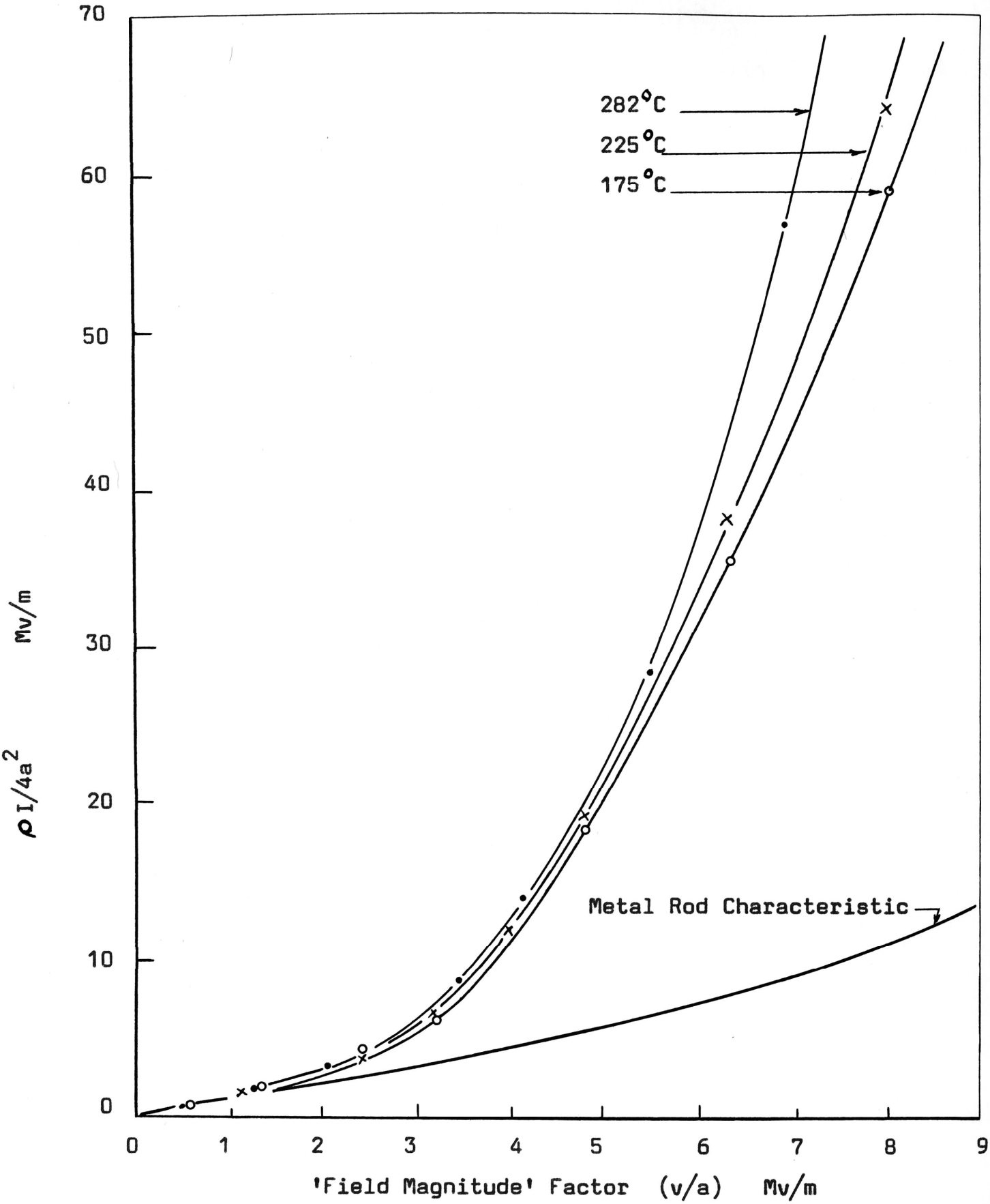

FIGURE 5.1 METAL BALL TO BOROSILICATE GLASS BULK CHARACTERISTIC. TEMPERATURE = 175, 225 AND 282°C.

actual value used in the plot is the average of the two.

(ii) The 'points positive' characteristic was obtained by applying a steady positive potential to the ball electrode and recording the current - time characteristic. Readings were taken at a number of voltages up to 500 volts. For each set of readings at a new voltage, the points were moved to a 'clean' area on the glass surface.

(iii) The 'points negative' characteristic was obtained in a similar manner except that the ball electrode was held at negative potential.

On a number of occasions during tests (ii) and (iii), the voltage was left disconnected for several minutes and then reapplied. In all cases the current returned to the same value as that at the time of disconnection, confirming that a fairly permanent change had taken place in the region of the contact.

The borosilicate glass samples are the same as those used in the bulk characteristic tests of Section 3.6.3.

5.2.2. Results.

The results of the bulk characteristic tests are shown plotted in Figure 5.1 using co-ordinates of v/π and $\rho I/4\pi^2$.

The contact resistance at low electric fields was determined from the initial slope of the voltage-current

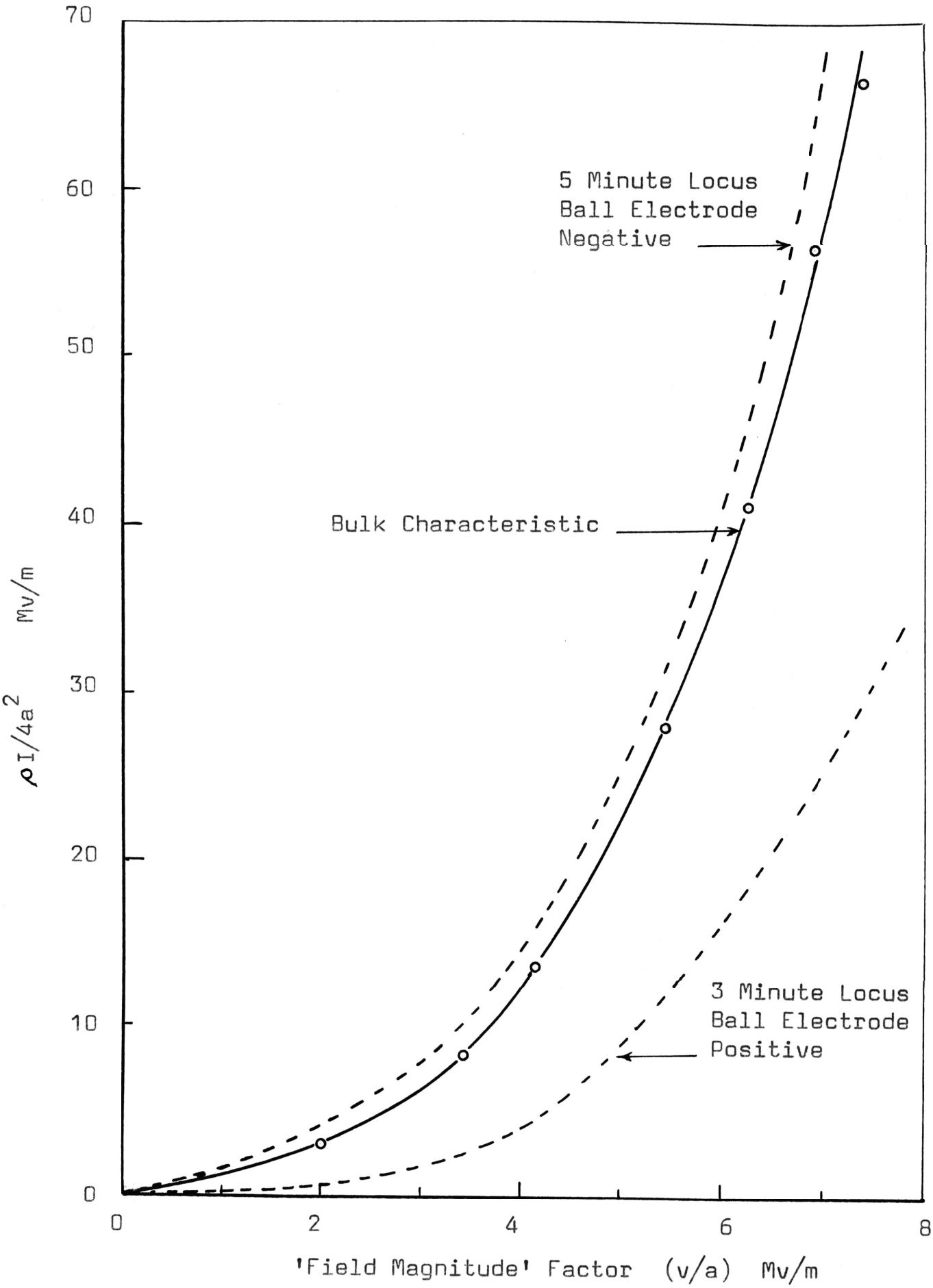

FIGURE 5.2 METAL BALL TO BOROSILICATE GLASS CHARACTERISTIC

TEMPERATURE = 282°C.

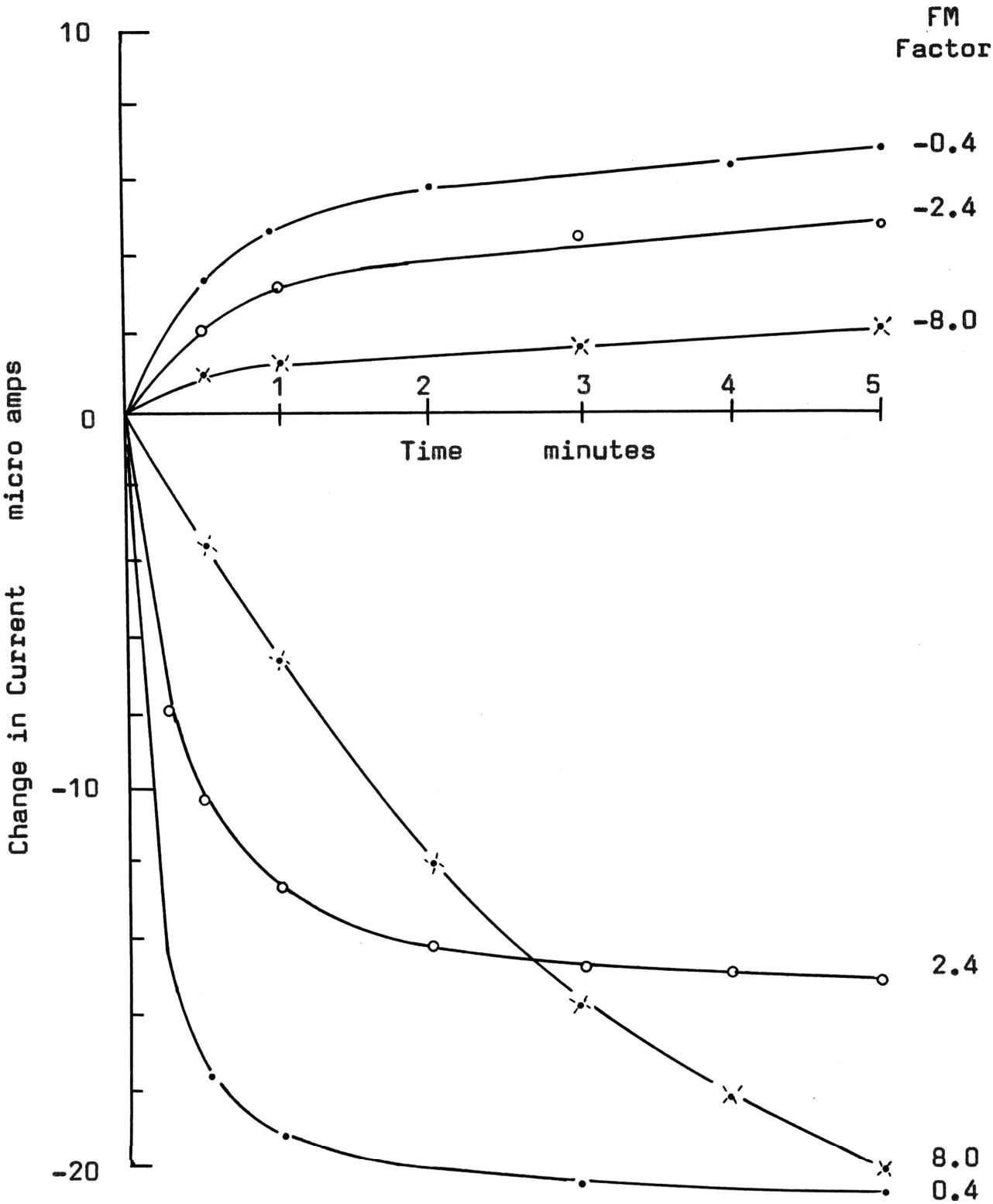

Multiply Vertical Scale:

by 1.0 for FM = 8.0
by 0.1 for FM = 2.4
by 0.01 for FM = 0.4

FIGURE 5.3 METAL BALL TO BOROSILICATE GLASS CHARACTERISTIC. CHANGE IN CURRENT AT TEMPERATURE OF 282°C.

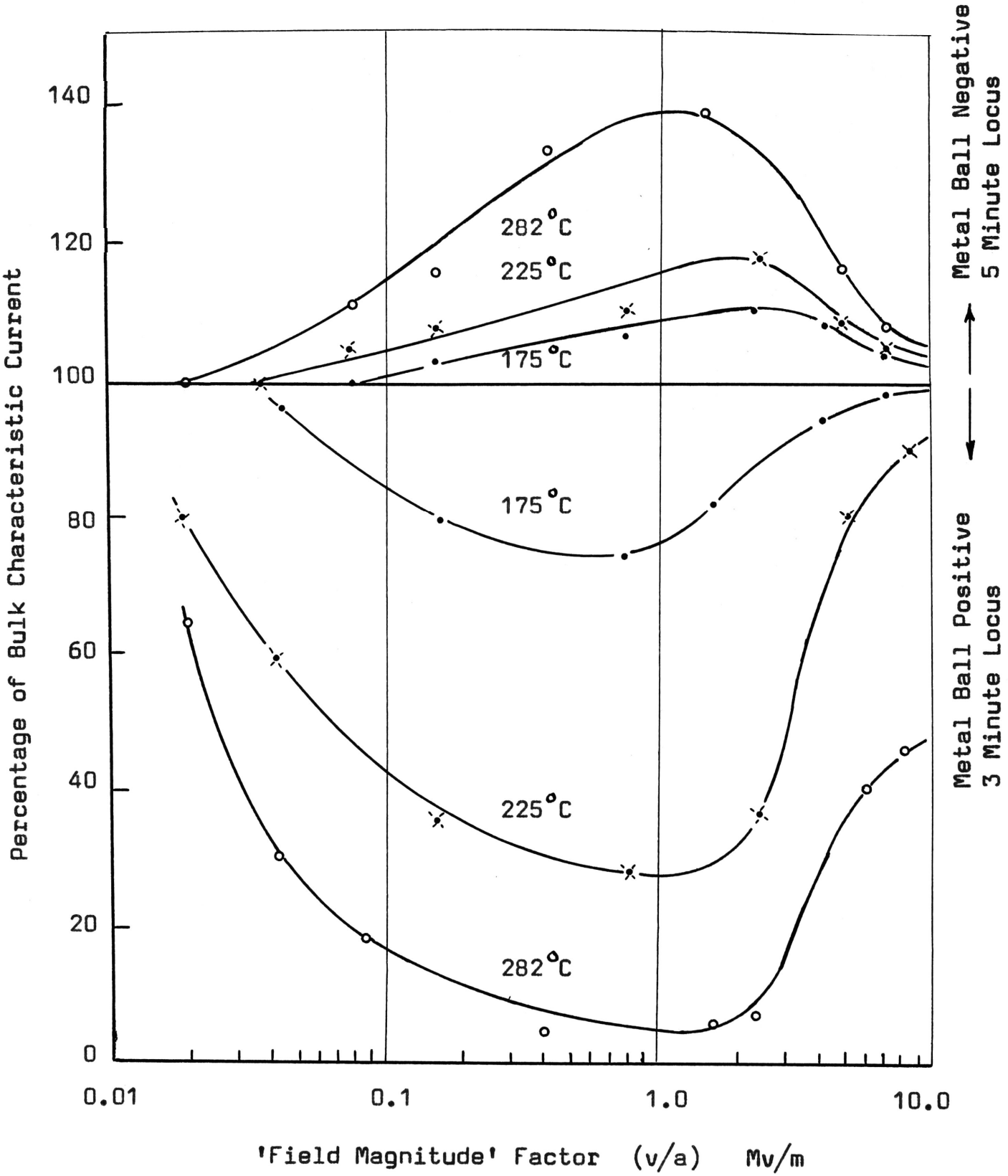

FIGURE 5.4 METAL BALL TO BOROSILICATE GLASS CHARACTERISTIC. SUMMARY OF CURRENT VARIATION WITH TIME.

curve. By using this, and the bulk resistivity of the material given by Figure 3.3, the Holm equivalent radius was calculated.

Table 5.2 gives a summary of the radii as calculated from the Holm and Hertz equation for a number of different temperatures.

It is rather difficult to show in a concise manner the time variations of the current for constant applied voltage and polarity. Figure 5.2 shows a typical bulk characteristic for a temperature of 282°C. The lower dotted line is the locus of the curve when the ball electrode is held at a positive potential for three minutes and the upper dotted line is the locus when the ball is held at a negative potential for five minutes. Figure 5.3 shows the actual change in current for different values of 'FM' over a period of five minutes at a temperature of 282°C.

Figure 5.4 gives a summary of the results for the three temperatures of 175, 225 and 282°C. Here the percentage deviation of the current from the bulk value is plotted against the 'FM' factor for both positive and negative polarities.

5.3 Metal Rod to Borosilicate Glass Contacts.

5.3.1 Experimental Method.

The preparation of the borosilicate glass surface, the arrangement of the rod electrodes and the

TABLE 5.2

RADII OF CONTACT FOR METAL BALL TO BOROSILICATE GLASS TESTS.

Temperature °C	Radius (microns)		Holm radius
	Hertz Equivalent	Holm Equivalent	Hertz radius
283	125	145	1.16
250	125	142	1.14
225	125	126	1.01
204	125	154	1.24
175	125	125	1.00

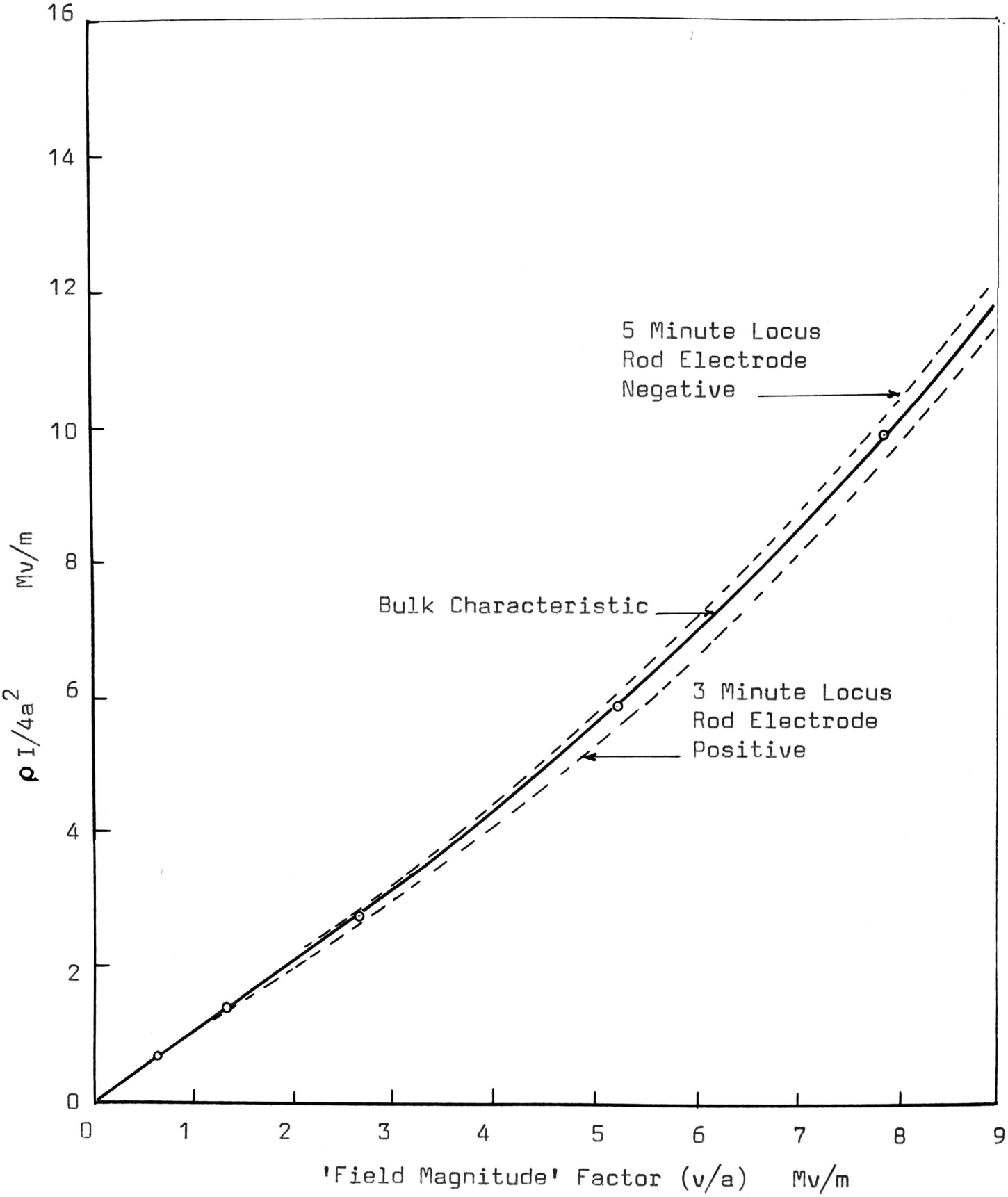

FIGURE 5.5 METAL ROD TO BOROSILICATE GLASS CHARACTERISTIC.
TEMPERATURE = 175°C.

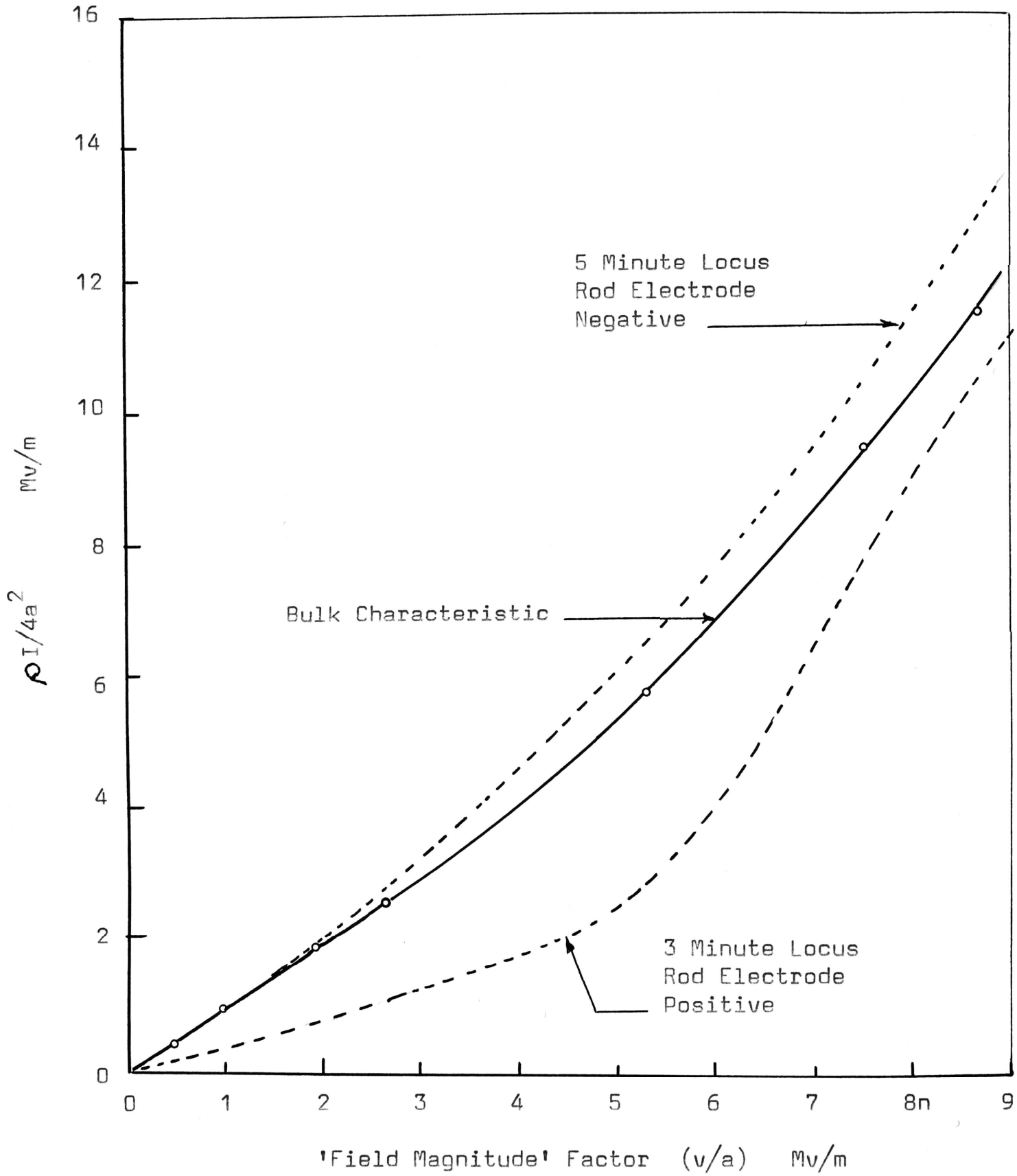

FIGURE 5.6 METAL ROD TO BOROSILICATE GLASS CHARACTERISTIC.

TEMPERATURE = 225°C.

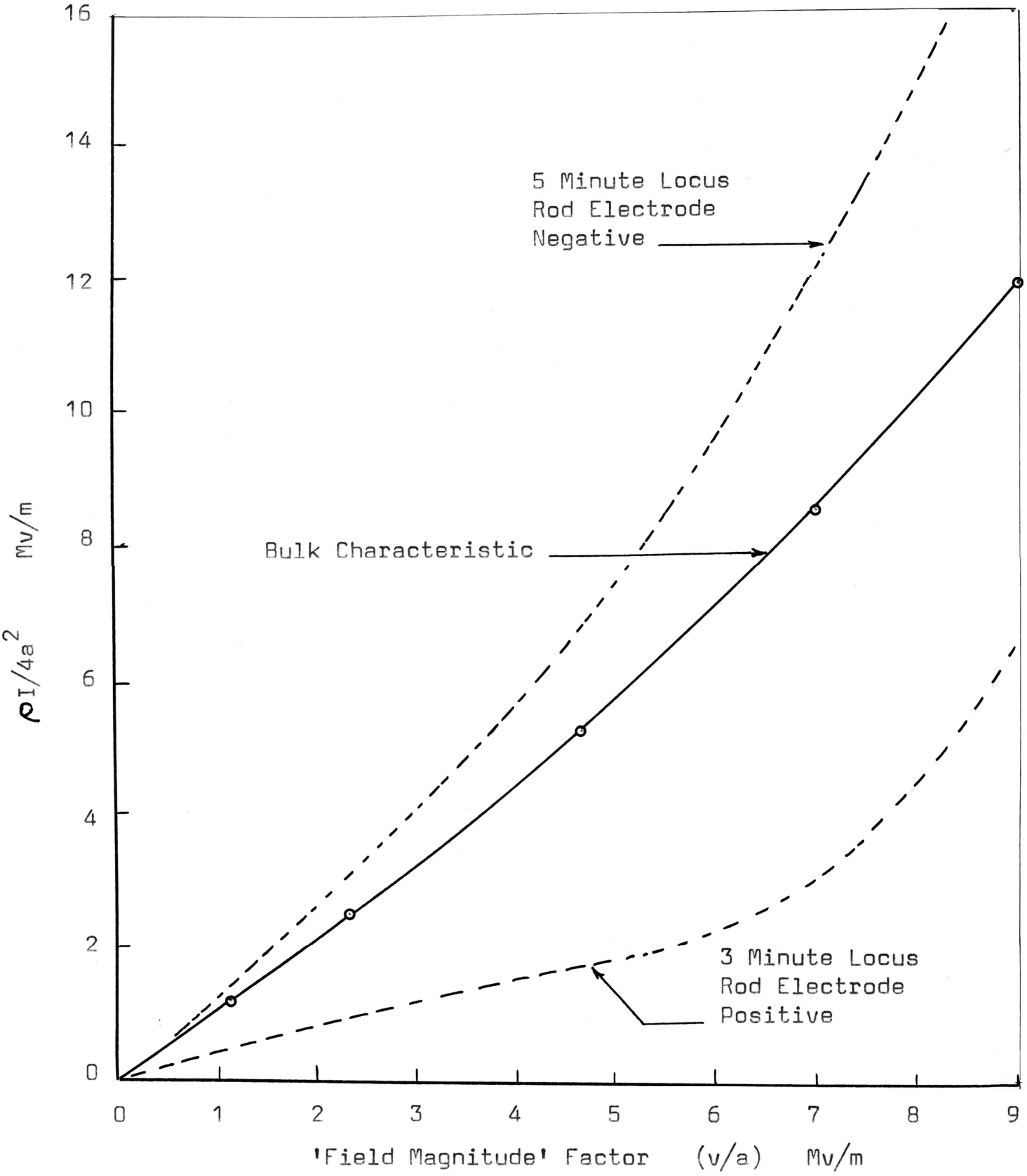

FIGURE 5.7 METAL ROD TO BOROSILICATE GLASS CHARACTERISTIC.

TEMPERATURE = 282°C

electrical connections are the same as for the corresponding tests on silica described in Section 4.3.

As was the case with the metal ball to plane tests of the previous section it is necessary to conduct three sets of tests.

(i) Bulk characteristic.

(ii) Electrode positive.

(iii) Electrode negative.

These were carried out in the same manner as described in Section 5.3.

5.3.2 Results.

A summary of these results is shown plotted in Figures 5.5, 5.6 and 5.7. The solid line is the bulk characteristic, the lower dotted curve is the locus of the current when the metal rod electrode is held at positive potential for three minutes and the upper curve is the locus of the current when held at a negative potential for five minutes.

Table 5.3 records the Holm equivalent radius, calculated in the same way as in the earlier sections.

5.4 Discussion.

5.4.1 Contact Radii.

The general relationships between the Holm

TABLE 5.3

CONTACT RADIUS OF METAL RODS ON BOROSILICATE GLASS

Temperature ^{o}C	Radius (Microns)	
	Optically Measured	Holm Equivalent
175	125	38
225	125	42
275	125	52

Equivalent radii to the physical radius of the points and the radius calculated by the Hertz Equation are similar to that obtained with silica. The comments made in Section 4.4.1 on the contacts with silica will apply in the case of borosilicate glass. The main difference between the two is that the Holm Equivalent radius shows a greater variation with borosilicate glass than with silica. This is probably due to the greater unevenness of the borosilicate glass surface.

5.4.2 Bulk Characteristics.

The bulk characteristic of the borosilicate glass with the rod to plane geometry has the same non-linear features as obtained with silica. The upward sweep of the curve in Figures 5.5, 5.6 and 5.7 is the result of the decrease in resistivity of the glass due to the region of high electric field stress around the point of contact. As described in Chapter 3, this phenomenon is known as the Pool Effect and has been well investigated for glass. The variation of the resistivity with the electric field is given by Equation 3.5.

The net effect of this is that the effective resistance of the contact is reduced at higher values of 'FM', and hence electric fields, and the total current increases.

The three experimental curves plotted in Figures 5.5, 5.6 and 5.7 can be made to fit the relationship;

$$\rho I / 4a^2 = FM \epsilon^{0.3\ FM} \quad \ldots\ldots\ldots\ldots\ldots\ldots \quad 5.1$$

Where FM is expressed in Mv/m.

Close examination of the bulk characteristic (although it is not so obvious in the plotted results) shows that the non-linearity begins at lower 'FM' values for higher temperatures. This is consistent with the experimental results in Section 3.6 where it is shown that the departure from linearity is temperature dependent. The higher the temperature the lower is the applied electric field at which this occurs. The effect on the rest of the characteristic however is negligible.

Figure 5.1 shows a plot of the bulk characteristic curves with the ball to plane geometry on which is also plotted the rod to plane characteristic. As is the case with silica, the characteristic of the ball to plane geometry is much more non-linear than that of the rod to plane geometry. The explanation given in Section 4.4.3 for silica applies equally well with borosilicate glass. This may be summarised as follows. The non-linearity of the ball to plane geometry is due in part to the variation of the bulk resistivity of the glass around the point of contact and also in part to the field enhanced thermionic electron emission from adjacent surfaces across the air gap in the

region of the contact. The temperature dependence of the bulk characteristics is consistent with this model. As is the case with silica, the characteristics due to electron emission dominates.

5.4.3 'Electrode Positive' Characteristic.

For both the rod to plane and the ball to plane tests, the total current decreased with time when these electrodes were held at a positive potential.

Consider a volume of the glass of thickness 'd' and a square surface of unit area. If one of these square surfaces is against the metal electrode, then under the influence of an applied electric field, cations will move out of the volume and oxygen defects will be created within this volume and move towards the electrode. This will cause two effects to occur.

(i) The build up of a negative space charge cloud.

(ii) Decrease in the mobile ion concentration in this volume.

Both of these effects could account for the characteristics observed.

The build up of the negative space charge would cause a voltage to be developed across this region and so produce a fall off of the total current. There is some experimental evidence to show that the voltage drop at the anode is usually less than at the cathode (35)(59)(60).

This may be due to the distribution of the negative charge but is more likely due to these electrons being detached from the oxygen atoms by thermal excitation and migrating to the anode under the influence of an electric field. Hence, considering the temperatures at which these tests are carried out and the order of the externally applied electric fields, the build up of a negative space charge at the anode is very unlikely.

The reduction in the concentration of the mobile ionic carrier is a more likely explanation. The author has shown (61) that this can account for the fall of current observed in the tests.

If N_o is the ionic carrier density of the glass before the application of any voltage and J the current density, the total number of mobile ions which will migrate out of this given volume of unit area and thickness 'd' is given by;

$$\int \frac{J}{e} \, dt$$

Hence the density of the volume has been reduced by;

$$\int \frac{J}{ed} \, dt$$

The new density is now;

$$N_o - \int \frac{J}{ed} \, dt$$

This assumes that the remaining ions redistribute themselves evenly throughout the volume. If this volume is subject to an even electric field E, the current density is given by;

$$J = e \mu E \left(N_o - \int \frac{J}{ed} \, dt \right) \quad \ldots\ldots\ldots\ldots\ldots \quad 5.2$$

Where e is the electron charge,

μ is the ion mobility.

Solving this differential equation,

$$J = J_o \epsilon^{-\mu E t/d} \quad \ldots\ldots\ldots\ldots\ldots\ldots\ldots \quad 5.3$$

Where J_o is the initial current density.

This equation indicates that the total current decrease is a function of the electric field strength, mobility and time.

Because of the field pattern of the rod or ball to plane configuration, it is not easy to apply this equation in any quantitative way. This is further complicated by the variation of conductivity with electric field strength and its time dependence because of the ion concentration depletion. However approximations of the nature given by equation 5.3 often give surprisingly good results as has been recently shown by Huey and Vongpanitlerd (62).

Equation 5.3 indicates that the current fall off is a function of time and this is confirmed by all the experimental results.

This equation also predicts that the percentage current fall off over a given period of time increases with the electric field strength. Examination of Figure 5.4 confirms this for 'FM' factors up to 2.0 Mv/m. At higher values however, the experimental results do not follow this pattern. This is probably due to the electron transfer across the air gap which begins at values of 'FM' greater than 2.0 Mv/m. At these higher electric fields, the component of current across the air gap is added to the initial current and this masks the current characteristics at the actual contact with the electrode. The net result is that the percentage current decay decreases at the higher values of 'FM'.

The only feature of the test results which at first does not appear to fit this equation is the temperature dependence of the current decay. These tests results show that the rate of current decay increases with temperature. In Section 3.6.3, it is shown that at the higher electric fields, the jump distance of the ions increases with temperature. Table 3.2 shows that this varies by an order of eight for the temperature range considered in these tests. Since the mobility, as used in Equation 5.3, is proportional to the jump distance, it follows that as the temperature increases, the mobility term in Equation 5.3 will increase and consequently the current decay at the higher temperatures will be greater.

5.4.4 'Electrode Negative' Characteristic.

When the electrode is held at a steady negative potential, the current gradually increases. This result is rather unexpected as, according to the conventional theory there should be a build up of positive space charge of the Na cations at this electrode. This would cause a voltage drop to be developed across this region and result in a current decay.

It has been shown by a number of workers (63)(64)(48) that when a metal surface is brought in contact with glass, it donates electrons. Other than making the observation, very little quantitative work has been done. It would be reasonable to assume that the number of electrons donated would increase with temperature and the author (61) has argued that it will also increase with the magnitude of the applied electric field. Once these electrons enter the glass, two processes may take place.

(i) Recombination. In this case the space charge is neutralized by recombination with the oxygen atom. The actual mechanism may be as indicated by Murray(38). He suggested that the metallic electrons are bound to the non-bridging oxygen atoms. These then combine with the mobile cations creating immobile Na_2O states and so neutralize part of the space charge.

(ii) In addition, it is necessary to speculate

on the existence of a space cloud of electrons which diffuses through the region. These electrons do not recombine with the cations but they do establish a negative space cloud which will neutralize the positive space cloud of the cations.

In order to account for the characteristics observed in the tests, it is necessary to postulate the build up in density of a cloud of mobile electrons around the contact point which gradually diffuses into the glass. The existence of the mobile charges around the contact area reduces the effective resistance of the contact and causes the current to increase. As the density of electrons builds up and the electrons, with time, diffuse further into the glass, then the current will also increase with time. This is consistent with the experimental results observed.

This increase in current could be attributed to the increase in temperature because of internal losses. That this is not the case is proved by the test in which the voltage was removed for five minutes at the end of a test run and then reapplied. Each time this was done, the current returned to the same value as it was at the point of switching off, and not the bulk value, as would be expected if the characteristic was determined by temperature effects. The permanence of the change is consistent with the model proposed.

CHAPTER 6.0

INSULATOR TO INSULATOR CONTACTS.

6.1 Introduction.

This chapter continues the investigation of the electrical characteristics of contacts. In addition to the metal to particle contacts which occur at the interface between the metal electrodes and particles, there are also the contacts between the particles themselves. These form the main bulk of the contacts in the particulate solid being considered in this thesis.

By using a scaled up model of these contacts, their electrical characteristics are examined. It is shown that for both silica to silica and borosilicate glass to borosilicate glass contacts, the voltage-current characteristic is non-linear. This is attributed to the Pool Effect and electron transfer between the surfaces of the particles adjacent to the points of contact.

It is also shown, that with ionic conducting material, there is a gradual fall off of current if a constant voltage of sufficient magnitude is applied for a period of time. This is attributed to the build up of space charge at the contacts.

The results of this chapter, together with those of the previous two, will be used to account for the overall characteristics of particulate solids in Chapter 8.

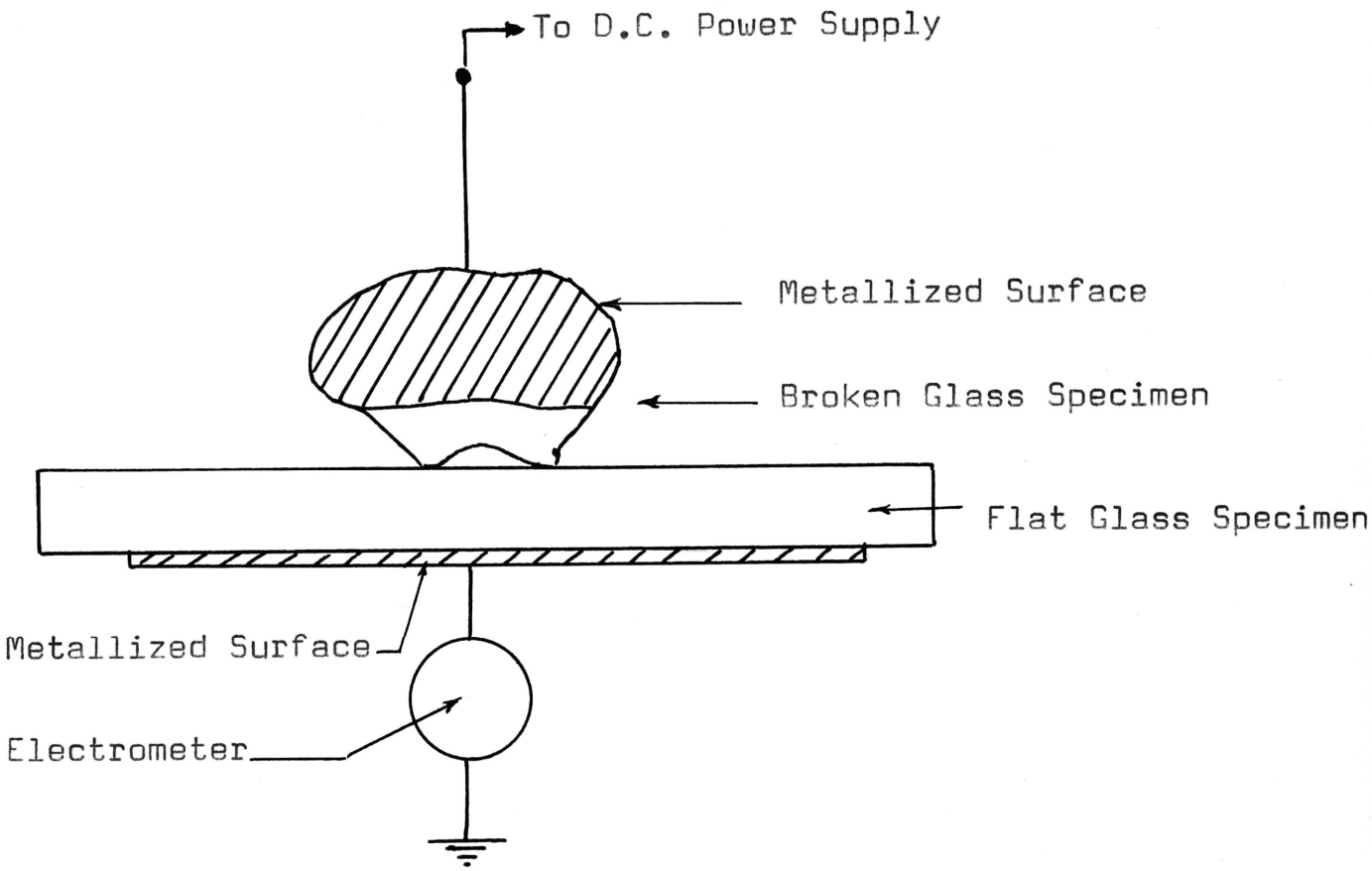

FIGURE 6.1 ARRANGEMENT FOR INSULATOR TO INSULATOR TESTS

6.2 Characteristics.

6.2.1 Experimental Method.

The main problem is to determine some suitable means of representing these contacts on a scale large enough to enable tests to be carried out. For both silica and borosilicate glass, Figure 6.1 shows the arrangement used. A sample of the glass to be examined is broken and metallized over all its surface except one of the freshly broken edges. After cleaning, the specimen is placed with this edge on the clean surface of the flat sample of the same material. The whole arrangement is placed in an oven and heated to various temperatures.

At each temperature the following measurements were made:

(i) Voltage-current characteristic.

(ii) Variation of the current with time with a constant applied voltage. Readings were also recorded for different voltages and polarity of the broken specimen.

(iii) After some of the (ii) test runs, the polarity was reversed and the variation of the current observed.

For each test run, a new broken specimen was used and this was placed on an unused part of the surface of the flat specimen.

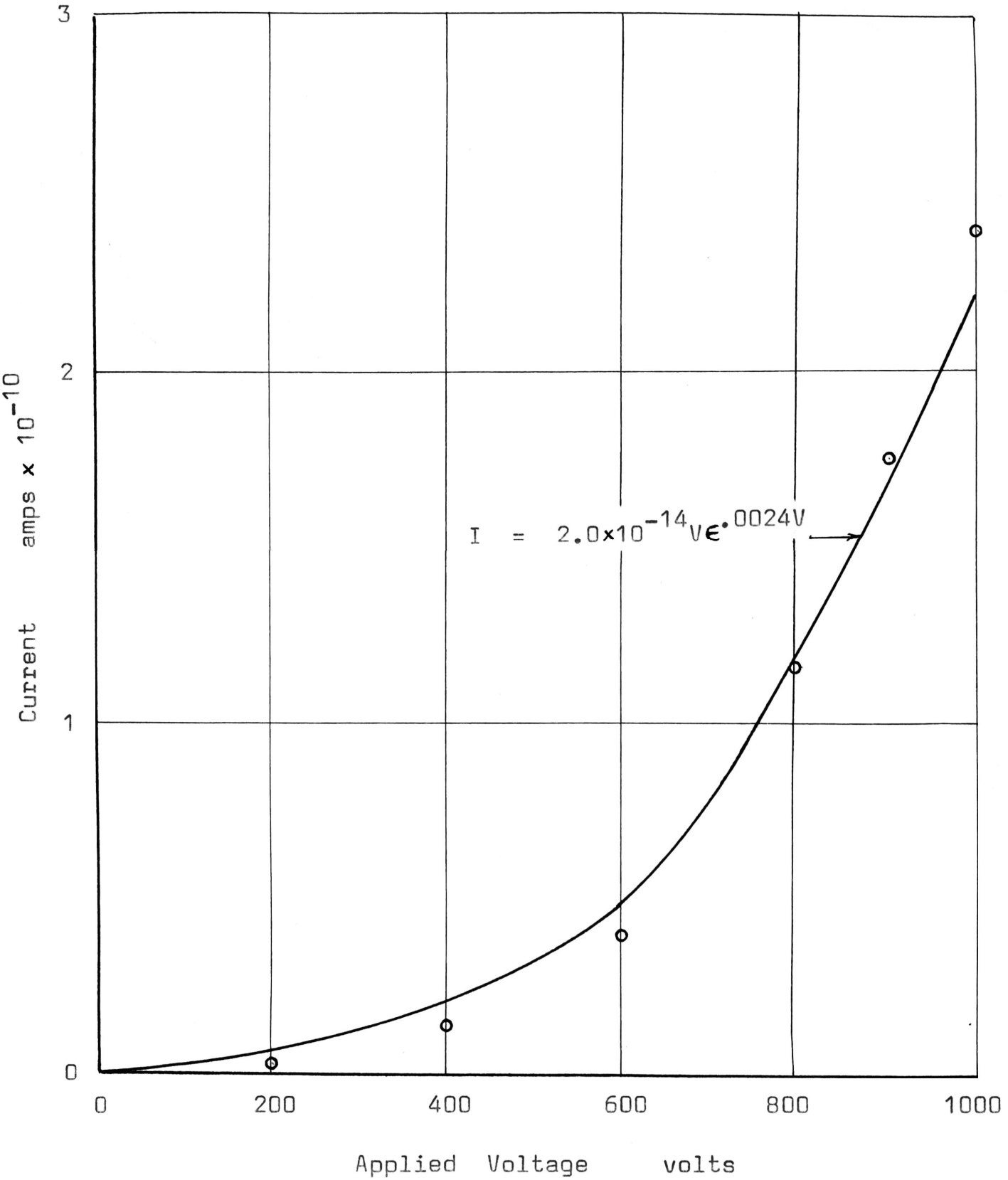

FIGURE 6.2 SILICA TO SILICA VOLTAGE-CURRENT CHARACTERISTICS

TEMPERATURE = 275 ^{o}C

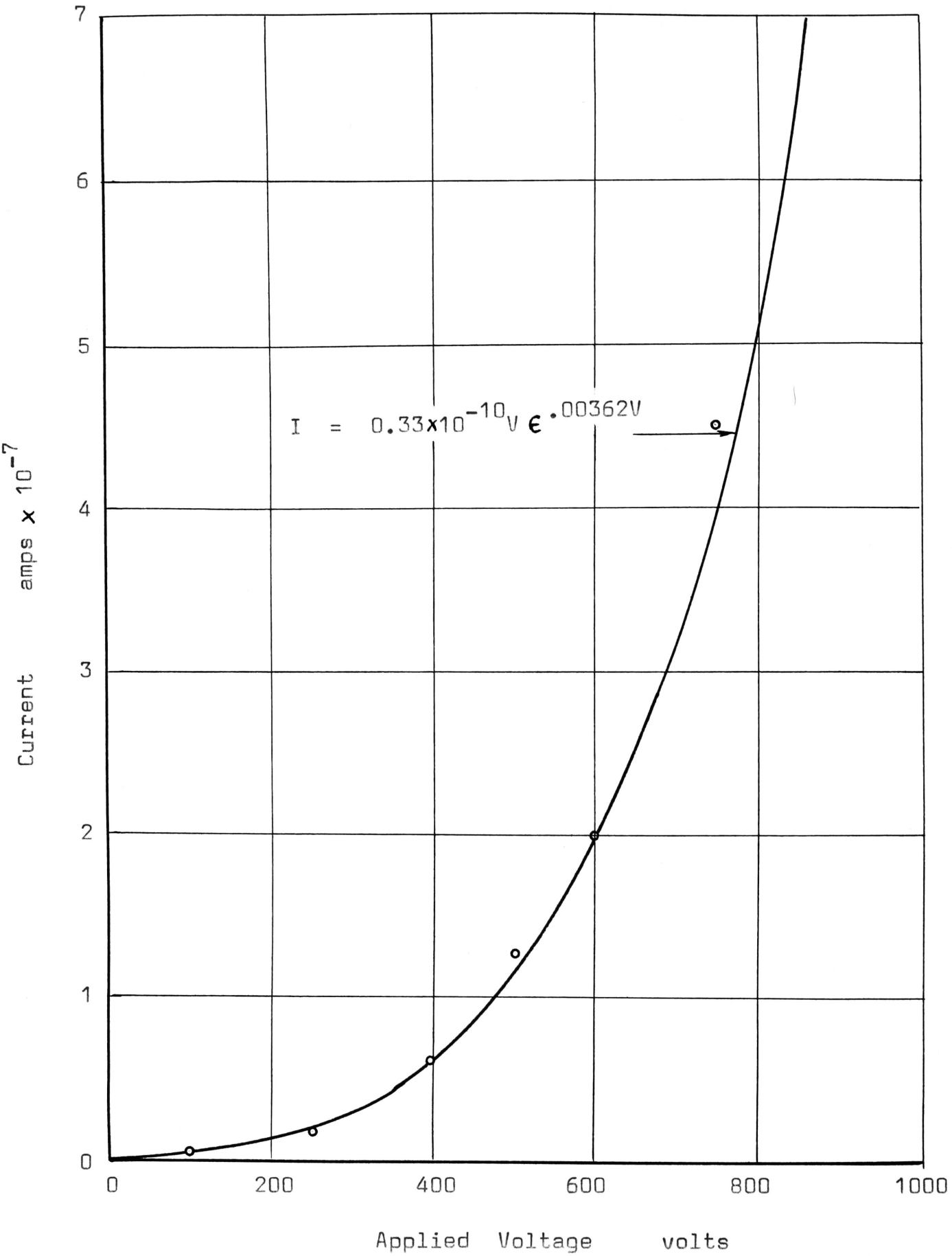

FIGURE 6.3 BOROSILICATE GLASS TO BOROSILICATE GLASS VOLTAGE-CURRENT CHARACTERISTICS. TEMPERATURE = 225°C

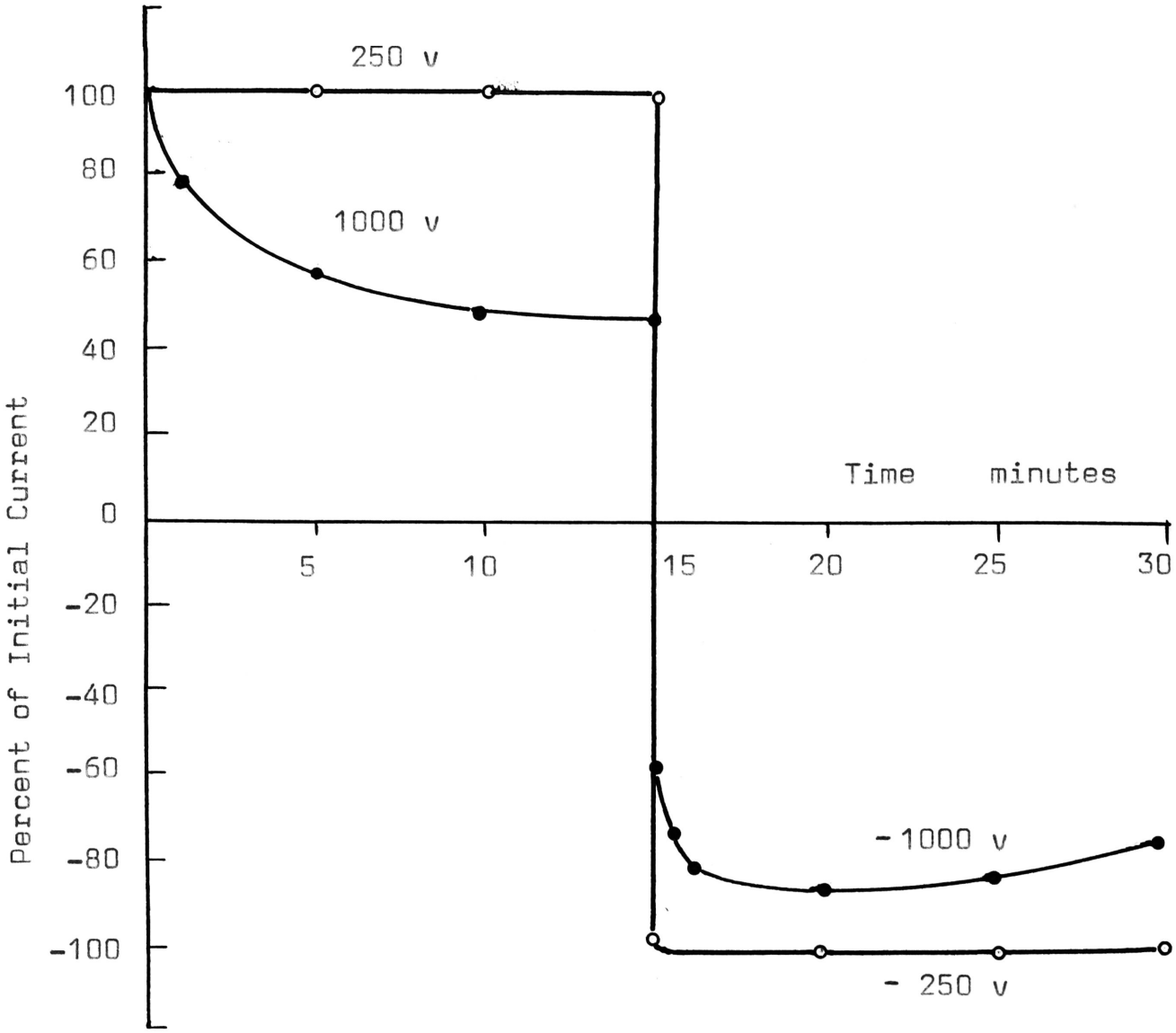

FIGURE 6.4 BOROSILICATE GLASS TO BOROSILICATE GLASS CURRENT-TIME CHARACTERISTICS. POLARITY REVERSED AFTER FIFTEEN MINUTES. TEMPERATURE = 225°C.

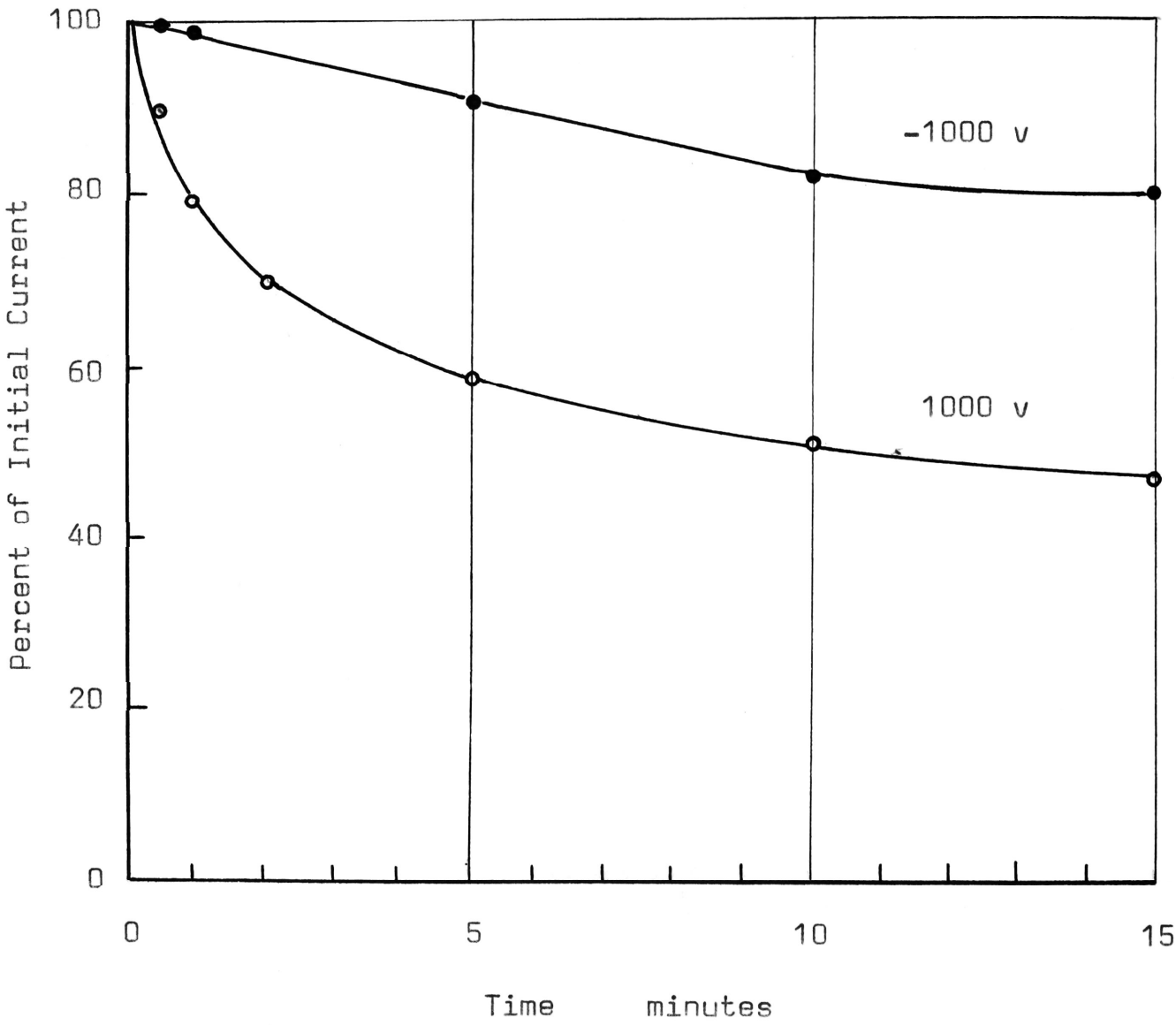

FIGURE 6.5 BOROSILICATE GLASS TO BOROSILICATE GLASS CURRENT-TIME CHARACTERISTICS. TEMPERATURE = 225°C.

6.2.2 Results - Silica.

Figure 6.2 shows a typical voltage-current characteristic for voltages up to 1,000 volts at a temperature of 275°C. The characteristics at other temperatures are of the same general shape but are not recorded in the thesis.

No variation of current with time for a constant applied voltage was observed.

In general no spurious pulses were observed even for voltages up to 2,500 volts.

6.2.3 Results - Borosilicate Glass.

Figure 6.3 is a typical voltage-current characteristic for voltages up to 1,000 volts at a temperature of 225°C. The characteristics at other temperatures are similar to this.

Figure 6.4 shows the variation of the current with time at a temperature of 225°C. The broken sample was initially held at a positive potential for fifteen minutes and then the polarity was reversed and the voltage held at the same magnitude for a further fifteen minutes. Tests were conducted at voltages of 60, 250 and 1,000 volts. Results are similar for other temperatures.

Figure 6.5 records the current-time characteristic for a positive voltage of 1,000 volts applied to the broken sample. The curve for a negative voltage of the same

magnitude is also recorded. In both cases fresh samples were used and the temperature held at 225°C.

6.3 Discussion.

6.3.1 Voltage-current Characteristic.

The voltage-current characteristics of both the silica and borosilicate glass pieces are non-linear. In both cases this is due to:

(i) The increase in the conductivity of the material due to the very high electric fields in the region around the points of contact. This reduces the effective resistance of the contact and causes the current to increase at a greater rate than it would if the resistivity remained constant. This is the same as the explanation offered for the voltage-current characteristics of the metal to glass contacts in Chapters 4 and 5. A general discussion of the reasons for the increase in conductivity with high electric fields is given in Chapter 3.

(ii) The second factor which contributes to this non-linearity is electron emission between the sample surfaces adjacent to the points of contact. The existence of this has been demonstrated in Chapters 4 and 5. In this case however, since the broken surface of the top sample is usually resting on a raised edge, it is probable that the two surfaces separate more quickly than in the case of a

ball placed on a smooth surface. In addition, it is shown in Equation 6.1 that the voltage-current characteristic is proportional to V (hence 'FM') in the exponent of the exponential. This is a feature of the bulk characteristic curves given in Figures 4.5 and 5.1 where electron transfer across the air gap is reduced to a minimum. It may be concluded that electron transfer between surfaces will exist but it does not dominate to the same extent as it does with the ball to plane geometry.

With both silica and borosilicate glass, the voltage-current characteristics can be made to fit the relationship:

$$I = A V \epsilon^{BV} \quad \ldots\ldots\ldots\ldots\ldots\ldots\ldots\ldots \quad 6.1$$

Where A and B are constants and V is the applied voltage.

The equations which fit the two sets of experimental results recorded in Figures 6.2 and 6.3 are:

For silica $$I = 2.0 \times 10^{-14} V \epsilon^{0.0024 V} \quad \ldots\ldots \quad 6.2$$

For borosilicate glass $$I = 3.3 \times 10^{-11} V \epsilon^{0.00362 V} \quad \ldots\ldots \quad 6.3$$

It is almost impossible to relate the 'FM' factor to the applied voltage with any degree of certainty. This is because of the difficulty in determining the number and nature of the contacts between the two samples. If however

it is assumed that contact takes place at three points and that each contact is essentially circular, then it may be shown from the results recorded in Figure 6.2 that the effective radius of each silica contact is 30 microns. The approximate 'FM' factor at 1,000 volts is 33 Mv/m. In the case of the borosilicate glass contacts, the calculated radius is 12 microns which gives a 'FM' factor at 1,000 volts of 84 Mv/m.

6.3.2 Current Time Characteristic.

When a constant voltage is applied to the silica contacts there is no drop off in current with time. Since the main charge carrier is the electron, this result is as expected.

In the case of borosilicate glass samples the fall off in current was observed for voltages of 1,000 volts but not for voltages up to 250 volts over a time period of fifteen minutes. Over greater lengths of time however a drop off was observed at the lower voltages.

There are three factors which are associated with this phenomenon;

(i) A high electric field.

(ii) Points of contact and

(iii) Ionic conduction.

The most likely explanation for this, is the

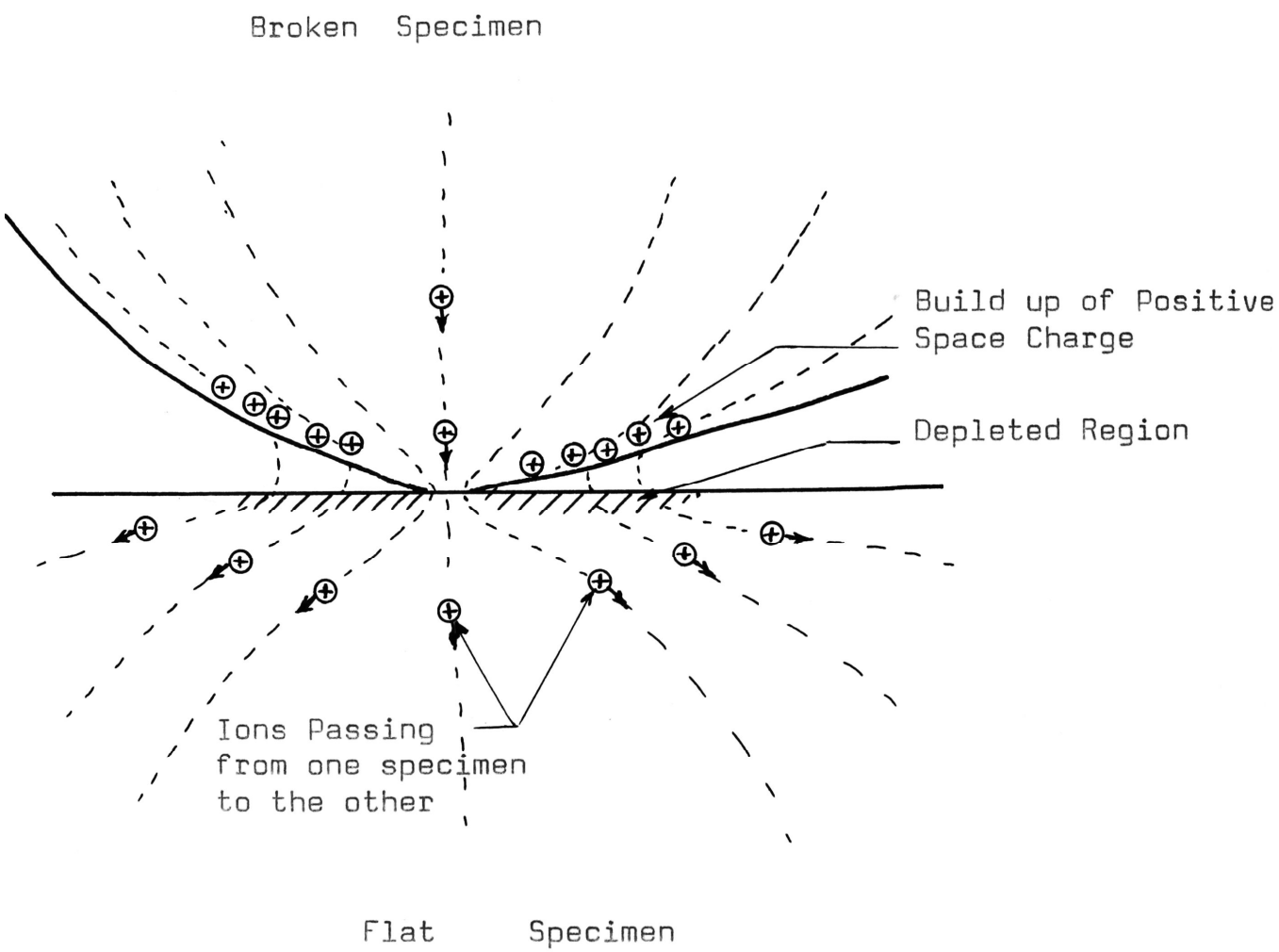

FIGURE 6.6 DIAGRAMATIC REPRESENTATION OF SPACE CHARGE BUILD UP AT CONTACT

build up of a space cloud of ions in the region of the contact. One possible mechanism by which this may occur is illustrated in Figure 6.6. The dotted lines represent the flow lines some of which cross the air gap. An ion on one of these will come to the surface of the particle and not be able to move across the gap as an electron can. It will then be fixed at this point. With time there will be a build up of a space charge which will slowly choke the current flow in this region. Normal conduction will continue at the actual point of contact except in so far as the field pattern is modified by the space charge. On the other side of the gap there will develop a deficiency of mobile carriers which will also contribute to the fall off of current.

Figure 6.5 provides some additional evidence to support this model. This shows that the current fall off with time is greater when the polarity of the broken specimen is made positive. Consider the case where a known voltage is applied across the contacts. In the initial stages, the field pattern will be independent of the direction of the field, as also will be the current. Irrespective of the polarity, the number of ions forming the space cloud around the contact points will be the same. If the broken specimen is made the anode, these ions will build up in the specimen as shown in Figure 6.6. Because of the geometrical shape of the region around the point, the ion concentration will

be greater in this case than it would be if the flat specimen was made the anode. This greater ion concentration in the former case will result in a greater space charge voltage drop and cause the current to fall off quicker than it would with the polarity reversed.

6.3.3 Spurious Pulses.

The absence of spurious pulses in these tests is consistent with the explanation of their origin given in Appendix II. This model assumes that metallic electrodes form an essential part of the pulse generating process and the absence of a metallic electrode in the high field region must mean that pulses cannot be generated.

CHAPTER 7.0

C O M P A C T I O N

7.1 Introduction.

Particulates found in their natural state are non-uniform in size and shape, and are not arranged in any predictable pattern. When compacted together this makes it very difficult to arrive at a suitable analytical expression for predicting their effective resistivity when compacted to form a particulate solid.

In order to obtain some understanding of the factors which govern the effective resistivity of compacted particulates, the effective resistivity of spherical particles packed in regular arrays is analysed. It is shown that the resistivity depends on the mode of packing and is independent of particle size for a constant applied pressure. A relationship between the effective resistivity and the bulk value of the material is established and a term is introduced to account for the effect of the applied electric field.

The random packing of spherical particles of uniform size is analysed and it is suggested that the effective resistivity may be related to the porosity in the same manner as it is for regular arrays. The effect of including small sized particles into a network of larger particles is discussed qualitatively.

A general expression is derived for the effective resistivity of a particulate solid. This takes into account the compaction, bulk characteristics of the material, the

Simple Cubic

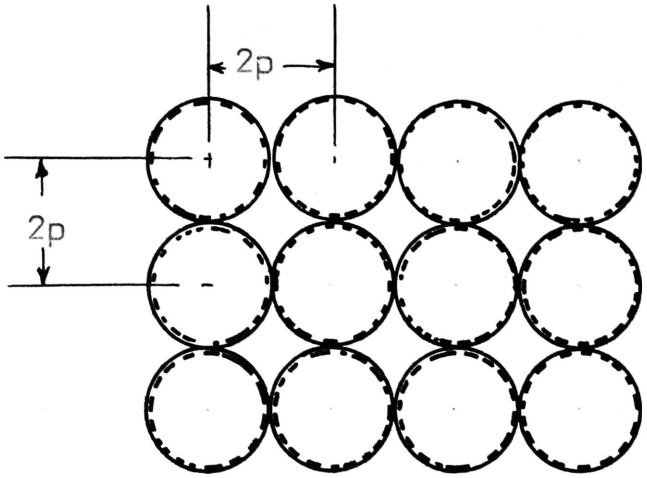

Orthorhombic

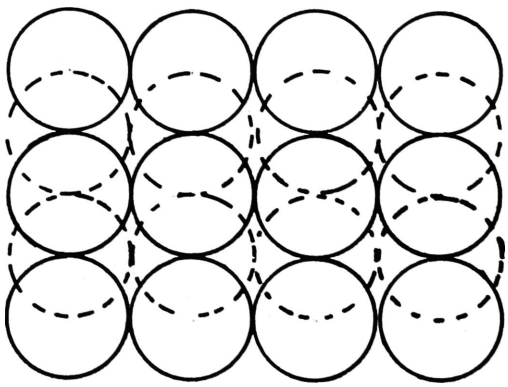

Pyramidal

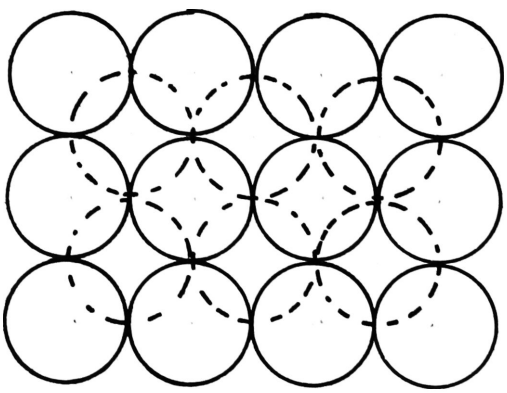

FIGURE 7.1 PACKING MODES FOR PARTICLES OF EQUAL SIZE. SQUARE BASE.

Cubical-Tetrahedral

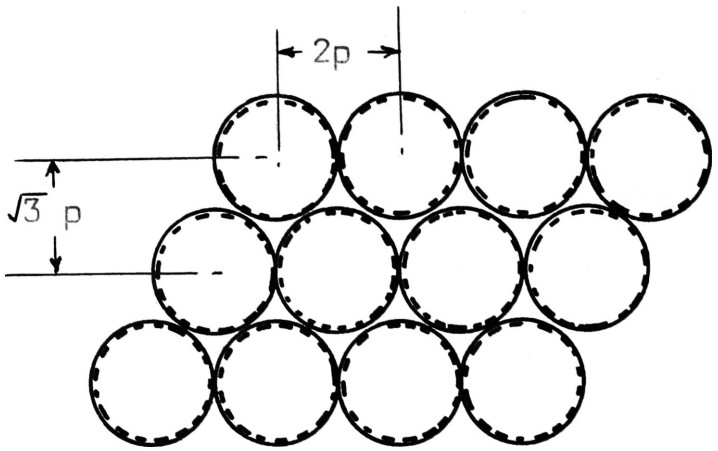

Tetragonal-Sphenoidal

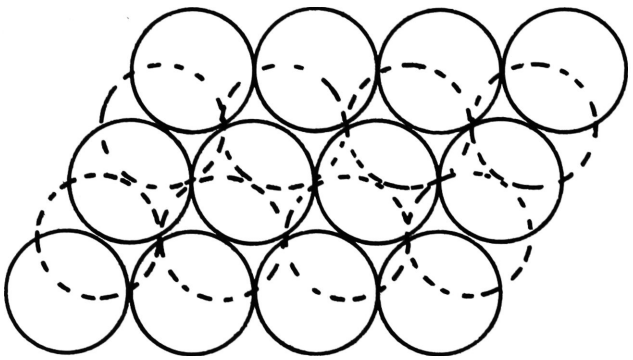

Tetrahedral

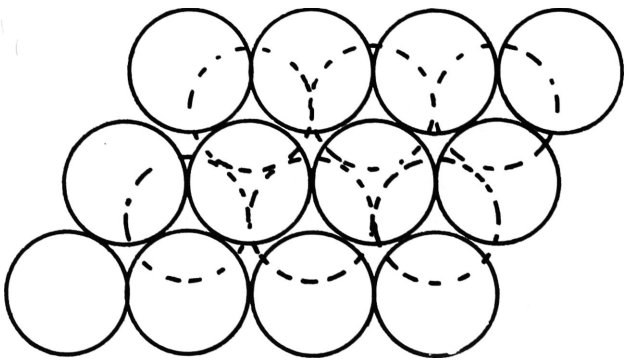

FIGURE 7.2 PACKING MODES FOR PARTICLES OF EQUAL SIZE. RHOMBIC BASE.

contact characteristics and the strength of the applied field.

7.2 Effective Resistivity of Regular Arrays.

7.2.1 Introduction.

It is possible to calculate the effective resistivity of a particulate solid made up of spherical particles of equal size compacted in a regular array between two parallel electrodes. In order to do this it is first of all necessary to consider the different manner in which the particles may be assumed to be packed. Figures 7.1 and 7.2 show the different packings considered (65). There are two basic types of layer; one is square and the other is rhombic. Each layer of the same type may be placed on a similar layer in three different ways so that a total of six different combinations are possible. Each diagram is a plan view of the array with one layer of particles shown by a solid line and the next layer by dotted lines.

If it is assumed that the compacted spheres are subject to a constant pressure, then the effective resistivity may be calculated providing the following assumptions are made:

(a) There are no frictional forces between adjacent particles, and between the walls of the container and the particles.

(b) At the points of contact between the particles,

elastic deformation takes place and the radius of the contact circle is given by the Hertz Equation.

(c) Only volume conduction takes place.

(d) The resistance of each contact is given by Holm's Equation. This assumes that the special effects due to high electric fields, type of charge carrier and dissimilar contact materials are negligible.

In order to have some point of reference, the effective resistivity of the simple cubic array is taken as standard, and all other combinations are expressed as a percentage of this.

7.2.2 Variation with Mode of Compaction.

The effective resistivity of each array will depend on how the pattern of the array will affect such parameters as the radius of contact, force at the contacts, number of contacts in series through which the current must flow, and the number of parallel paths available for the current flow.

Irrespective of the method of packing, the radius of contact between two particles is given by Equation 2.11

$$a = \sqrt[3]{\frac{3(1 - \nu^2)\, Fc\, p}{4Y}}$$

where the symbols have the meaning given to them in Chapter 2

and F_c is the force normal to the plane of contact.

If the particles are all made of the same material, this equation may be written as;

$$a = K_1 \sqrt[3]{F_c\, p} \qquad \text{..... 7.1}$$

Where $K_1 = \sqrt[3]{\frac{3(1 - \nu^2)}{4Y}}$

If the Holm Equation is used to calculate the effective resistance of these contacts, then the resistance of each contact is given by;

$$R_o = \frac{\rho}{2a} = \frac{\rho}{2 K_1 \sqrt[3]{F_c\, p}} \qquad \text{..... 7.2}$$

If it is assumed that the resistance of each contact is the same and that the resistance of the bulk of the particle is negligible compared with the contacts, then a close examination of each array will show that the flow of current will follow a regular pattern. The number of parallel paths for the current is equal to the number of particles in any one layer times the number of parallel paths in each particle. The number of contacts in series in any one of these parallel paths will also depend on the number of particles through which the current has to flow. This is a function of the particle size and the packing.

Given Ns as the number of series contacts per unit distance,

Np as the number of parallel paths per unit area,

then the effective low field resistivity is,

$$\rho_{eo} = \frac{\rho}{2 K_1 \sqrt[3]{F_c p}} \frac{Ns}{Np} \quad \ldots\ldots\ldots\ldots\ldots\ldots \quad 7.3$$

This equation is perfectly general for the arrays to be considered. The main task is to calculate the values of Fc, Ns and Np. These are shown in Table 7.1 for each of the arrays.

If the radius of each particle is p, then the number of these particles which will make up a unit distance with their centres all in a line is,

$$n = 1/2p \quad \ldots\ldots\ldots\ldots \quad 7.4$$

The number of contacts in series Ns in any one of the parallel paths is the same as the number of layers of particles in one unit of thickness. In the two cases where each layer is mounted directly above the lower layer, the number of layers per unit distance is n. Table 7.1 lists the values of Ns for other types of packing.

The number of parallel paths Np for the current is given by the number of particles per unit area of a layer, times the number of parallel paths in each particle. The number of particles in a unit area for a square layer is n^2 and $n^2 2/\sqrt{3}$ for the rhombic layer. Table 7.1 lists the values of Np for the different packing arrays.

If the total applied pressure P is the same for all arrays, then the force on each particle in contact with

TABLE 7.1

EFFECTIVE RESISTIVITY OF REGULAR ARRAYS OF SPHERICAL PARTICLES

Type of Packing	C	Porosity	Ns	Np	PP	Fc	RR
Simple Cubic	6	.4769	n	n^2	1	P/n^2	1.00
Cubical-Tetrahedral	8	.3954	n	$2n^2/\sqrt{3}$	1	$\sqrt{3}P/2n^2$	0.91
Orthorhombic	8	.3954	$2n/\sqrt{3}$	$2n^2$	2	$P/\sqrt{3}n^2$	0.70
Tetragonal-Sphenoidal	10	.2595	$2n/\sqrt{3}$	$4n^2/\sqrt{3}$	2	$P/2n^2$	0.63
Pyramidal	12	.2595	$\sqrt{2}n$	$4n^2$	4	$P/2\sqrt{2}n^2$	0.50
Tetrahedral	12	.2595	$\sqrt{3}n/\sqrt{2}$	$6n^2/\sqrt{3}$	3	$P/2\sqrt{2}n^2$	0.50

C = Co-ordination number.

Ns = Number of contacts in series per unit distance.

Np = Number of contacts in parallel per unit area.

PP = Current paths per particle.

Fc = Normal force at each contact point.

RR = Relative resistivity factor.

the electrode is P/n^2 for the square layer and $P\sqrt{3}/2n^2$ for the rhombic layer. The actual force 'Fc' normal to the contact surface depends on the number of contacts per particle and the angle the contact surface makes with the verticle. A summary of these values of Fc for the different arrays is tabulated in Table 7.1.

The effective resistivity of any array may now be found by substituting the appropriate values of K_1, Fc, Ns, Np and ρ in Equation 7.3. If the effective resistivity of the simple cubic array is taken as reference, then the effective resistivity of the other arrays can be expressed as a per unit value of this. The results for the different arrays are given in Table 7.1.

7.2.3 Variation with Particle Size.

The general expression for the resistivity of a regular array is given by Equation 7.3. If the variables in this are expressed as functions of 'n', then it can be easily shown that the resistivity is independent of 'n' and hence of the particle size.

For a constant applied pressure, the p/a ratio is constant. Using Equations 7.1 and 7.4 and that Fc is proportional to 1/n, it may be shown that:

$$p/a = K_2 / \sqrt[3]{P} \quad \ldots\ldots\ldots\ldots\ldots\ldots \quad 7.5$$

$$= \text{constant (For constant pressure).}$$

7.2.4 Variation with Pressure.

For particles compacted in a regular array, there would be no variation of the bulk density of the mixture with pressure. The slight variation due to the elastic deformation would be negligible. From Equation 7.3 the effective resistivity may be shown to be given by;

$$\rho_{eo} = \frac{K_3}{\sqrt[3]{P}} \quad \ldots\ldots\ldots\ldots\ldots\ldots\ldots \quad 7.6$$

The value of the constant will vary with the packing array. This equation shows that the resistivity varies inversely as the cube root of the pressure.

7.2.5 Relationship to Bulk Resistivity.

The effective resistivity of a particulate solid will be greater than that of the bulk value of the material itself. The general relationship is given by Equation 7.3, and this is equal to,

$$\rho_{eo} = H\rho \quad \ldots\ldots\ldots\ldots\ldots\ldots\ldots \quad 7.7$$

Where H is given by;

$$H = \frac{Ns}{Np\ 2\ K_1 \sqrt[3]{F_c\ p}} \quad \ldots\ldots\ldots\ldots \quad 7.8$$

Consider the case of a Simple Cubic array where the values of Ns, Np and Fc are given in Table 7.1. Hence it may be shown that,

$$H = p/a$$

For other packing arrays, the value of 'H' must be multiplied by the relative resistivity (RR) factor given in Table 7.1. The more general expression for 'H' is;

$$H = RR\ p/a = p/a'$$

Hence these packing arrays may be reduced to an equivalent Simple Cubic array, with an equivalent contact radius of;

$$a' = a/RR$$

7.2.6 Effect of High Electric Fields.

The analysis given in the previous sections assumes that the average electric field across the layer is sufficiently low to ensure that the voltage-current characteristics of the contacts are linear. For high electric fields however, this characteristic becomes non-linear. This feature has already been investigated in previous chapters.

Assume the different packing arrays are subject to the same average electric field E_{av}. The voltage across each contact Vc is given by;

$$Vc = E_{av}/Ns \qquad \ldots\ldots\ldots 7.9$$

It has already been shown in Chapter 2 that the basic parameter by which the electric field condition around the contact points may be examined is the 'FM' factor.

By definition,

$$FM = V_c / 2a$$

$$= \frac{E_{av}}{K_4 \, Ns \sqrt[3]{F_c/n}} \quad \text{from Equations 7.1 and 7.9}$$

In order to determine the value of the 'FM' factor for the different arrays, it is necessary to know the values of Ns and Fc. For the six regular arrays considered, these values are shown tabulated in Table 7.2. In the case of the Simple Cubic array, the expression reduces to;

$$FM = \frac{E_{av}}{K_4 \sqrt[3]{P}} \quad \ldots\ldots\ldots\ldots\ldots\ldots \quad 7.10$$

If this is taken as reference, then for a given applied electric field, the values of the 'FM' factor at the contacts with other packing arrangements may be expressed as a percentage of this. This is referred to as the relative field magnitude factor (RFM), and its magnitude for the different packing arrays is shown in Table 7.2. The net effect of the denser packing arrangements is to generally increase the 'FM' factor of the contacts above that for a Simple Cubic array, but in no case is this greater than fifteen percent.

A more general expression for the 'FM' factor is obtained by including the 'RFM' factor in Equation 7.10.

TABLE 7.2

RELATIVE 'FM' FACTORS FOR REGULAR ARRAYS

Type of Packing	N_s	F_c	RFM
Simple Cubic	n	P/n^2	1.00
Cubical-Tetrahedral	n	$\sqrt{3}P/2n^2$	1.05
Orthorhombic	$2n/\sqrt{3}$	$P/\sqrt{3}n^2$	1.04
Tetragonal Spheroidal	$2n/\sqrt{3}$	$P/2n^2$	1.09
Pyramidal	$\sqrt{2}n$	$P/2\sqrt{2}n^2$	1.00
Tetrahedral	$\sqrt{3}n/\sqrt{2}$	$P/2\sqrt{2}n^2$	1.15

$$\text{Hence} \qquad FM = \frac{E_{av}\, RFM}{K_4 \sqrt[3]{P}} \qquad \ldots\ldots\ldots\ldots\ldots\ldots \quad 7.11$$

$$= L\, E_{av} \qquad \ldots\ldots\ldots\ldots\ldots\ldots\ldots \quad 7.12$$

It has been shown in the previous chapters that for increasing values of the applied voltage across the contact, the voltage-current characteristic becomes non-linear and the resistance of the contact decreases. In the case of insulator to insulator contacts and the bulk characteristics of the metal to glass contacts, the contact resistance between two particles follows the general relationship,

$$Rc = Ro\, \epsilon^{-B\, FM}$$

From Equations 7.2 and 7.12;

$$Rc = Ro\, \epsilon^{-B\, L\, E_{av}}$$

$$= \frac{\rho}{2a}\, \epsilon^{-N\, E_{av}} \qquad \ldots\ldots\ldots\ldots\ldots\ldots \quad 7.13$$

Where $N = B\, L$

Consider one of the series paths with Ns contacts. The total resistance is given by;

$$Rs = \frac{Ns\rho}{2a} \epsilon^{-N E_{av}}$$

Since there are Np parallel paths in a unit area, the effective resistance, and hence resistivity, of the unit cube is;

$$\rho_e = \frac{\rho}{2a} \frac{Ns}{Np} \epsilon^{-N E_{av}} \quad \ldots\ldots\ldots\ldots \quad 7.14$$

$$\rho_e = \rho_{eo} \epsilon^{-N E_{av}}$$

Where ρ_{eo} is the effective resistivity of the array for low electric fields and is given by Equation 7.3.

7.2.7 General Expression for Effective Resistivity.

It is now possible to write down a general expression for the effective resistivity of a particulate solid made up of spherical particles arranged in a regular array. Using Equation 7.7 and 3.17, the effective resistivity for low average electric fields is;

$$\rho_{eo} = H A \epsilon^{\phi/kT} \quad \ldots\ldots\ldots\ldots\ldots\ldots \quad 7.15$$

Where the value of H is given by Equation 7.8.

It has already been shown in the previous section that this resistivity is reduced at higher values of applied electric field. Modifying Equation 7.15 by Equation 7.14, the general expression becomes;

$$\rho_{e} = H A \epsilon^{\phi/kT} \epsilon^{-N E_{av}} \quad \ldots\ldots\ldots\ldots \quad 7.16$$

7.3 Non-uniform Array.

7.3.1 Particles of Constant Size.

A further extension of this work is to consider the case of uniform spherical particles packed in some random manner. Assume that the particles do not cling together to create large voids.

Experiments on the random packing of equal spherical particles by Westman and Hugill (66) and by White and Walton

(67) have shown that packing porosities between 37.7 and 44.7 percent were obtained. Smith, Foote and Busang (68) carried out tests to determine the number of contacts with each particle as a function of the porosity. Deresiewicz (69) was able to find theoretically a relationship between the average number of contacts per sphere 'C' and the porosity 'V'. This is given by,

$$C = 26.4868 - 10.7262/(1 - V) \quad \ldots\ldots \quad 7.17$$

For a porosity of 0.3954, the calculated value of the average number of contacts is 8.7. It is of interest to note from Table 7.1 that this number of contacts per sphere is reasonably close to that for uniform spheres packed to give the same porosity.

Ridgway and Tarbuck (70) have given a summary of the experimental work of a number of investigators and have arrived at the empirical relationship:

$$V = 1.072 - 0.1193\,C + 0.00431\,C^2 \quad .. \quad 7.18$$

It is not possible to arrive at any simple analytical expression for the effective resistivity of randomly packed spherical particles, but it is quite likely that the relationships between resistivity, porosity and co-ordination number that exist for uniformly packed spherical particles will give some guidance for randomly packed particles. The

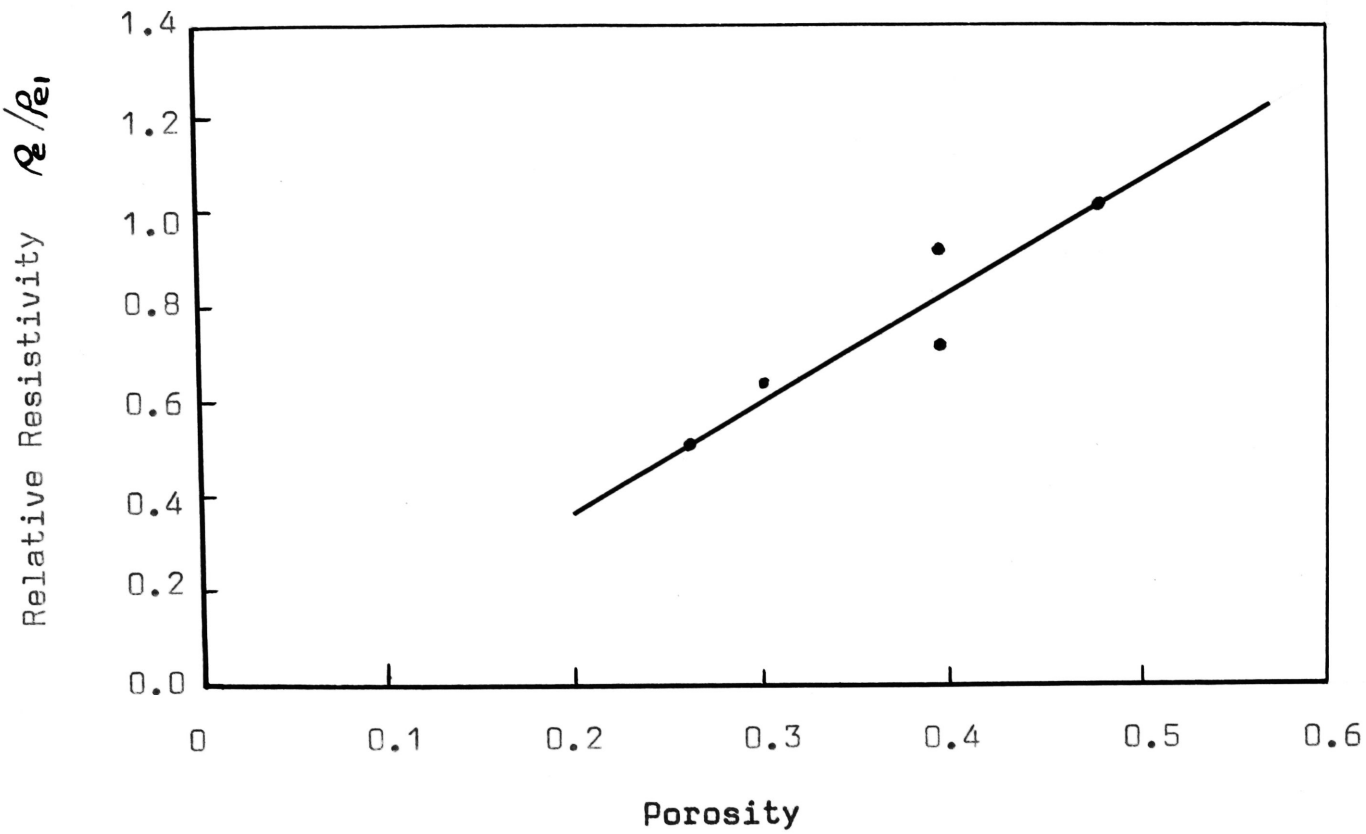

ρ_{e1} = Effective resistance of a simple cubic array

FIGURE 7.3 RELATIONSHIP BETWEEN RELATIVE RESISTIVITY AND POROSITY FOR REGULAR PACKING MODES OF SPHERICAL PARTICLES

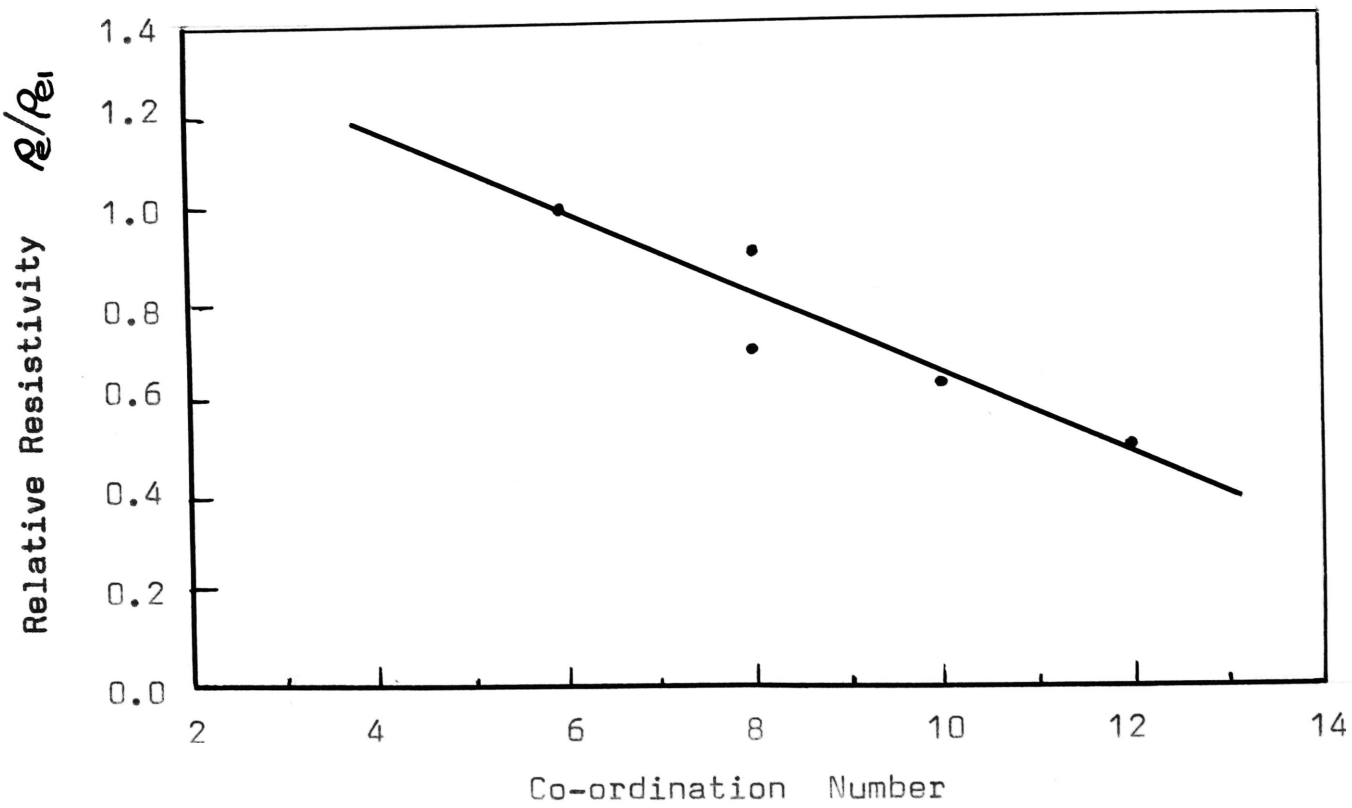

ρ_{e1} = Effective resistivity of a simple cubic array

FIGURE 7.4 RELATIONSHIP BETWEEN RELATIVE RESISTIVITY AND CO-ORDINATION NUMBER FOR REGULAR PACKING MODES OF SPHERICAL PARTICLES

relationships for uniformly packed spherical particles are shown plotted in Figures 7.4 and 7.3.

From an electrical point of view, it would be expected that the number of contacts per particle would be more significant than the porosity. Since however there is a very close relationship between the co-ordination number and the porosity, and since it is much easier to measure the porosity of a mixture than the average number of contacts per particle, Figure 7.3 may be used to indicate the possible relationship between the porosity and relative resistivity of randomly packed uniformly spherical particles.

If porosities between 37.7 and 44.7 percent are normal for this type of packing, then the relative resistivity could be expected to vary between 77 and 93 percent of the value for a simple cubic array, assuming the applied pressure is the same in all cases. Hence the effective resistivity of a random compaction would be less than that for a simple cubic array but never less than half.

7.3.2 Variable Sized Particles.

Powders found in practice usually have different sized particles which often follow a normal or log-normal distribution. This, combined with the random packing obtained in practice, makes it very difficult to find a simple analytical expression to determine the effective resistivity.

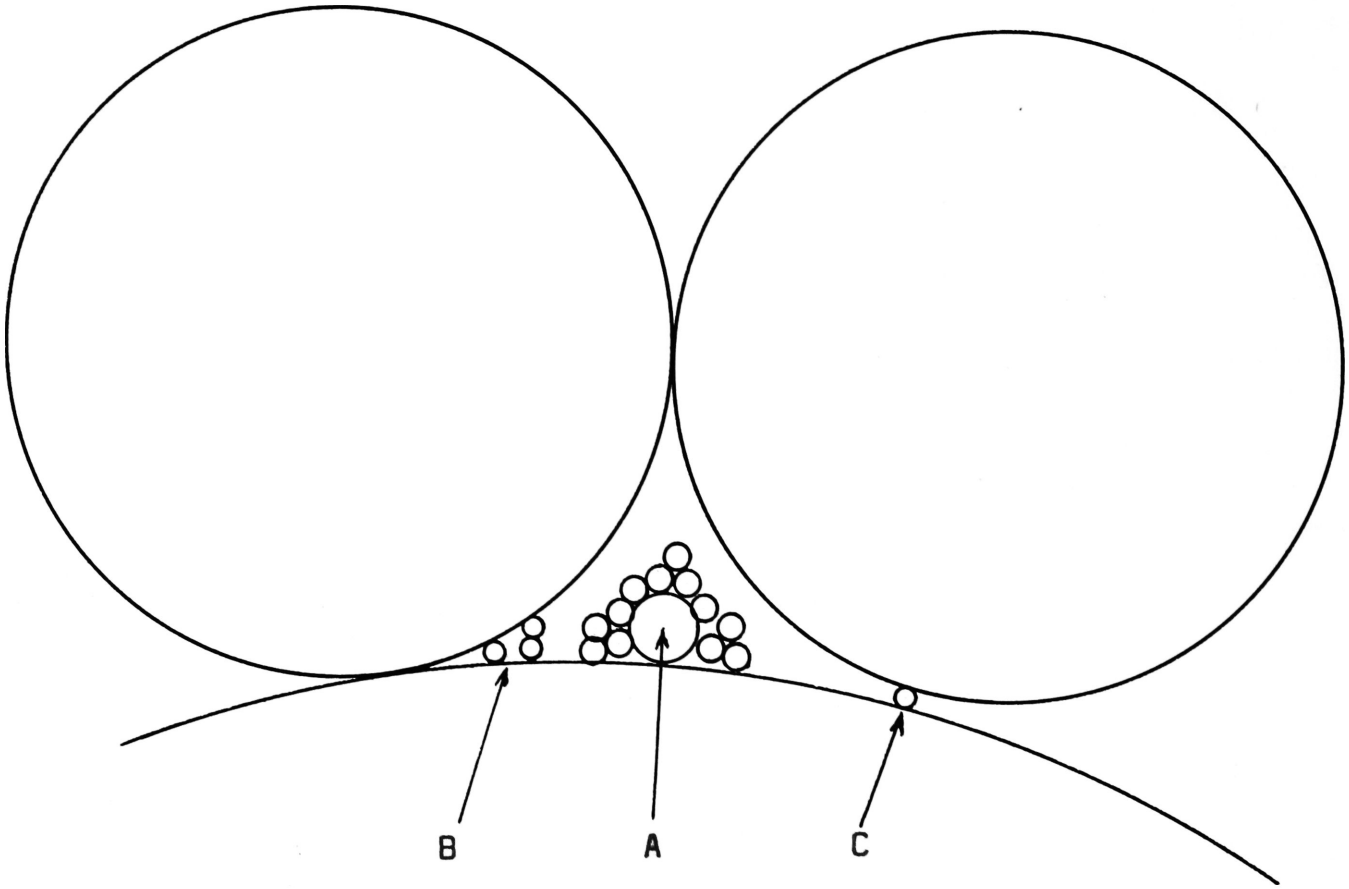

FIGURE 7.5 POSSIBLE POSITIONS OF SMALL DIAMETER PARTICLES IN A NETWORK OF LARGER PARTICLES

In order to obtain some understanding of the effect of the size distribution of particles, consider the case where a number of small particles is added to an existing mixture made up of much larger particles. These smaller particles may affect the mixture in three different ways.

(1) Some of the particles will fill in the voids between the larger particles in such a way as to reduce the porosity but not contribute in any way to the overall conductivity of the mixture. This is represented by 'A' in Figure 7.5.

(2) Other particles will fill the voids between the larger particles and also contribute to the improvement of the overall conductivity by providing an additional parallel path to that of the main contact. This is represented by 'B' in Figure 7.5.

(3) Other particles may place themselves between two large particles in such a way so as to only slightly increase the porosity but considerably increase the resistance of the current flow in that area. This is represented by 'C' in Figure 7.5.

It is to be expected that a mixture of sizes will generally reduce the porosity but it is not possible at this stage to predict how the effective resistivity will vary. The experimental work in Chapter 8 however, indicates

that the effect of adding small diameter particles to a mixture of larger particles is to reduce the effective resistivity of the resultant particulate solid.

7.3.3 General Expression for Effective Resistivity.

Consider the case of a unit cube of the particulate solid. The total resistance of any one of the parallel paths through the cube is the sum of the individual resistances of the contacts. If it is assumed that the effective electric field through the particulate solid is constant E_{av}, the total resistance of one of the parallel paths is;

$$Rs = Rc_1 + Rc_2 + Rc_3 + \cdots + Rc_{Ns}$$

Substituting in this series Equation 7.13, the total series resistance becomes;

$$Rs = \frac{\rho}{2} \sum_{n=1}^{Ns} \frac{\epsilon^{-N_n}}{a_n} E_{av}$$

The summation of this series gives an expression which cannot be conveniently used in calculations. The series can be modified to a more useful form by replacing each contact in the series path by the same number of contacts of radius a_e. The value of this effective radius is such that the total resistance of the path is unchanged. The resistance of the series path now becomes;

$$Rs = \frac{\rho\, Ns}{2\, a_e}\, \epsilon^{-N'E_{av}} \qquad \ldots\ldots\ldots\ldots\ldots \quad 7.19$$

where N' is the effective value of the constant in the exponent of the exponential.

If it is now assumed that the number of parallel paths in a unit area is Np, and that the total resistance of each path is approximately the same, the effective resistivity of the unit cube is;

$$\rho_e = (\rho\, Ns/2\, a_e\, Np)\, \epsilon^{-N'\, E_{av}}$$

$$= \rho\, H' \epsilon^{-N'\, E_{av}} \qquad \ldots\ldots\ldots\ldots\ldots\ldots \quad 7.20$$

$$= H'\, A\, \epsilon^{\emptyset/kT}\, \epsilon^{-N'\, E_{av}} \qquad \ldots\ldots\ldots\ldots \quad 7.21$$

Equation 7.21 is of the same form as Equation 7.16, the general expression for a regular array. It is not possible to predict the magnitudes of the constants H' and N' by any simple analytical means, and at this stage they can only be obtained empirically.

The relationship between the current density and the applied electric field is;

$$J = (E_{av}/\rho\, H')\, \epsilon^{N'\, E_{av}} \qquad \ldots\ldots\ldots\ldots\ldots \quad 7.22$$

CHAPTER 8.0

CONDUCTION IN PARTICULATE SOLIDS

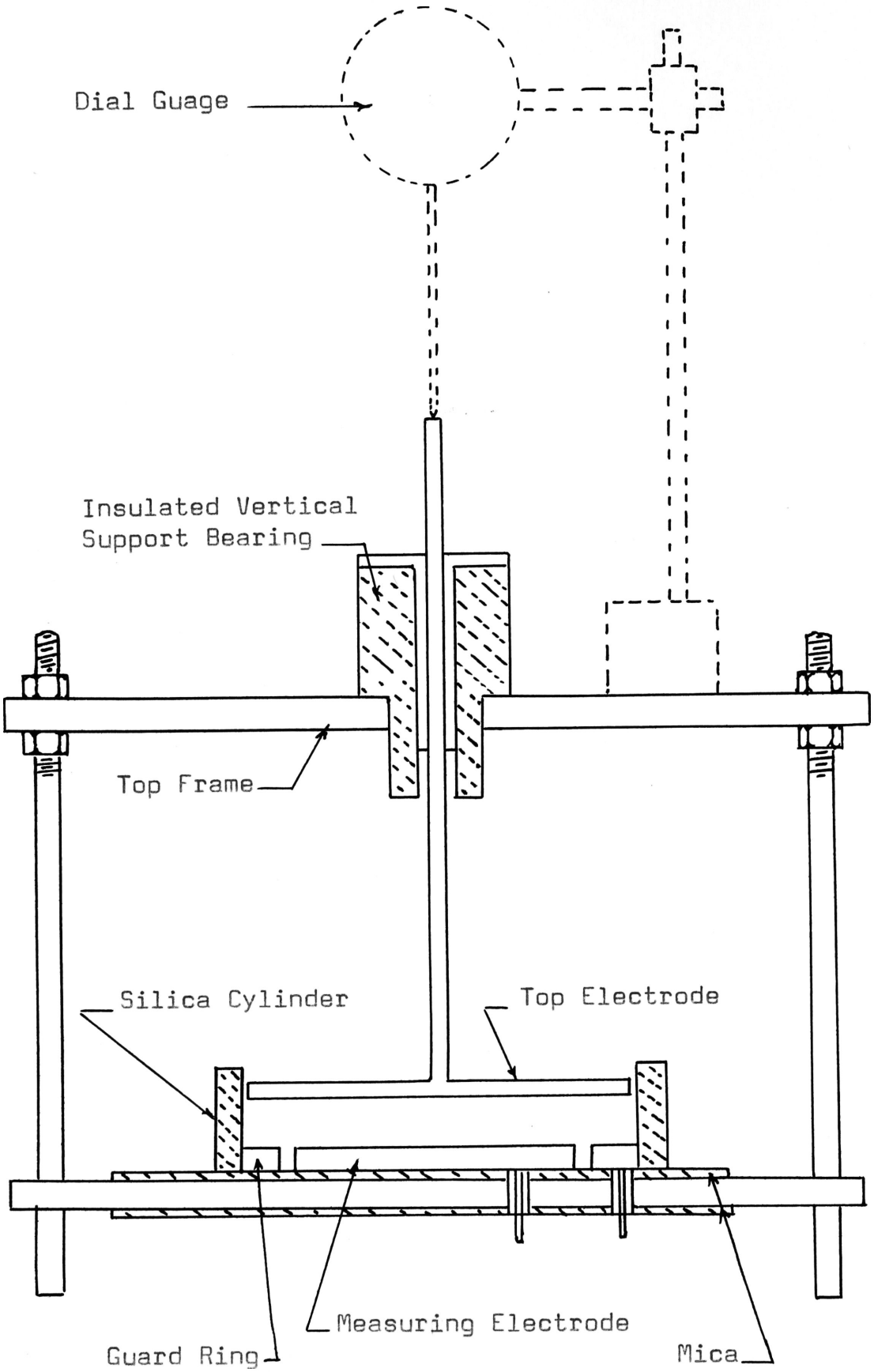

FIGURE 8.1 APPARATUS FOR MEASURING RESISTIVITY OF PARTICULATE SOLIDS

8.1 Introduction.

This chapter records some typical overall electrical characteristics of the borosilicate glass and silica samples after they have been ground to a powder and compressed between two metal electrodes. These are then explained in terms of the characteristics of the scaled up models of the point contacts, the bulk characteristics of the glass and the mode of compaction.

In order to illustrate the work in the rest of the thesis, a set of results has been obtained for a sample of fly-ash and its characteristics are explained in terms of the theory developed in the thesis.

8.2 Characteristics of Glass Samples.

8.2.1 Experimental Method.

The apparatus used for these tests is shown in Figure 8.1. This comprises two parallel plates with a guard ring around the bottom plate. The top electrode is free to move in the vertical axis and can be adjusted in the horizontal axis by means of nuts on the vertical supports. A d.c. voltage is applied to the top electrode and the current through the bottom measuring electrode is measured by the Keithley Electrometer 610B. An insulated coaxial screened cable is used to connect the bottom measuring electrode to the instrument. The guard ring current is carried by the

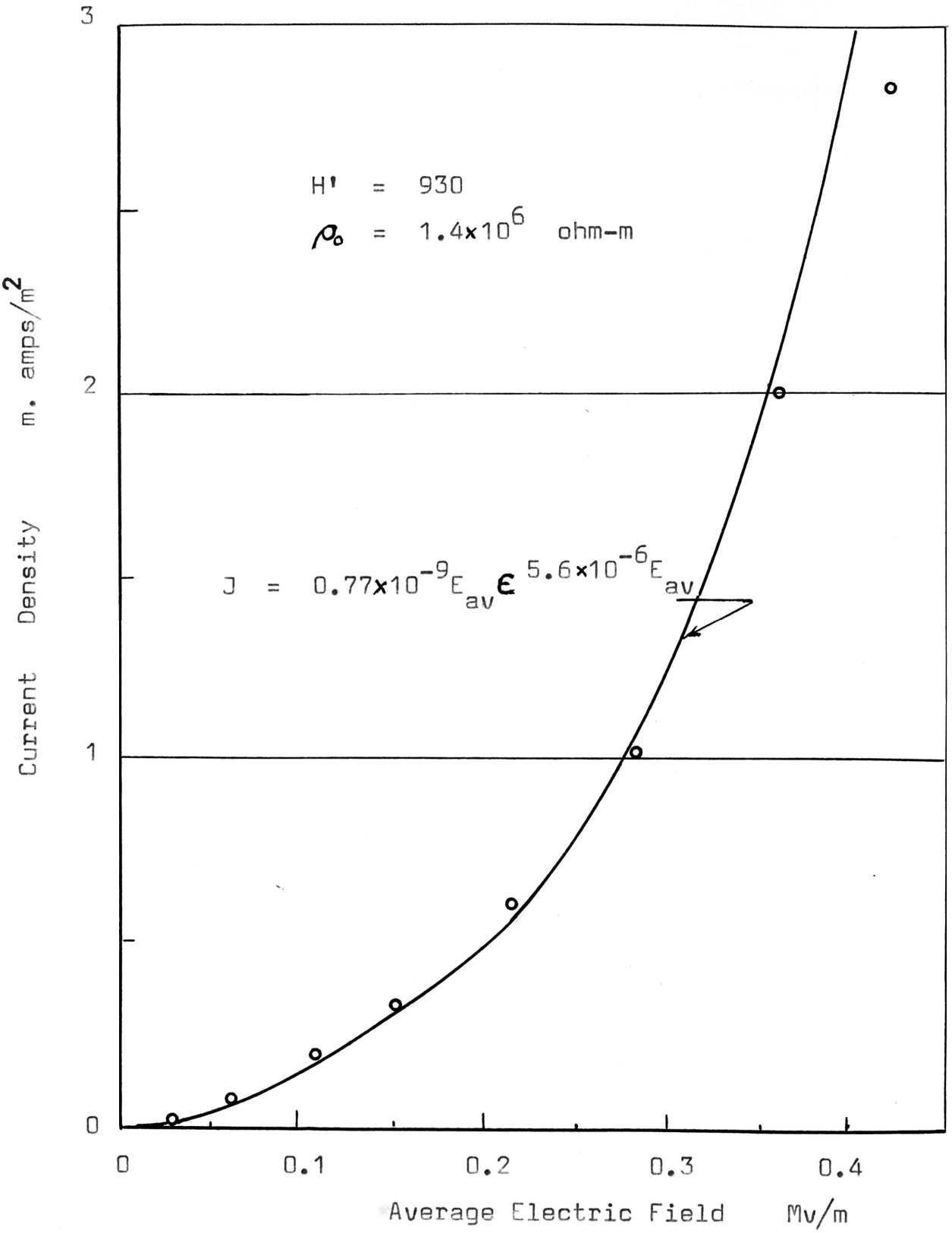

FIGURE 8.2 VARIATION OF CURRENT DENSITY WITH ELECTRIC FIELD. BOROSILICATE GLASS PARTICLES. SIZE 210 - 300 MICRONS. TEMPERATURE = 225 °C.

screen to earth. Considerable care is necessary to eliminate the effects of external electric fields.

The samples of silica and borosilicate glass to be tested were cleaned in alcohol and then ground to a powder. This was then sieved and the following mixtures made up:

A. Full range of sizes resulting from the grinding.

B. 210 to 300 micron range.

C. Less than 210 microns.

D. A mixture of equal volumes of B and C.

The sample to be tested was placed on the bottom electrode of the apparatus, the top electrode lowered onto the surface of the layer and the sample compressed with a weight of two kilogrammes.

For each of the mixtures, the following tests were carried out at a number of different temperatures.

(i) E-J characteristics.

(ii) The time variation of current for a constant applied voltage.

(iii) The time variation of current for different values of applied voltage.

8.2.2 Borosilicate Glass Results.

Figure 8.2 shows a typical plot of the

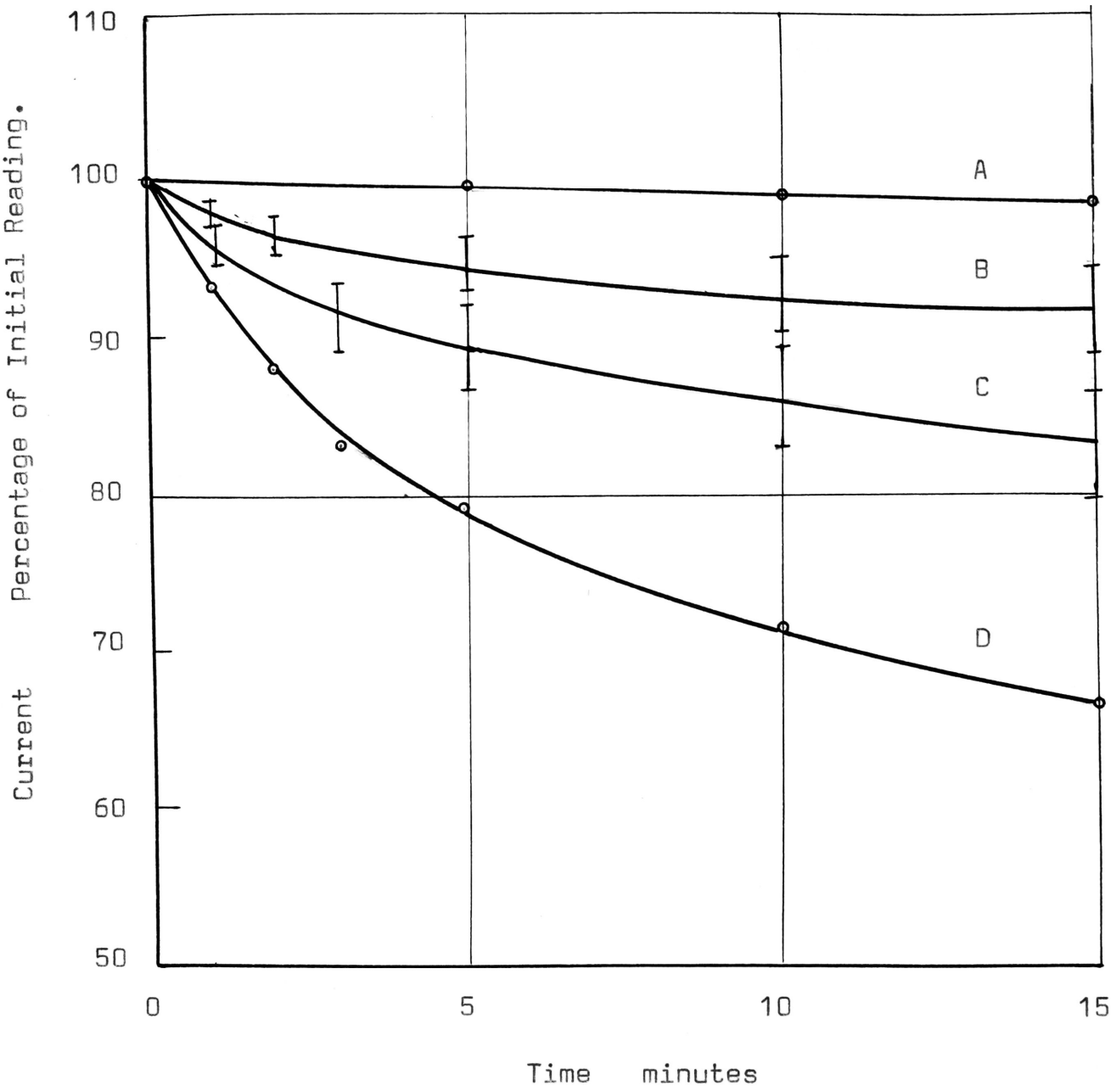

A Full range including 2,000 microns.

B Less than 210 microns.

C Equal volumes of 210 - 300 micron size range and the size range less than 210 microns.

D 210 - 300 microns.

FIGURE 8.3 CURRENT-TIME RELATIONSHIP FOR DIFFERENT MIXTURES OF BOROSILICATE PARTICLES. TEMPERATURE = 225°C. ELECTRIC FIELD STRENGTH = 0.33 MV/M.

variation of current density with applied electric field for a particle range of 210 to 300 microns at a temperature of 225°C. The characteristics for other temperatures and mixtures were similar. Equation 7.22 is also shown plotted with constants H' and N' adjusted to fit the experimental points.

If the effective resistivity for the given mixture is plotted against the reciprocal of the absolute temperature on semi-log graph paper then it follows the equation:

$$\rho_e = H' A \epsilon^{9,800/T} \quad \ldots\ldots\ldots\ldots\ldots\ldots \quad 8.1$$

In order to obtain some indication of the effect of the different mixtures of particle sizes on the effective resistivity of the particulate solid, the effective resistivities at low electric fields were compared with the bulk value of the material at that temperature. The results are shown tabulated in Table 8.1.

For any one mixture, the value of H' recorded is the average of a number of readings taken at different temperatures.

Figure 8.3 records the variation of the current with time for a fixed temperature of 225°C and applied electric field of 0.33 MV/m but with different mixtures of particle sizes.

In order to illustrate the effect of temperature,

TABLE 8.1

THE 'H' VALUES OF PARTICULATE SOLIDS

BOROSILICATE GLASS

Size Range microns		Electric Field MV/m	H'
210 - 300	B	0.01	930
Mixture	D	0.01	850
Less than 210	C	0.01	700

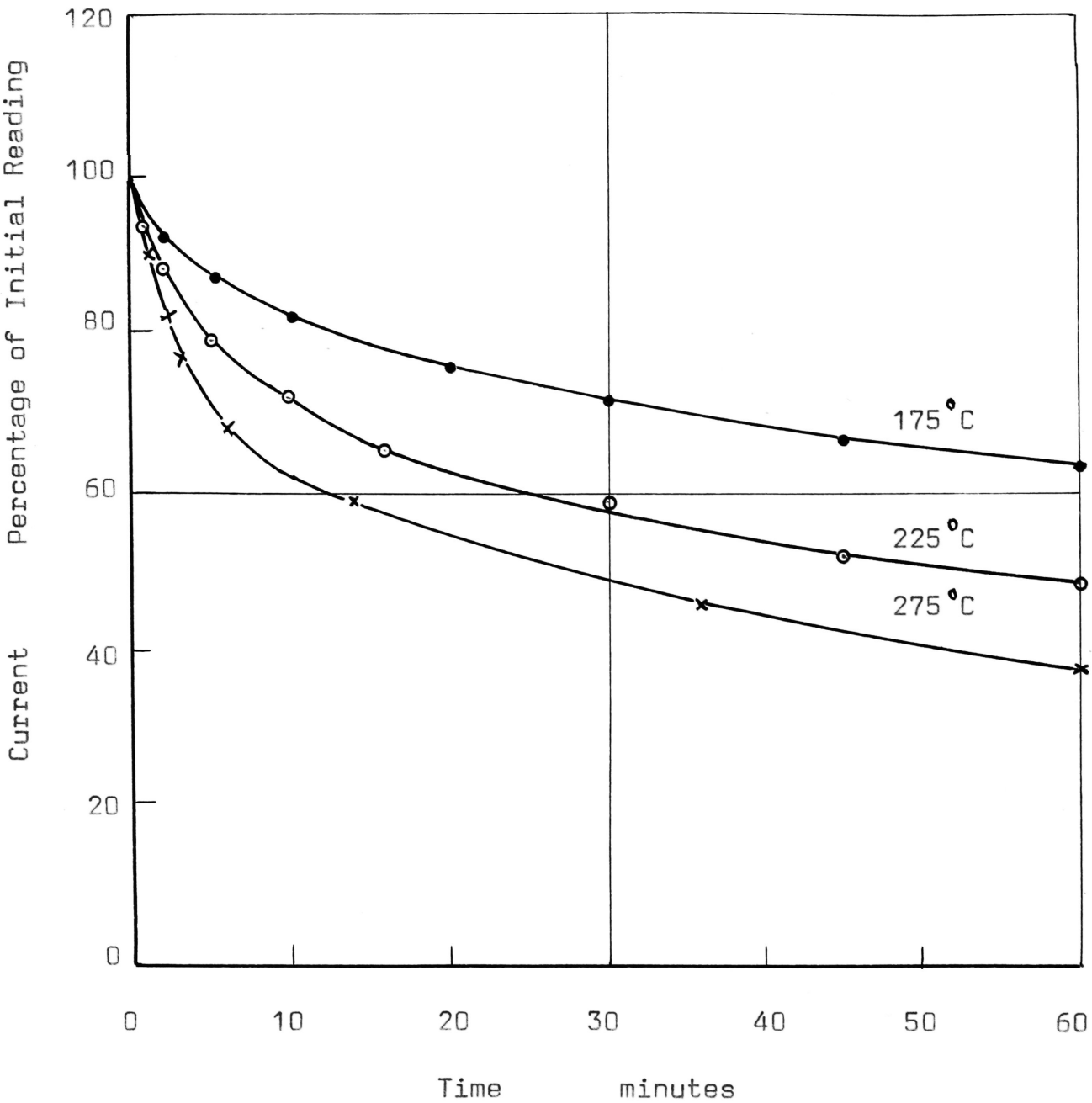

FIGURE 8.4 CURRENT-TIME RELATIONSHIP FOR DIFFERENT TEMPERATURES. BOROSILICATE GLASS PARTICLES 210 TO 300 MICRONS.

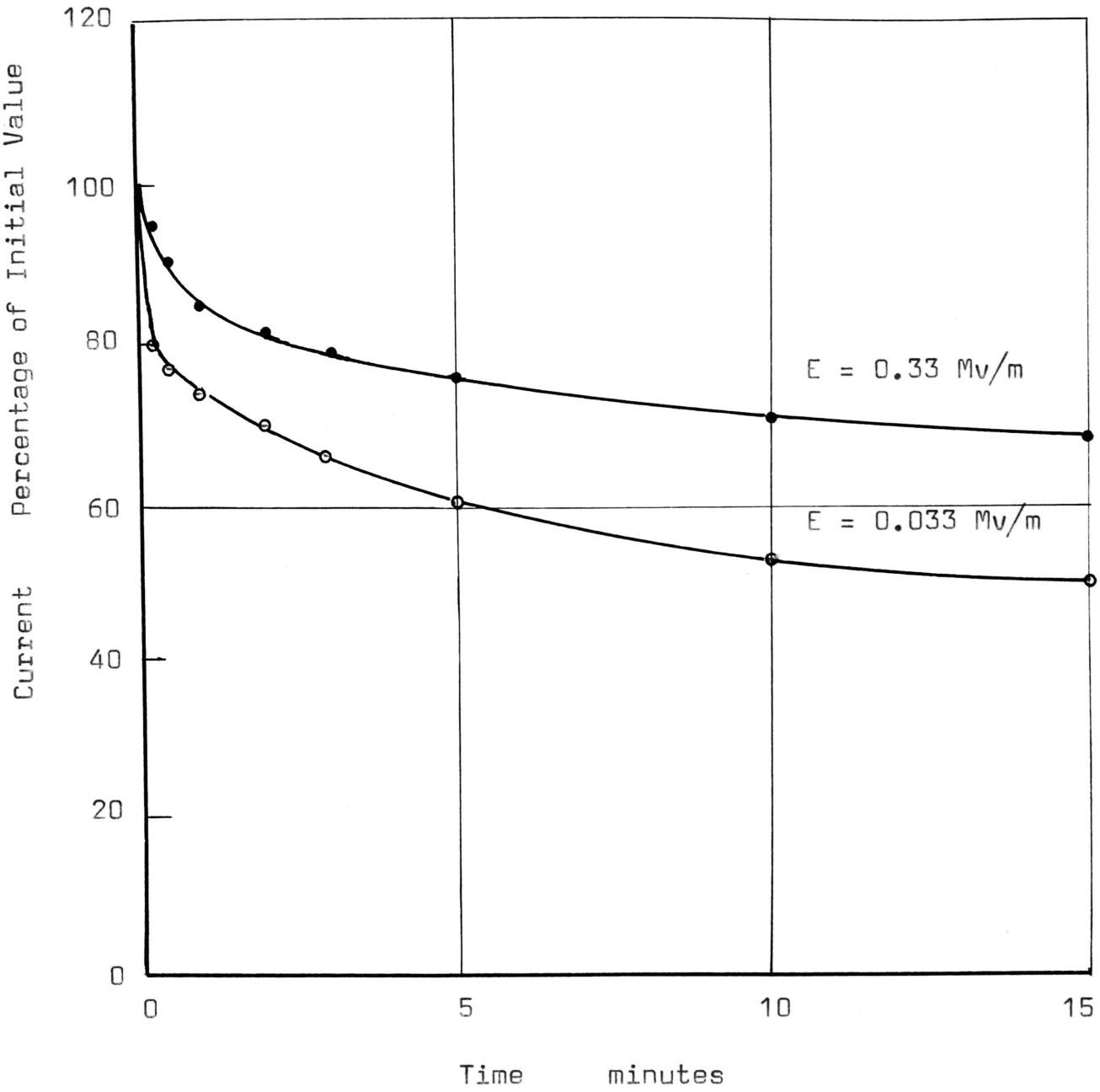

FIGURE 8.5 CURRENT-TIME RELATIONSHIP FOR DIFFERENT ELECTRIC FIELDS. BOROSILICATE GLASS PARTICLES 210 TO 300 MICRONS. TEMPERATURE = 225 ^{o}C.

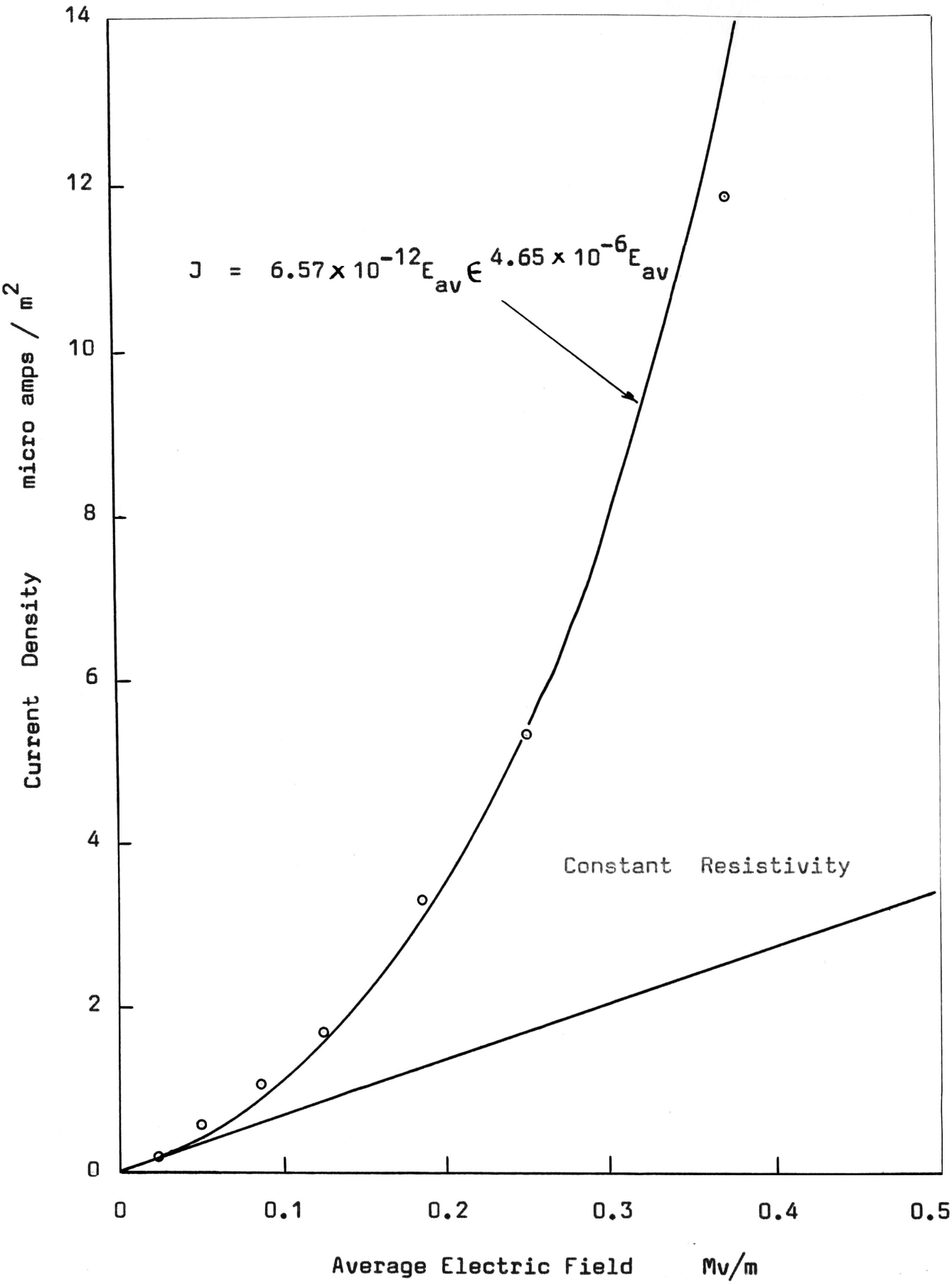

FIGURE 8.6 VARIATION OF CURRENT DENSITY WITH ELECTRIC FIELD. SILICA PARTICLES. SIZE 210 - 300 MICRONS. TEMPERATURE 282 °C.

Figure 8.4 records the current variation for the mixture 210 to 300 microns at temperatures 175, 225 and 275°C. In each case the applied electric field is 0.33 MV/m.

Figure 8.5 records a typical set of current-time characteristics for different values of applied electric field.

8.2.3 Silica Results.

Voltage-current characteristics were obtained for mixtures containing the size ranges shown in Table 8.2 for a number of different temperatures. A typical result is shown in Figure 8.6 for a mixture containing particle sizes between 210 and 200 microns at a temperature of 282°C. Equation 7.22 is also shown plotted with the constants H' and N' adjusted to fit the experimental points.

If the effective resistivity of the mixture is plotted against the reciprocal of the absolute temperature on semi-log graph paper then it follows the equation;

$$\rho_e = H'A' \epsilon^{15,300/T}$$

The temperature dependence of the bulk resistivity of the particular sample of silica used for this test is given by;

$$\rho = 7.0 \times 10^{-4} \epsilon^{15,320/T}$$

From these results, a comparison is made of the effective resistivity of the particulate solid with the bulk

resistivity of the material itself, at the same temperature. This is done for three different mixtures of particles and the results are recorded in Table 8.2. For any one mixture, the value of H' recorded is the average of a number of readings taken at different temperatures.

The current-time variations for constant applied voltage that were observed, were due entirely to the parameters of the measuring circuit. It was found that the time constant of the decay increased with a decrease in temperature and that it always settled to a steady value. Each time the test was repeated, the current transient followed the same curve and settled at the same steady state value.

When a voltage was first applied to a fresh mixture of particles the presence of spurious pulses were observed in the current flow. These pulses tended to have the following characteristics.

(i) They only existed with fresh mixtures of particles.

(ii) They were most numerous when the voltage was first applied. Over an initial period they were of both signs but later were mainly of negative polarity.

(iii) After a period of five minutes they disappeared altogether.

(iv) They were temperature dependent, being more obvious at lower temperatures than at higher temperatures.

TABLE 8.2

THE 'H' VALUES OF PARTICULATE SOLIDS

SILICA

Size Range microns		Electrie Field Mv/m	H'
210 - 300	B	0.01	223
Mixture	D	0.01	170
Less than 210	C	0.01	92

8.3 Discussion of Glass Characteristics.

8.3.1 The E-J Characteristics.

For both silica and borosilicate glass, the point of deviation from linearity begins at much lower electric fields when the glass is in the particulate form than it does when in the solid form. Table 8.3 gives the values of the electric field at which the deviation is 10 percent.

This non-linear relationship is attributed to the electrical characteristics of the point contacts between the particles themselves, and between the surface particles and metal electrodes. A detailed description of this phenomenon is given in Section 4.5 and 5.4. Because of the particulate form of the layer, the current in passing from one particle to another, must do so by flowing through their common points of contact. As has been shown in Chapter 2, very high electric fields are produced in the region adjacent to the points of contact, thus affecting the overall characteristics in two ways.

(i) The bulk resistivity of the material is reduced with increasing electric field.

(ii) Charge transfer takes place across the airgap in the region adjacent to the contact.

The effect of both of these is to reduce the effective resistance of the contacts and so reduce the

TABLE 8.3

ELECTRIC FIELDS GIVING TEN PERCENT DEVIATION FROM LINEARITY FOR SOLIDS AND PARTICULATES.

Material	Form	Temperature °C	Electric Field Mv/m.
Silica	Solid	275	1·500
	Particulate	275	0·025
Borosilicate Glass	Solid	225	2·500
	Particulate	225	0·030

overall resistance of the layer, causing the effective resistivity to decrease with electric field strength.

Since low average electric fields through the layer cause high electric fields to exist around the points of contact, the deviation from linearity of the E-J characteristic will begin at much lower applied fields when the glass is in the particulate form than it does when the glass is in the solid form.

The non-linear characteristics of both materials in the particulate form can be made to fit Equation 7.22 derived in Chapter 7.

$$J = \frac{E_{av}}{\rho H'} \epsilon^{N'E_{av}} \quad \ldots\ldots\ldots\ldots\ldots\ldots \quad 8.2$$

Where H', N', and ρ are constants.

The only other factor which could cause the non-linearity is the internal heating due to the Joule effect. This could be detected by observing a current increase with time, but for the test conditions described in this thesis, this did not occur. This is also consistent with the observations made with the scaled up point contacts. Although some heating must take place at the contacts, it must be regarded as having negligible effect on the overall characteristics.

8.3.2 Temperature Dependence.

The activation energy for both silica and

borosilicate glass in the particulate form is the same as when the glass is in the solid form. This result is in agreement with the model developed in Section 7.3.3 for the general expression for the effective resistivity. There is no reason to expect anything different.

8.3.3 Compaction.

Tables 8.1 and 8.2 indicate that the effect of introducing smaller diameter particles into a network of larger particles is to reduce the effective resistivity. Although it is possible, as discussed in Section 7.3.2, that some of the smaller particles may place themselves between two larger particles and so increase the resistance, many more must provide parallel paths for the current and so reduce the effective resistance of the contacts.

The results also indicate that the resistance is further reduced if a wide distribution of particle sizes is present as in the case of the mixture with particles of less than 210 micron diameter.

The effective resistivity of a particulate solid at low applied electric fields may be from 100 to 1,000 times the bulk resistivity of the material itself. The exact value depends on the pressure, particle size distribution and the shapes of the particles themselves. Because of the non-linearity characteristic, this value will be

reduced by an order of one magnitude for electric fields of 0.1 Mv/m.

One of the main difficulties in obtaining consistent results, is the uneven compaction of the particulates in the measuring chamber. Since the particles do not flow like a liquid, it is possible to obtain pressure differentials over the surface of the layer so that a firm contact is only made at a few points on the surface. By taking care in spreading out the particulates evenly before the top plate is lowered, the effect of this can be minimised.

8.3.4 Equation for the Effective Resistivity.

It is now possible to write the general equation for the effective resistivities of particulate solids made from silica and borosilicate glass.

Silica.

$$\rho_e = H'(7.0 \times 10^{-4} \epsilon^{15,320/T}) \epsilon^{4.65 \times 10^{-6} E_{av}} \quad .. \quad 8.3$$

Borosilicate Glass.

$$\rho_e = H'(3.8 \times 10^{-3} \epsilon^{9,810/T}) \epsilon^{5.6 \times 10^{-6} E_{av}} \quad ... 8.4$$

8.3.5 Time Dependence of the Current.

(a) Silica.

The transient observed when the voltage is first applied is due entirely to the time constant of the measuring circuit. This is consistent with the characteristics observed in Section 3.5.2.

(b) Borosilicate Glass.

The time dependence of the current is a contact phenomenon. At the cathode the effective resistance of the contacts between the electrode and the first layer of particles will gradually decrease. This is due to the injection of electrons into the particles at their point of contact with the metal electrode and their drift into the particle. This has been described in some detail in Section 5.4.4. Since however these are in series with the contacts in the bulk of the layer, their effect on the overall characteristic is negligible.

The main factor responsible for the current decay is the characteristic of the contacts at the anode. A detailed description of the effects taking place at the anode is given in Section 5.4.3. It is attributed to the depletion in the density of mobile carriers adjacent to the points of contact with the metal electrode. This increases the resistance of the contacts and so reduces the overall current.

That this effect is the same as described in

Section 5.4.3 is confirmed by the following observations.

(i) The temperature dependence is the same. As can be seen by comparing Figures 8.4 and 5.6, the rate of current decay increases with temperature in both cases.

(ii) In both cases, when the voltage was removed after a current-time run, and then re-applied after a lapse of five minutes, the current was the same as that just before the voltage was removed. This indicates that the same type of 'permanent' change has taken place.

(iii) The percentage variation of the current decay expressed as a function of the electric field is similar in both cases. As can be seen from Figures 8.5 and 5.6 the variation in both instances is greater at lower electric fields.

The dependence of the current decay on particle size distribution is shown in Figure 8.3. In general the wider and the more even the size distribution, the less is the effect of the anode characteristic. The smaller particles will tend to fill up the spaces between the larger particles at the contact surface and so increase the effective area of contact with the electrode. As the contact area increases, the current decay will decrease. At the limit where contact is made over the whole area there would be no fall off in the current with time.

The very small drop in current with the full range of particle sizes is due to the presence of the large

particles. It was observed that some of these were on the surface of the layer with their flat sides facing upwards against the anode. If the main current flow from the anode into the particulate solid took place through these points, then no current decay would be expected.

8.4 Characteristics of Flyash.

8.4.1 Introduction.

The purpose of this section is to record some typical characteristics of flyash and then use the results of the previous sections to explain the characteristics observed. The sample tested was supplied by the Electricity Commission of New South Wales from hoppers of the electrostatic precipitators of Tallawarra Power Station, New South Wales. This flyash has the highest resistivity in the State and is particularly difficult to precipitate. Some chemical and other details of this flyash are given in the Appendix I.

8.4.2 Experimental Method.

The apparatus used for these tests is shown in Figure 8.1. The flyash to be investigated was first placed in a flat dish and heated to a temperature of 200^{o}C for twenty-four hours to thoroughly dry it out. This was then placed in the measuring chamber and the top

electrode carefully lowered. Particular care was taken to ensure that contact was made over the whole surface. The total weight of the top electrode was 300 gms. The depth of the dust was measured with the dial gauge. The whole apparatus was placed in the oven and reheated again at maximum temperature for a further period of twenty-four hours. Voltage-current measurements were then made at temperatures of 268, 220, 197, 164, 143, 135 and 76°C. During these tests the layer of flyash was left undisturbed. Some of the flyash was then removed out of the chamber and the procedure repeated. Complete sets of readings were obtained for four different depths. In every case, the current transients were allowed to die away before readings were taken.

A separate series of measurements were made to determine the time dependence of the current decay. The circuit used is the same as in Figure 8.1. A step voltage was applied to the top electrode and the current decay measured with a storage C.R.O. and a stop-watch. Tests were carried out between the temperatures of 145 and 240°C and for each temperature the time constant of the circuit was altered by varying the input resistance of the electrometer used to measure the current.

8.4.3 Results.

A typical plot of the electric field

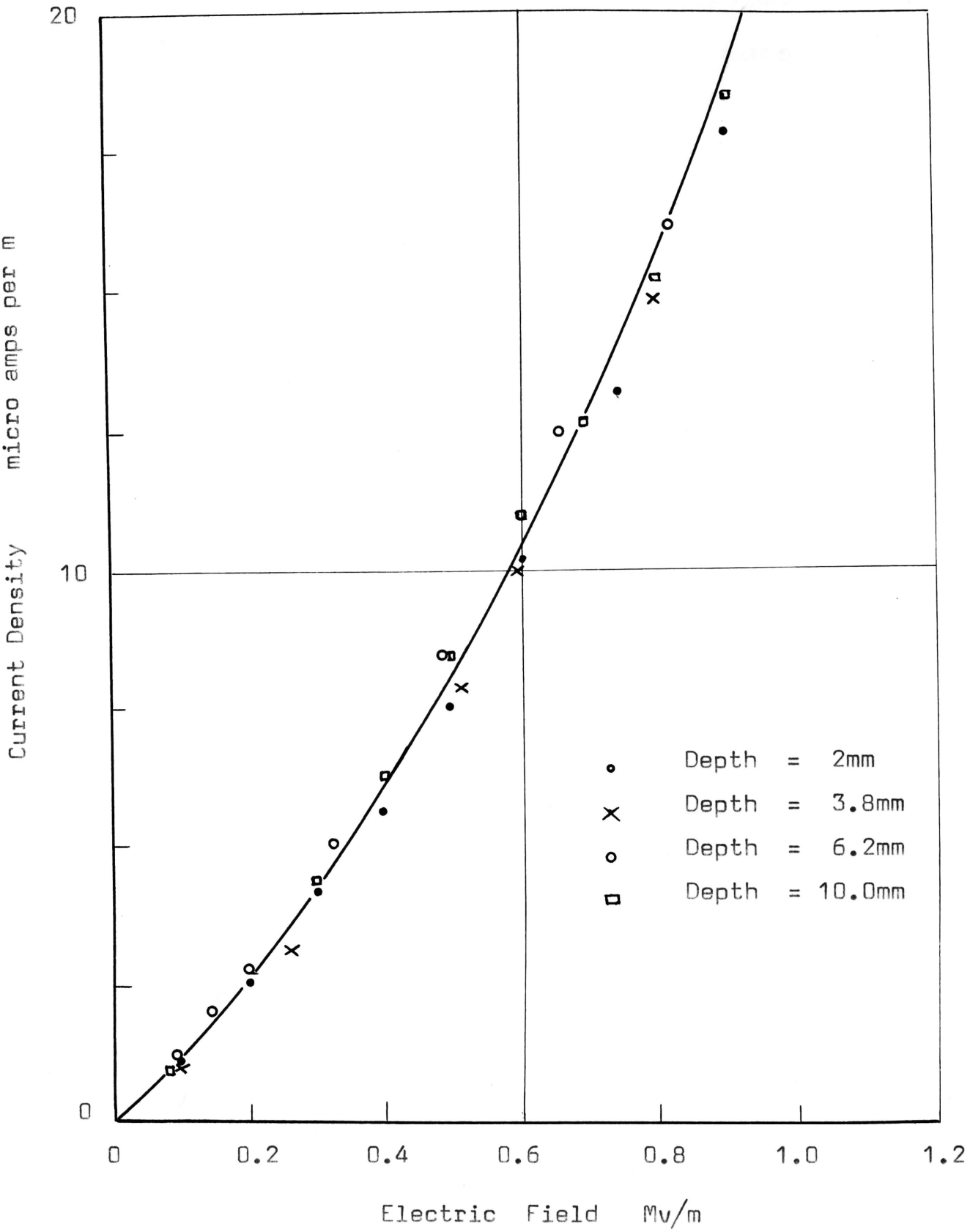

FIGURE 8.7 CURRENT DENSITY - ELECTRIC FIELD CHARACTERISTIC FOR FLYASH. TEMPERATURE = 195°C.

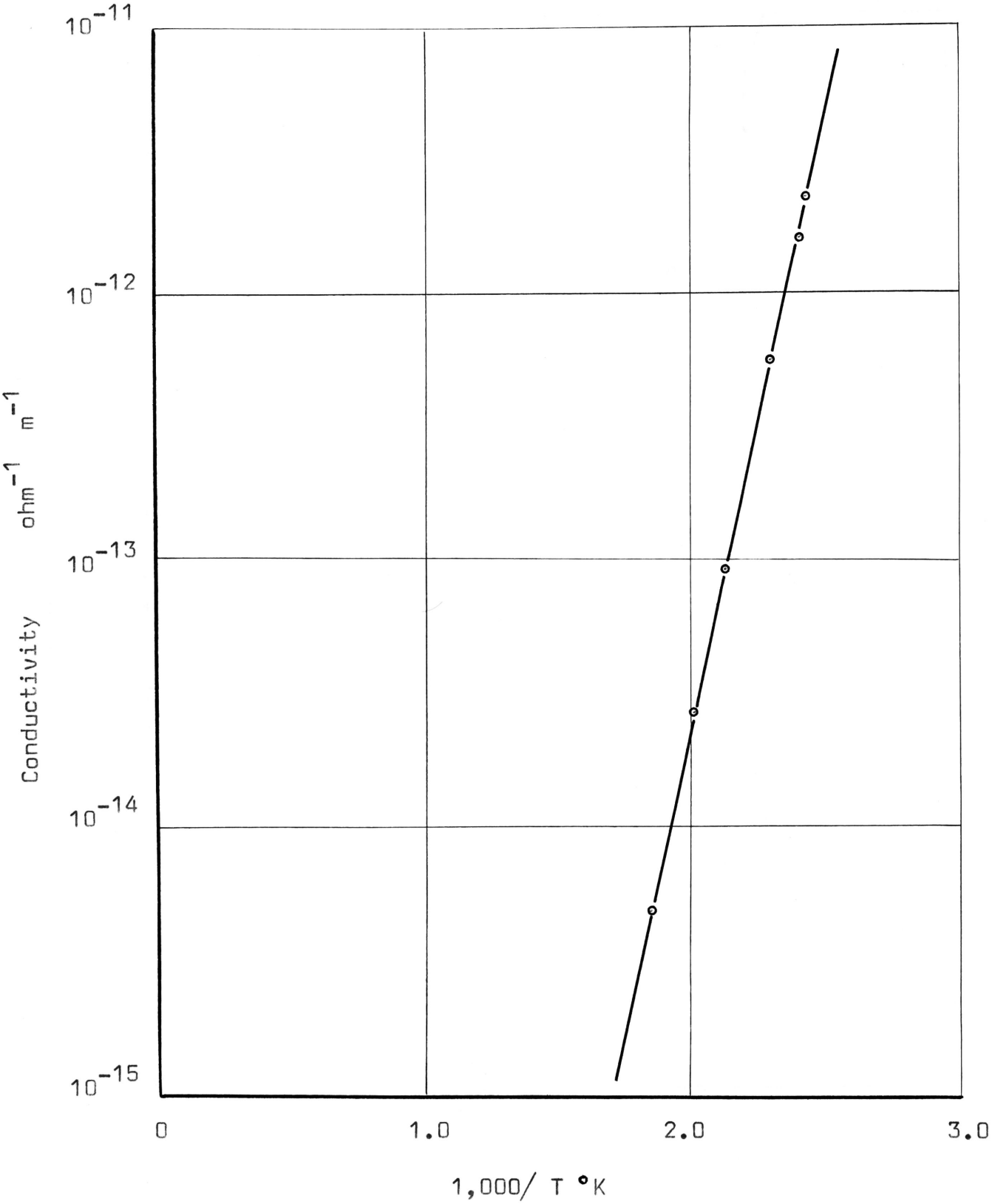

FIGURE 8.8 VARIATION OF FLYASH CONDUCTIVITY WITH THE RECIPROCAL OF THE ABSOLUTE TEMPERATURE. ELECTRIC FIELD = 0.16 MV/M.

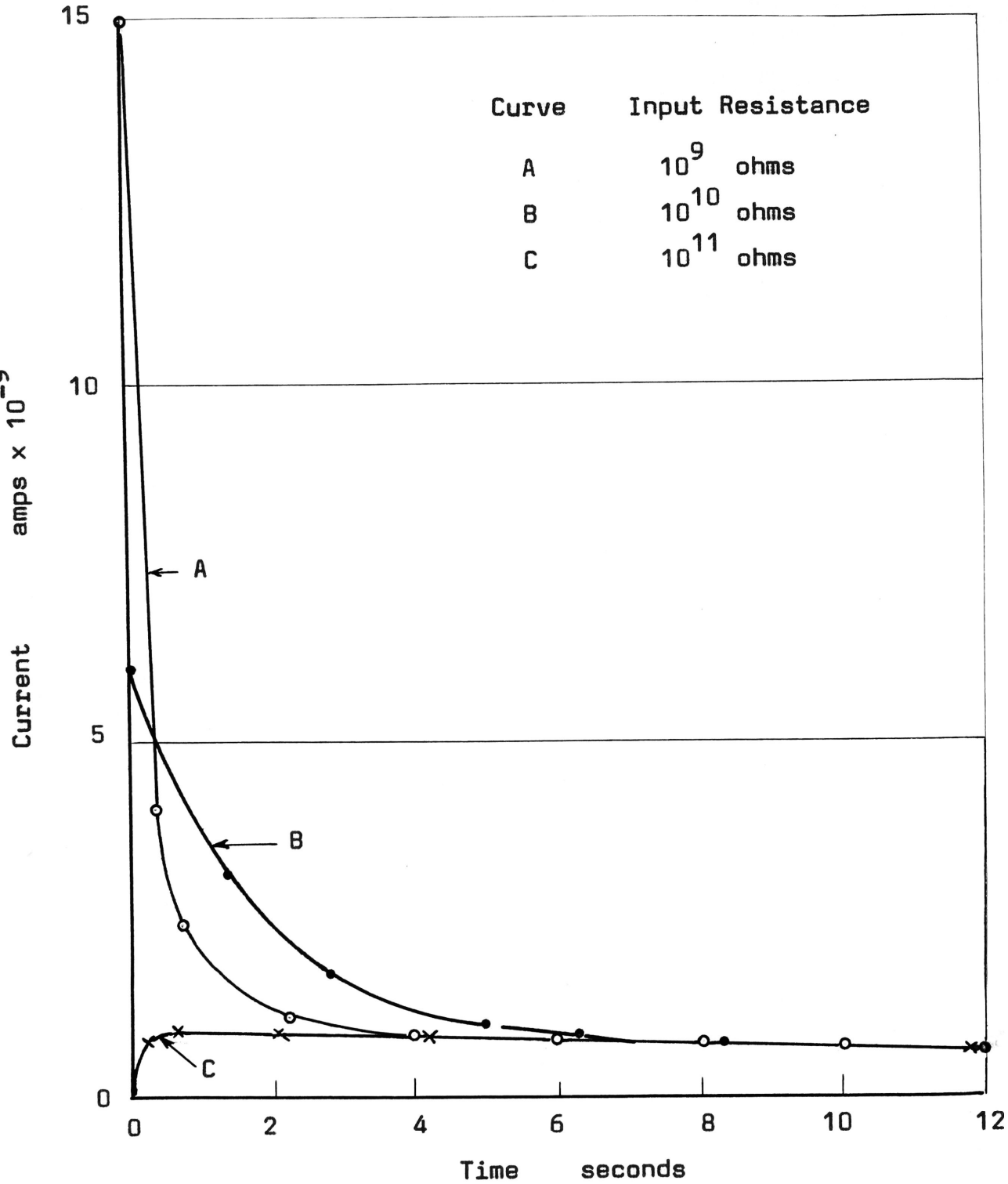

FIGURE 8.9 FLY ASH CURRENT-TIME TRANSIENTS FOR VARYING INPUT RESISTANCES TO THE ELECTROMETER. TEMPERATURE = 172°C. APPLIED VOLTAGE = 500 VOLTS.

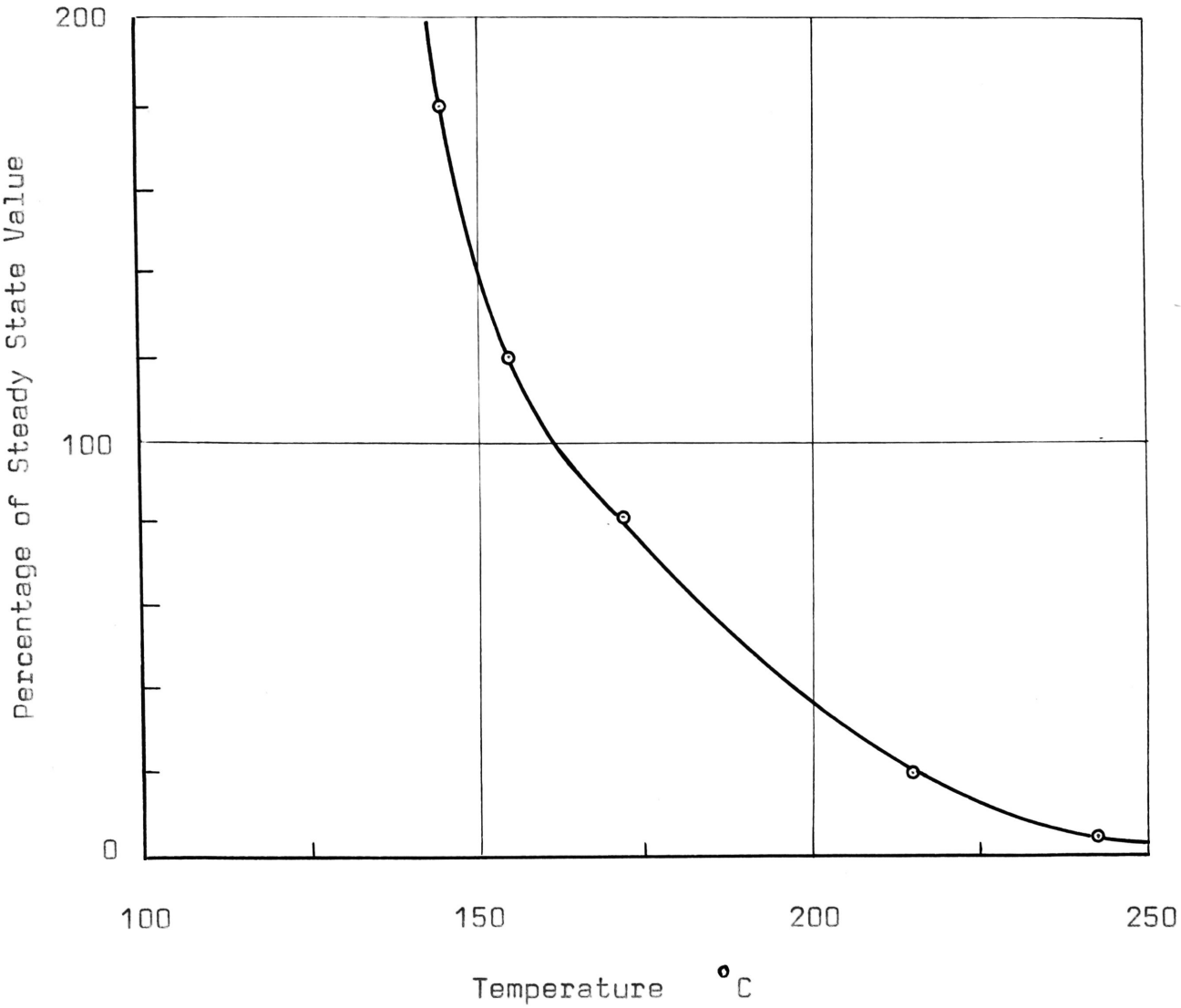

FIGURE 8.10 ABSORPTION CURRENT. PERCENTAGE OF STEADY STATE VALUE AFTER FIFTEEN SECONDS AT DIFFERENT TEMPERATURES. APPLIED VOLTAGE = 500 VOLTS.

against current density at a temperature of 195°C and for four different thicknesses is shown in Figure 8.7. This characteristic is similar to that obtained for the particulate form of silica and borosilicate glass. It is linear for very low electric fields and becomes non-linear at values above 0.1 MV/m. The deviation from linearity can also be made to fit the relationship,

$$J = A_1 E_{av} \epsilon^{B_1 E_{av}} \quad \ldots\ldots\ldots\ldots\ldots\ldots \quad 8.5$$

where $A_1 = 8.9 \times 10^{-12}$

$B_1 = 0.77 \times 10^{-6}$

This is shown drawn in Figure 8.7.

Figure 8.8 is a plot of the resistivity against the reciprocal of the absolute temperature on a semi-log scale. All points fit on a straight line giving an activation energy of 0.883 eV. The relationship is,

$$\rho = 3{,}000\ \epsilon^{10{,}210/T} \quad \ldots\ldots\ldots\ldots\ldots\ldots \quad 8.6$$

Figure 8.9 records a typical set of current-time characteristics for input impedances to the electrometer of 10^9, 10^{10} and 10^{11} ohms, at a temperature of 175°C. Characteristics at other temperatures were also obtained but only the variation of the absorption current is recorded. This is shown in Figure 8.10. Here the value of this current

after fifteen seconds, is expressed as a percentage of the steady state current for different temperatures.

8.4.4 Discussion.

The electric field-current density characteristic is linear for electric fields up to 0.1 Mv/m but for higher values it becomes non-linear. This non-linearity is due to the particulate form of the layer. Current flowing from one particle to another must pass through their common points of contact. This causes high electric fields to be generated in the region of the contacts which in turn reduced the bulk resistivity of the particles and causes charge transfer to take place between adjacent surfaces in the region of the contact points. The net effect of this is to reduce the effective resistance of the contacts and so reduce the effective resistivity of the particulate solid. The non-linear electric field-current density characteristic can be made to fit Equation 8.2.

The low electric field resistivity of the compacted layer depends on the temperature and compaction. The temperature dependence is given by Equation 8.6. The constant 3,000 in this equation contains a term H' which accounts for the mode of compaction, particle size distribution, particle shape and the applied pressure. Since it is not possible to determine the bulk resistivity of the

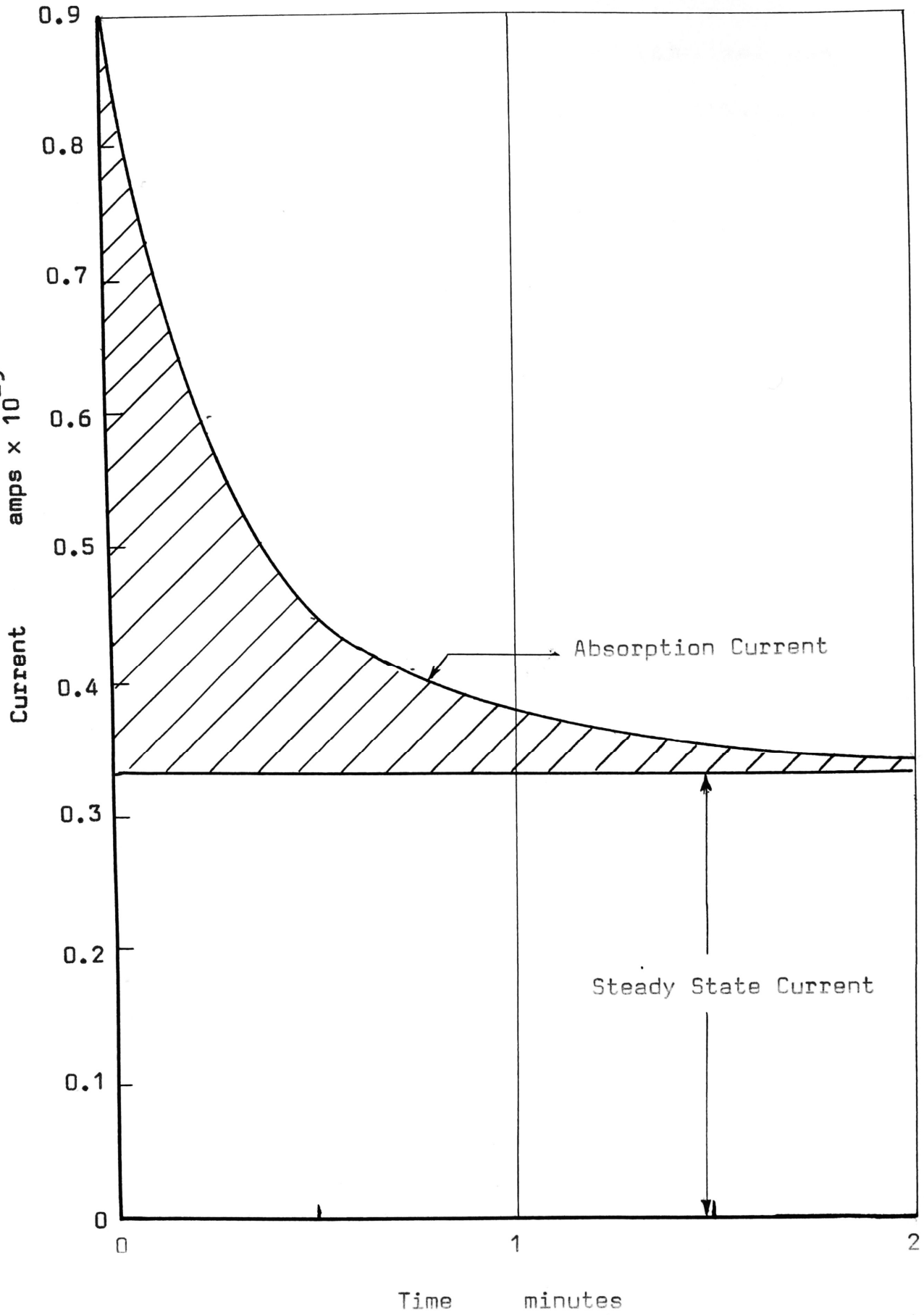

FIGURE 8.11 FLY ASH ABSORPTION CURRENT. TEMPERATURE = 172°C. APPLIED VOLTAGE = 500 VOLTS.

particle material itself, the actual value of H' is unknown. If the work on the silica and borosilicate glass particulate solids are of any guide, then H' could be expected to vary between 100 and 1,000.

The general equation for the effective resistivity of the flyash sample is given by,

$$\rho_e = 3{,}000\, \epsilon^{10{,}210/T}\, \epsilon^{-0.77 \times 10^{-6} E_{av}} \quad \ldots\ldots\ldots \quad 8.7$$

The transient component of the current is shown in Figure 8.9 clearly divides itself into two parts. The first is associated with the measuring circuit constants and can be separated out by varying the input resistance to the current measuring electrometer. The second component is independent of the measuring circuit parameters and must be a characteristic of the flyash itself. This is known as the absorption current and has been discussed in Section 3.5. Figure 8.11 is a plot of this absorption current for an applied electric field of 0.1 Mv/m and a temperature of 172°C.

The relative magnitude of this absorption current with respect to the steady state current decreases with increasing temperature as shown by Figure 8.10. This is consistent with the observations made by other investigators (50)(53).

Once the absorption current falls to zero, the total current is steady. On the basis of the work with the particulate form of the borosilicate glass, it may be concluded that the main charge carrier in the flyash is electronic. This is confirmed by the closeness of the E-J characteristics for different depths which indicates that there are no special contact effects taking place as would be the case if the main charge carrier was ionic.

REFERENCES

REFERENCES

1. WHITE, H.J. 'Industrial Electrostatic Precipitation', Addison-Wesley, U.S.A., 1963.
2. ROSE, H.E. and WOOD, A.J. 'An Introduction to Electrostatic Precipitation', London, Constable, 2nd Edn., 1966.
3. McLEAN, K.J. Trans. I.E. Aus., Vol.EE 4, No.1, p 141, March, 1968.
4. CARTWRIGHT, C.H. Phy.Rev., Vol. 49, p 443, March, 1936.
5. DAS, J.N. Int.J.Control, Vol. 3, No.1, p 79, 1966.
6. REGEL, A.R. and TAGIEV, B.G. Soviet Phys.-Solid State. Vol.7, No.3, p 742, 1965.
7. ALBERTS, L., BOHLMANN, M. and MEIRING, G.L. Brit.J. Applied Phys., Vol.17, p 951, 1966.
8. ZELNEY, L. Agr. Eng. p 252, April, 1954.
9. JOHNSTONE, H.F., Univ. Ill. Exp. Sta. Cir. No. 20, 1929.
10. WHITE, H.J. Chem. Eng. Progress, Vol. 52, p 244, 1956.
11. SPROULL, W.T. and NAKADA, Y. Ind.Eng.Chem., Vol. 43, No.6, p 1350, 1951.
12. DANIELS, R.O. 'A Study of the Effects of Adsorbed Films upon the Surface Electrical Conductivity of Powders'. Ph.D. Thesis, Uni. Utah, 1952.
13. LAKEY, J.R.A. and BOSTOCK, W. Trans.Inst.Chem.Eng., Vol. 33, p 252,1955.
14. MASUDA, S. E.T.J. of Japan, p 108, 1961.

15. MASUDA, S. Staub, Vol.25, p 175, May, 1965.

16. WHITE and ANDERSON developed this method and it is described in Ref. 11.

17. WALKER, A.B. Information Report No.2. Jn.Air Poll. Con.Ass., Vol.15, No.6, p 257, 1965.

18. ISAHAYA, F and ECHIZENYA, S. Hitachi Rev., Vol.17, No.2, p 40, 1968.

19. COHEN, L and DICKINSON, R.W. Jn.Sci.Instrum., Vol.40, 1963.

20. TASSICKER, O.J., HERCEG, Z. and McLEAN, K.J. Uni.N.S.W., Wollongong, Bulletin No.10, 1966.

21. TASSICKER, O.J., HERCEG, Z. and McLEAN, K.J. 'A New Method and Apparatus to Assist the Prediction of Electrostatic Precipitator Performance'. Trans.I.E. Aus., 1969 (In print).

22. EISHOLD, H.G. Staub, Vol.26, No.1, p 11, 1966. (In German)

23. JONES, F.L. 'The Physics of Electrical Contacts'. Great Britain, Oxford Uni. Press, 1957.

24. WINDRED, G. 'Electrical Contacts'. London, Macmillan, 1940.

25. HOLM, R. 'Electric Contacts Handbook'. Stockholm, Hugo Gebers Forlag, 3rd Ed., 1958.

26. SMYTHE, W.R. 'Static and Dynamic Electricity'. New York, McGraw-Hill, 2nd Ed., 1950.

27. WEBER, E. 'Electromagnetic Fields'. Vol.1, New York, John Wiley, 1950.

28. TIMOSHENKO, S. and GOODIER, J.N. 'Theory of Elasticity', 2nd Ed., New York, McGraw-Hill, 1951.

29. GREENWOOD, J.A. Brit.Jn.Appl.Phys., Vol.17, p 1621, 1966.

30. WEYL, A.W. and MARBOE, E.C. 'The Constitution of Glasses'. Vol.1 and 11. John Wiley, N.Y., 1967.

31. STEVELS, J.M. 'Encyclopedia of Physics'. Vol.13, Springer-Verlag, Berlin, 1962.

32. CARMAN, P.C. 'Chemical Composition and Properties of Engineering Materials'. Edward Arnold and Co., London, 1949.

33. ZACHARIASEN, W.H. Jn. Am. Chem. Soc., Vol.54, p 3841, 1932.

34. WARREN, B.E. Jn.Appl.Phys., Vol.8, p 645, 1937.

35. OWEN, J. 'Progress in Ceramic Science'. Vol.3, Pergamm Press, London, 1966. Editor J.E. Burke.

36. MAURER, R.J. Jn.Chem.Phys. Vol.9, p 579, 1941.

37. CHARLES, R.J. Jn.Appl.Phys., Vol.33, No.6, p 1115, 1961.

38. MURAY, J.J. Jn.Appl.Phys., Vol.9, p 1517, 1962.

39. WHITEHEAD, S. 'Dielectric Breakdown of Solids'. Oxford Calender Press, 1950.

40. FRENKEL, J. Phys. Rev., Vol.54, p 647, 1938.

41. ZENER, C. Proc. Roy. Soc., Vol.A145, p 523, 1934.

42. LAMB, D.R. 'Electric Conduction Mechanisms in Thin Insulating Films'. Methuen, London. 1967.

43. FROHLICH, H. 'Theory of Dielectrics', Claredon Press, Oxford 2nd Ed., 1958.

44. ROE, D.W. Jn. Electrochem. Soc., Vol.112, No.10, p 1005, 1965.

45. GREEN, R.L. and BLODGETT, K.B. Jn.Am.Cer.Soc., Vol.31, No.4, p 89, 1948.

46. ROHATGI, V.K. Jn.Appl.Phys., Vol.28, No.9, p 951. 1957.

47. NELSON, R.C. Jn.Appl.Phys., Vol.34, No.3, 1963.

48. DAVIES, D.K. Stat.Elec.Con., Ser. No.4, Inst.Phy. Soc., p 29, 1967.

49. DOREMUS, R.H. Jn. Elec. Chem. Soc., Vol.115, p 181, 1968.

50. SUTTER, P.H. and NOWICK, A.S. Jn. Appl. Phys., Vol.34, p 734, 1963.

51. JOFFE, A. 'The Physics of Crystals'. McGraw-Hill, New York, 1928.

52. LINDMAYER, J. Trans. I.E.E.E., Vol CP-11, p 212, 1964.

53. VERMEER, J. Physica, Vol.22, p 1257, 1956.

54. BEAN, C.P., FISHER, J.C. and VERMILYEA, D.A. Phy. Rev., Vol.101, p 551, 1956.

55. MEAD, C.A. Phy. Rev., Vol.128, p 2088, 1962.

56. FOWLER, R.H. and NORDHEIM, L. Proc.Roy.Soc., Vol.A119, p 173, 1928.

57. MURAY, J.J. Jn.Appl.Phys., Vol.33, p 1525, 1962.

58. AHMED, S.U. 'Sparking in Air for Gap Lengths of Ten to One Hundred Microns'. Thesis, Uni. N.S.W., 1969.

59. SUTTON, P.M. Jn.Am.Cer.Soc., Vol.47, p 219, 1964.

60. COHEN, J. Jn.Appl.Phys., Vol.28, p 795, 1957.

61. McLEAN, K.J. Elec.Lett., I.E.E., Vol.5, p 72, 1969.

62. HUEY, R.M. and VONGPANITLERD, S. Ins.R.E.E.Aus., Vol.30, p 124, 1969.

63. PETERSON, J. Jn.Appl.Phys., Vol.25, p 501, 1954.

64. WAGNER, P.E. Jn.Appl.Phys., Vol.27, p 1310, 1956.

65. GRATON, L.C. and FRASER, H.J. Jn.Geol., Vol.43, p 785, 1935.

66. WESTMAN, A.E.R. and HUGILL, H.R. Jn.Am.Cer.Soc., Vol.13, p 767, 1930.

67. WHITE, H.E. and WALTON, S.F. Jn.Am.Cer.Soc., Vol.20, p 155, 1937.

68. SMITH, W.O., FOOTE, P.D. and BUSANG, P.F. Phy.Rev., Vol.34, p 1271, 1929.

69. DERESIEWICZ, H. 'Advances in Applied Mechanics'. Vol.5, p 233, Academic Press, N.Y., 1958.

70. RIDGWAY, K. and TARBUCK, K.J. Bt.Chem.Eng., Vol.12, p 384, 1967.

A P P E N D I X

I Fly-ash Composition.

I.1 Chemical Analysis.

The following table gives a typical chemical analysis of the flyash from Tallawarra Power Station. The analysis was carried out by the Electricity Commission of New South Wales.

TABLE I.1

FLYASH COMPOSITION

Compound	Percent Content
Combustible	2.40
SiO_2	71.30
Al_2O_3	21.60
Fe_2O_3	2.80
CaO	0.96
MgO	0.22
S and SO_3	0.22

This table shows that 93 percent of the flyash is made up of SiO_2 and Al_2O_3.

Tests for trace elements have also been made. The following elements were detected and the concentration, in parts per million, is given in parenthesis.

B (150), Ba (400), Co (10), Cr (50), Cu (50), Ga (30), Ge (30), La (100), Mn (1000), Mo (10), Ni (25), Pb (70),

S (1500), Sc (30), Sr (500), V (200), Y (60), Zn (1000), Zr (800).

I.2 X-Ray Diffraction Pattern.

An X-ray diffraction pattern was taken to determine the mineral combination of the silica and alumina. The flyash had a pattern similar to that of silimanite. The pattern also indicated that the basic oxides present are probably in solution in the alumino-silicate. The conclusion that the ash consists of an alumino-silicate of the silimanite type cannot account for some 50 percent of the SiO_2. Since the diffraction patterns show no strong lines, this would indicate that some polymorph of this oxide is present. One possible conclusion that may be drawn is that this SiO_2 is present in a non-crystalline form, either as SiO_2 or in some complex molecular form.

The X-ray diffraction patterns and interpretations were carried out by the Department of Metallurgy, Wollongong University College.

II Stray Pulses in Silica.

II.1 Introduction.

In carrying out tests on the bulk characteristics of silica it was observed that at high electric fields the reading of the current was made difficult

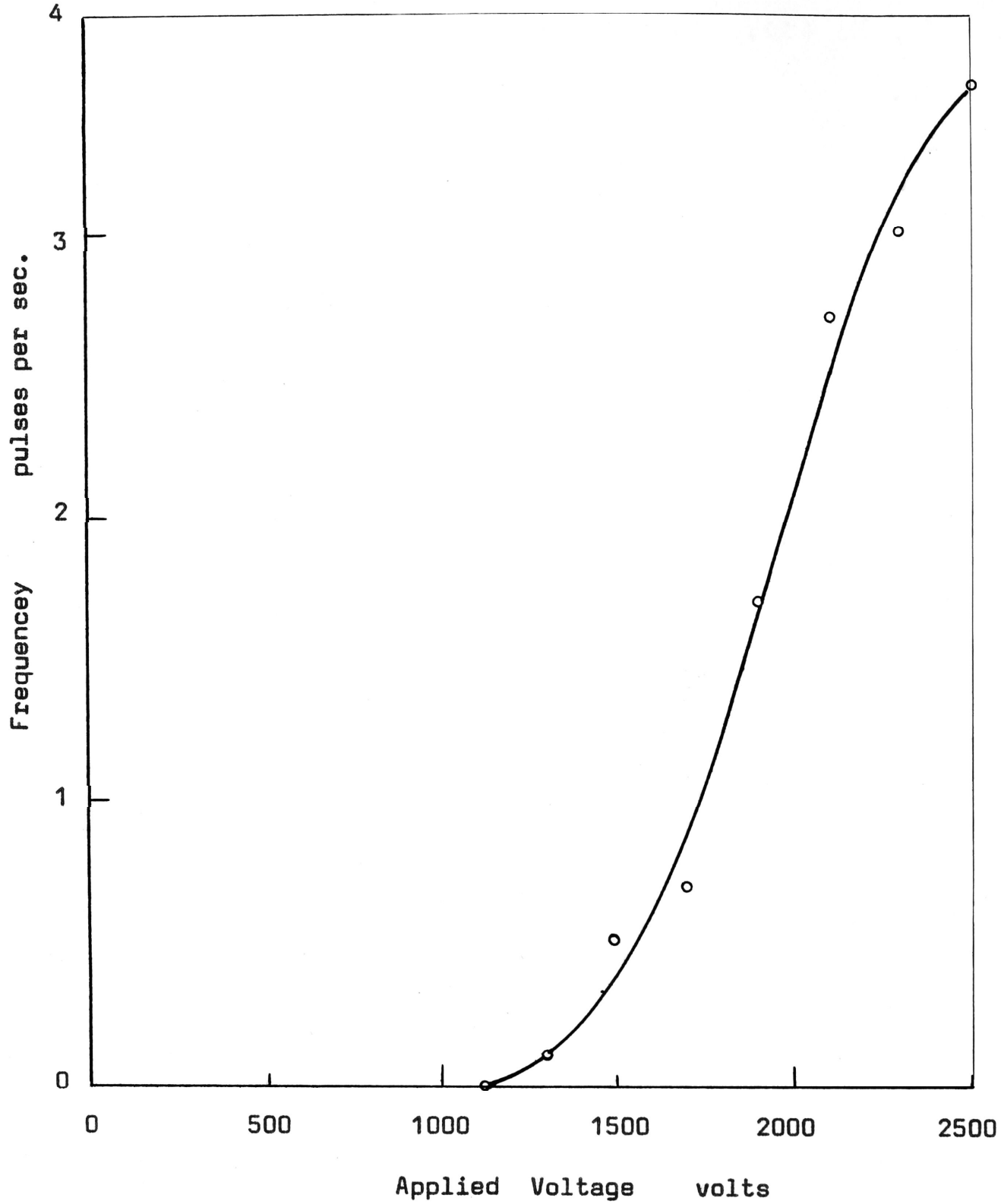

FIGURE II.1 VARIATION OF PULSE FREQUENCY WITH APPLIED VOLTAGE.

TEMPERATURE = 275 °C.

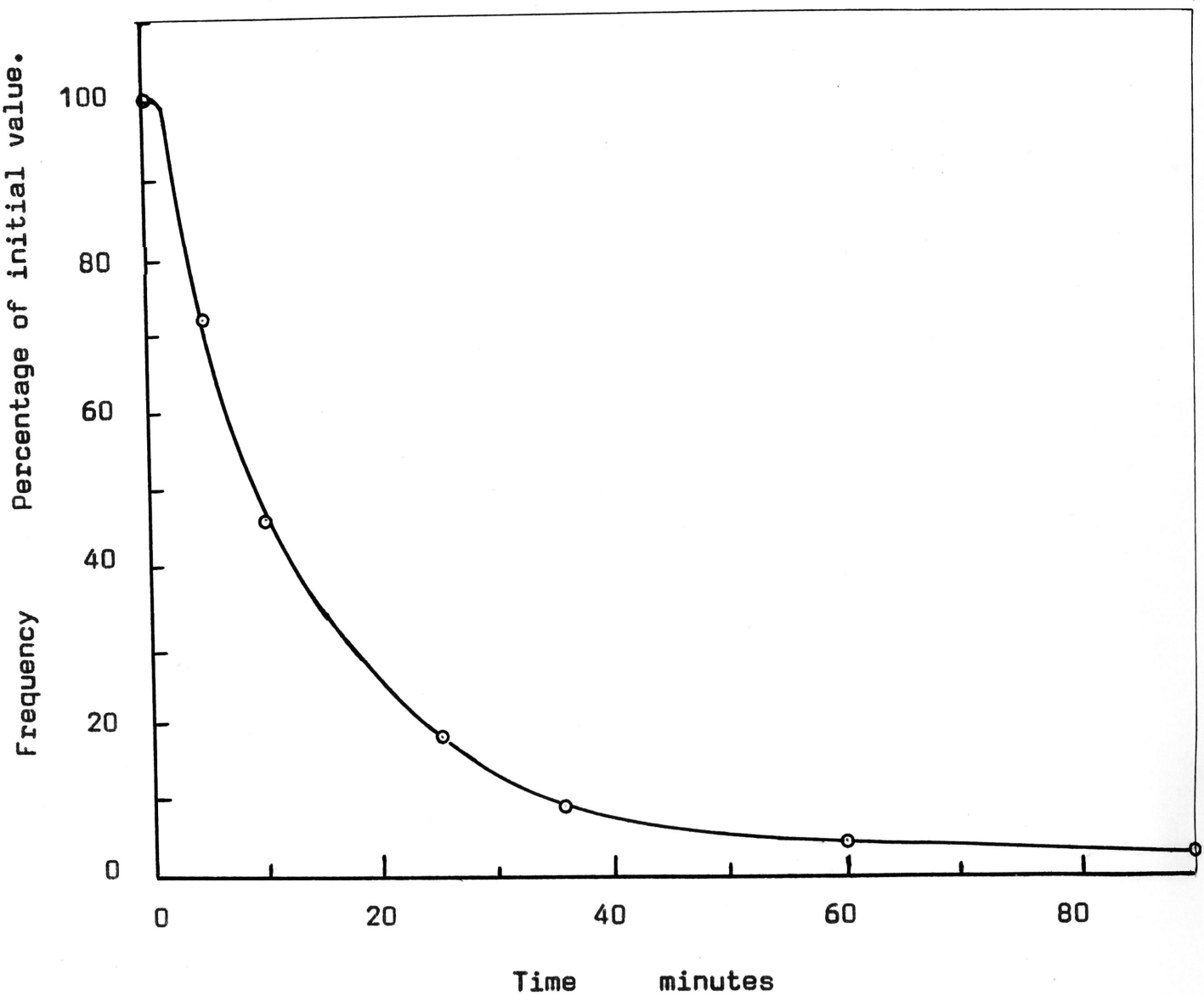

FIGURE II.2 VARIATION OF PULSE FREQUENCY WITH TIME FOR A CONSTANT APPLIED VOLTAGE OF 2,100 VOLTS

by the presence of spurious pulses superimposed on the d.c. current.

In order to investigate their origin and characteristics, the rod electrode system was used. This is essentially the same as shown in Figures 4.3 and 4.4. By using this geometry, a non-uniform electric field is established in the silica disc and by varying the polarity of the rod electrode the effect of the electrode polarity can be determined.

II.2 Procedure and Results.

The apparatus was placed in an oven and heated to a temperature of 275°C. The voltage was then increased and the presence of pulses observed on a storage oscilloscope. When the rod electrodes were held at negative potential, the pulses appeared at a voltage of 1,300 volts and their frequency increased with the voltage. Figure II.1 records a typical set of results. The characteristic for a temperature of 225°C was very similar to this.

It was also observed that if the voltage was held at one value for any length of time, the frequency of the pulses reduced with time. A typical example, taken for a voltage of 2,100 volts, is shown in Figure II.2. Results at other voltages and temperatures have the same general characteristic.

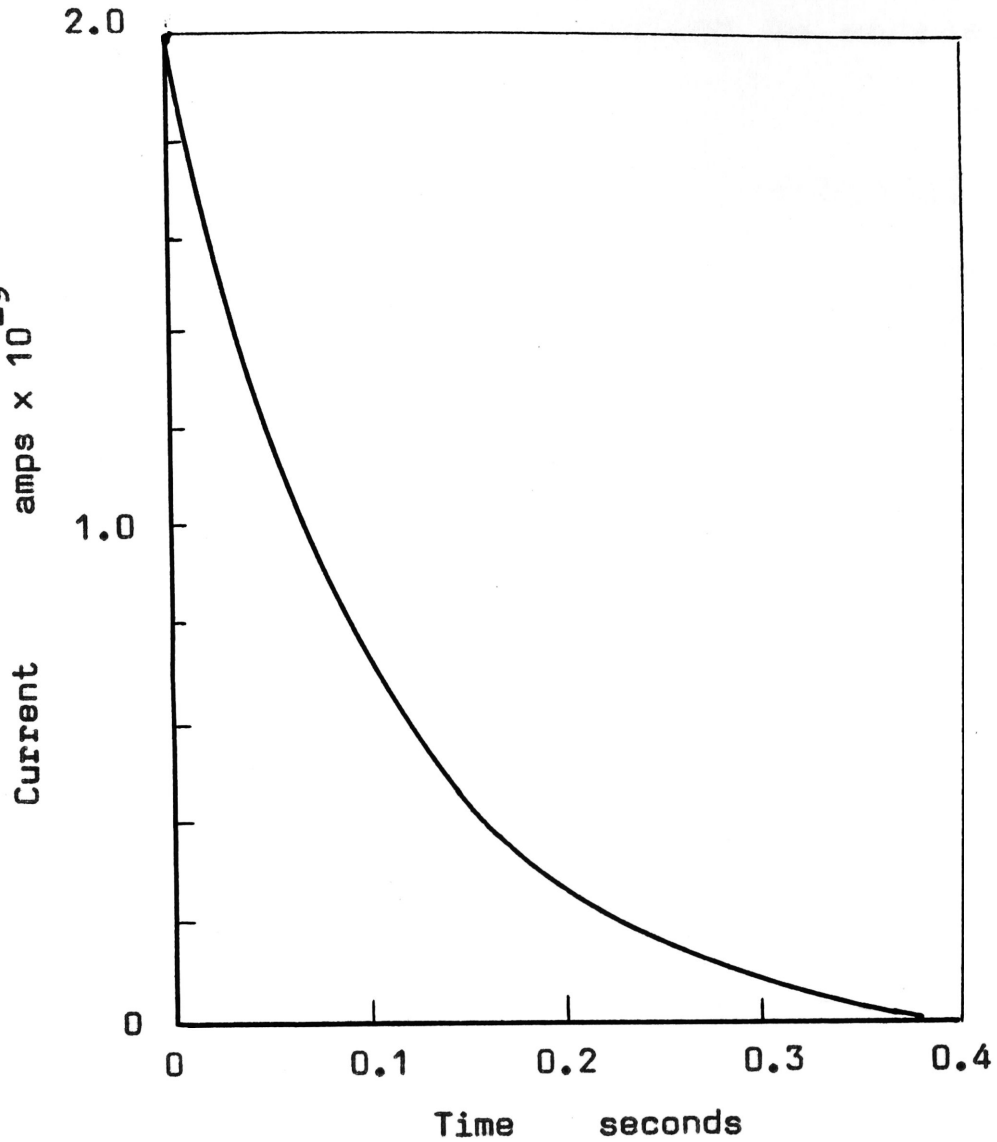

Input impedance to electrometer	10^9 ohms.
Temperature	275 °C.

FIGURE II.3 SHAPE OF TYPICAL PULSE.

Figure II.3 gives a typical shape of the pulses. The peak value of the pulses decreased and the time constant increased as the input resistance to the electrometer increased.

When the points were held at positive potential, no pulses were observed for voltages up to 2,500 volts. However, if this potential was maintained for more than a minute, then positive pulses began to appear. They gradually increased in magnitude and frequency over a period of three minutes after which time their intensity quickly reduced. After this, only spasmodic pulses were observed. The general shape and time constants were the same as those for the negative pulses.

II.3 Discussion.

Because of the exceptionally low mean free path of the mobile carriers in the silica, it is clear that the pulses observed are not due to sudden flow of charge through the insulator. The current observed in the external circuit must be due to the sudden generation of space charge in the silica itself. The actual charge associated with each pulse may vary by orders of magnitude. The charge in the pulse shown in Figure II.3 is given by,

$$\int I(t)\, dt$$

and is equal to 8.0×10^{-11} coulombs. This is equivalent

to 5.0×10^8 electrons.

The generation of noise in dielectrics has been investigated by a number of workers. The explanations offered for this phenomenon vary from that due to avalanches of electrons emitted from the metal electrode by Hawarth and Bozorth(71), the fluctuating motion of ions in the solid material by Boyer(72), the ionization of small voids due to poor electrode contact by Mason(73)(74), the presence of electrets by Baumann and Wiseman (75), to the solid state chemical activity at the contact surface by Northrip(76). In all the experimental work carried out by the above investigators, the samples were placed between two parallel plates. This electrode arrangement has some limitations as it is not possible to distinguish between the separate effects of the two electrodes. By using the rod to plane electrode system suggested in this thesis, this limitation is overcome.

Of the theories put forward, the only two which are likely to apply to silica are those offered by Hawarth and Bozorth, and Mason. Both are consistent with the much greater activity at the negative electrode. An alternative model which would be consistent with the experimental evidence is to consider a process analogous in some respects to the generation of Trichel pulses in negative corona discharges.

Consider a volume of the silica close to the point of contact between the rod electrode and the silica. If the rod electrode is held at a negative potential, then as this increases, the electric field in the silica increases until it is high enough to cause an avalanche of electrons, ~~to be separated from their parent atoms.~~ As the negative space charge is built up, it reduces the field strength around the contact point and chokes any further generation of free electrons. As this negative space cloud moves away from the electrode, the positive ion defects move towards the rod electrode where they are neutralized by the metallic electrons. The result of this process is that there is a net gain in negative space charge in the silica which appears as a current pulse in the external circuit. In the initial stages, the increase in the frequency of the pulses with the applied voltage is also analogous to discharges in gas. As the applied voltage increases, the space charge cloud is not so effective in reducing the electric field at the electrode below the ionization level, hence the pulses can be generated at a greater frequency.

In one respect these pulses are not analogous to the discharges in gas. For a fixed applied voltage, the pulses observed in the silica decreased in frequency and magnitude with time. This does not occur with the Trichel pulses. This characteristic of the pulses in silica can be attributed to the gradual build up of a negative space charge in the silica by the electrons emitted from the rod

electrode. As these move into the lower field areas, they are more likely to become trapped. The net effect of this is to cause the build up of a stationary space charge which will reduce the field strength around the rod electrode and so reduce the frequency of the pulses until they are completely choked.

The characteristics observed with the rod electrode positive cannot be explained in terms analogous to gas discharges. Under the influence of the high electric field, an avalanche of electrons is generated within the silica and moves to the electrode leaving behind a positive space cloud. This initially chokes the avalanche until it moves away from the area. The initial delay could be due to the very low drift velocity of the initial avalanche of electrons so that there is a delay from the time they are generated to the time of their arrival at the electrode. Once they arrive, there is a sudden appearance of a positive space charge which appears in the external circuit as a positive pulse. This process cannot go on indefinately because there is only a limited number of electrons capable of being separated from their parent atoms. Hence there is a sudden burst of pulses which quickly dies down as the area becomes depleted of easily ionizable electrons.

The absence of spurious pulses in the silica to silica tests recorded in Chapter 6 is consistent with this model and supports its validity.

II.4 References.

71. HAWARTH, F.A. and BOZORTH, R.M., Physics, Vol.5, p 15, 1934.

72. BOYER, R.F., Jn.App.Phys., Vol.21, p 469, 1950

73. MASON, J.H., Trans.I.E.E., Vol.98, Pt 1, p 44, 1951.

74. MASON, J.H., Jn.App.Phys., Vol.22, p 235, 1951.

75. BAUMANN, N.P. and WISEMAN, G.G., Jn App.Phys., Vol.25, p 1391, 1954.

76. NORTHRIP, J.W., Jn.App.Phys., Vol.31, p 2293, 1960

III Scaling and Method of Plotting Results.

III.1 Scaling.

Since it is physically impossible to investigate the characteristics of the contact points between actual particles, it is necessary to use a scaled up model of the contacts. In most engineering problems where it is desired to represent some actual situation with a scaled model, it is often difficult to do this in such a manner that the model represents the original in every respect. It is usual to arrange the model so that the main parameters are accurately represented and adjustments are made to the results for those parameters which are not accurately represented.

The main requirement of our model is that the current flow pattern in the ideal particle is the same as

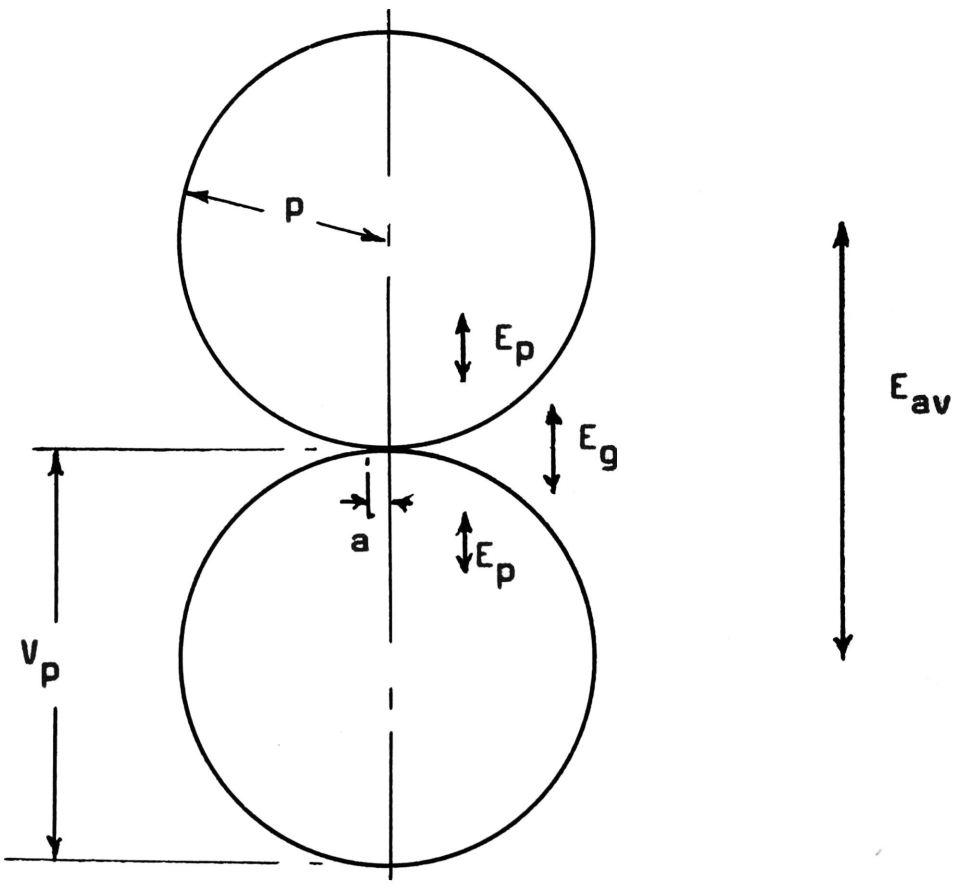

FIGURE 111.1 DIAGRAM SHOWING PARTICLE DIMENSIONS AND ELECTRIC FIELDS.

that in the model, and that the electric field strength is the same at corresponding points in the particle and the model. It will be shown in the next section that this condition is obtained if the voltage is increased in the same ratio as the radius of contact.

III.2 The 'FM' Factor.

Consider the case of circular metallic contact on the surface of a flat sample of high resistivity material. If the material is homogenous and of constant resistivity, the field pattern of the current flow is given by Holm's equation. This pattern will be the same for any radii and the magnitude of the field will vary with the applied voltage and the radius of the contact. Examination of the equations in Section 2.4.2 shows that the electric field strength across the axes considered are given by the relationship,

$$E_p = K\ (V/a)$$

Where V is the voltage across the contact, a is the radius of the contact circle and K is a constant which will vary with the axes.

The ratio of V to a is an important constant and is called the 'FM' or 'Field Magnitude' factor. If this value is the same for two different contacts, it may be assumed that the magnitude of the two fields are the same and that one contact correctly models the other.

The use of the term can be extended to describe the field condition in the particles compacted together to form a layer. If they are arranged in a simple cubic array, the voltage across each particle is given by,

$$V_p = E_{av}\ 2p$$

and the voltage across half the particle is,

$$V = V_p/2$$

Since it is assumed that the current pattern in the particle is given by the Holm equation, the electric field strength in the particle is,

$$E_p = K\ V_p/2a = K\ FM$$

Where $$FM = V/a = V_p/2a = E_{av}(p/a)$$

For a compacted layer of particles, the field strength in the particle increases in the same ratio as the average applied electric field across the layer.

The electric field strength between the surfaces of two particles in contact is given by Equation 2.27.

$$E_g = K\ FM\ (p/a)$$

In this case, for one particle to correctly model another, it is necessary that,

(a) their 'FM' factors be the same, and

(b) the ratio of p to a for each particle is the same.

III.3 Verticle Axis.

One of the main requirements of the method

adopted in plotting the results is that the results from different tests can be easily compared. Consider the case of the metal electrode to glass contacts described in Chapters 4 and 5. The resistance of the contact is:

$$R_c = V / I = \rho / 4a.$$

This may be rewritten as,

$$\frac{4aV}{\rho I} = 1.0$$

Dividing top and bottom terms by $4a^2$, the equation becomes;

$$\frac{V/a}{\rho I/4a^2} = 1.0$$

Hence if V/a is plotted against $\rho I/ 4a^2$ on rectangular axes using the same scale, the resultant curve will be a straight line inclined at 45^o providing the resistivity of the glass remains constant with the applied voltage and no electron emission takes place across the airgap. This will be true irrespective of the temperature and the radius of the contact circle. Any reduction in the resistivity with the applied voltage or any electron emission across the airgap will cause the resultant curve to sit above this 45^o line.